Optimization of Two Stage Process for the Growth of In_2S_3, $CuInSe_2$ and $CuIn(Se_{1-x}S_x)_2$ Thin Films for Solar Cell Application

Thesis submitted to
COCHIN UNIVERSITY OF SCIENCE AND TECHNOLOGY
in partial fulfillment of the requirements
for the award of the degree of
DOCTOR OF PHILOSOPHY

Rahana Yoosuf

Department of Physics
Cochin University of Science and Technology
Cochin – 682 022, Kerala, India

October 2007

Optimization of Two Stage Process for the Growth of In_2S_3, $CuInSe_2$ and $CuIn(Se_{1-x}S_x)_2$ Thin Films for Solar Cell Application

Ph.D thesis in the field of material science

Author:

Rahana Yoosuf
Optoelectronic Devices Laboratory
Department of Physics
Cochin University of Science and Technology
Cochin – 682 022, Kerala, India
email: rehna_y@yahoo.com

Supervisor:

Dr. M.K. Jayaraj
Reader
Optoelectronic Devices Laboratory
Department of Physics
Cochin University of Science and Technology
Cochin – 682 022, Kerala, India
email: mkj@cusat.ac.in

October 2007

Dr. M.K. Jayaraj
Reader
Department of Physics
Cochin University of Science and Technology
Cochin – 682 022

15th October 2007

Certificate

Certified that the work presented in this thesis entitled "*Optimization of Two Stage Process for the Growth of In_2S_3, $CuInSe_2$ and $CuIn(Se_{1-x}S_x)_2$ Thin Films for Solar Cell Application*" is based on the authentic record of research done by *Mrs. Rahana Yoosuf* under my guidance in the Department of Physics, Cochin University of Science and Technology, Cochin – 682 022 and has not been included in any other thesis submitted for the award of any degree.

Dr. M.K. Jayaraj
(Supervising Guide)

Phone : +91 484 2577404 extn 33 Fax: 91 484 2577595 email: mkj@cusat.ac.in

Declaration

Certified that the work presented in this thesis entitled "*Optimization of Two Stage Process for the Growth of In_2S_3, $CuInSe_2$ and $CuIn(Se_{1-x}S_x)_2$ Thin Films for Solar Cell Application*" is based on the original research work done by me under the supervision and guidance of Dr. M.K. Jayaraj, Reader, Department of Physics, Cochin University of Science and Technology, Cochin-682022 has not been included in any other thesis submitted previously for the award of any degree.

Cochin – 22
15th October 2007

Rahana Yoosuf

Acknowledgements

This thesis arose in part out of years of research and by that time, I have worked with a great number of people whose contribution in assorted ways to the research and the making of the thesis deserve special mention. It is a pleasure to convey my gratitude to them all in my humble acknowledgment.

In the first place I would like to record my gratitude to Dr. M. K. Jayaraj for his supervision, advice, and guidance from the very early stage of this research. I thank him also for giving me the chance to participate in several interesting research projects and attend various conferences.

I extend my sincere thanks to Dr.T.Ramesh Babu, the Head of the Department of Physics, and all other former Heads of the Department for allowing me to use the facilities. I gratefully acknowledge Prof.K.P.Vijayakumar, my doctoral committee and all other faculty members of the Department of Physics.

It is with a particular pleasure that I acknowledge Dr.Johny Isaac, my MSc project coordinator for the start of my research carrier. I am also indebted to Dr. Rani Joseph, Department of Polymer Science and her student Srikanth for their valuable advice in conducting polymers and providing me the sample.

I am grateful to all the office and library staff of the Department of Physics and the technical staff at USIC for all the help and cooperation. I acknowledge the financial support by the Ministry of Non-Conventional Energy Sources.

It is a pleasure to express my gratitude wholeheartedly to my colleagues at OED lab, Ajimsha, Aneesh, Anoop, Arun, Anila Teacher, Joshi Sir, Mini, Ratheesh, Saji and Vanaja madam. It was

great to collaborate with them all. I am grateful to all who helped me to revise parts of this thesis, particularly at the end of this project. I specially appreciate Aldrin Antony for his helpful advices during the initial stage of my research.

My special thanks go to Asha, Nisha, Reshmi and Manoj for giving me such a pleasant time when working together and for the hilarious lunch hours. With a deep sense of gratitude I thank Reshmi in particular, whose indispensable help dealing with the entire official and unofficial matters during my leave so I could optimally continue my research. It is also a pleasure to mention Anusha for being a good friend who was always ready to lend a hand.

I am thankful to Alex, Aravind, Teny, Jerome Sir, Sukesh, Jincy and Smitha for their friendship and sincere help extended to me at various stages in my life at CUSAT.

Collective and individual acknowledgments are also owed to my friends at hostel, whose presence somehow perpetually refreshed, and made memorable my stay at Athulya. Special thanks to Radhika who tolerated me for four years and Premi who offered a place in her room when I first came to CUSAT.

With a sense of gratitude, I remember Manjusha for all the support and positive criticism from the very day we met. Special thanks to my long time friends Shybi, Becky and Manju for their love and advices and constant support they extended throughout the years through phone calls and mails.

Finally, I wish to express my love and gratitude to my beloved parents, parent in laws and my husband. I am deeply and forever indebted to my parents for their love, support and encouragement throughout my entire life. I would like to express my deepest gratitude for the understanding and love that I received from my husband and

also for never advising me to quit this project. I am also very grateful to Resna and Refin for being supportive and caring siblings.

Words fail me to express my appreciation to my little daughter whose presence provided an additional and joyful dimension to my mission. I owe her for being such an understanding baby during the writing of this thesis.

I would like to thank everybody who was important to the successful realization of thesis, as well as expressing my apology that I could not mention personally one by one.

Rahana Yoosuf

Contents

Chapter 3

Growth of β -Indium Sulfide Buffer Layer by Two Stage Process

Preface

Over the last ten years, photovoltaic (PV) has emerged to an application with vast potential which has attracted the interest of increased numbers of students and researchers. Solar electricity is growing in popularity for several reasons. The main of them are increasing environmental concerns, desire for energy independence, utility deregulation etc. But widespread use of solar cells is handicapped by its high cost. One of the most promising strategies for lowering PV cost is the use of low cost manufacturing techniques. The objective of this thesis work was mainly focused on the development of a relatively low cost easily scalable two stage deposition technique, to produce uniform coatings of thin films on large area substrates. The thesis is organised into six chapters.

An over view of the development of thin film solar cells are briefly described in Chapter 1. It also review some basic aspects of solar cells and the major families of PV materials currently being developed, including various types of silicon, thin films, and new concepts.

Chapter 2 describes the different thin film deposition techniques used to deposit the chalcopyrite thin films and the different characterisation tools used to characterise the thin films. The thicknesses of the films were measured using Vecco Stylus profilometer. X-ray diffraction (XRD) studies were carried out to study the crystallograoghic properties of the thin films prepared. The energy dispersive X-ray analysis (EDX) and scanning electron microscopy (SEM) were used for evaluating the composition and morphology of the films. Optical properties were investigated using the UV-Vis-NIR spectrophotometer by recording the absorption spectra. The electrical properties and the temperature dependence of conductivity were measured using the two probe method.

The p-n heterojunction in thin-film solar cells is formed at the interface between the p-type absorber and the n-type buffer layer. The preparation and characterisation of both absorber and buffer layer is important for the performance of a solar cell. The growth of n-type Indium Sulfide (In_2S_3), p-type Copper Indium Selenide ($CuInSe_2$) and Copper Indium Sulfur Selenide $CuIn(S_{1-x},Se_x)_2$ thin films by two stage process and their characterisations are described in next three chapters.

In_2S_3 thin films appear to be promising candidates for many technological applications due to their stability, transparency, and wide band gap (2 - 2.3 eV) and their photoconductivity. In_2S_3 can be used as an effective replacement for CdS in $Cu(In,Ga)Se_2$ based solar cells. It is also a binary precursor for $CuInS_2$. In_2S_3 exists in three crystallographic modifications α, β and γ with β-In_2S_3 being a stable state with tetragonal structure. In the third chapter, the dependence of the processing parameters on structural, optical and electrical characteristics of the β - In_2S_3 films were reported.

In_2S_3 thin films were prepared by sulfurisation of thermally evaporated indium. The sulfurisation was carried out for 45 minutes at various temperatures ranging from 250° C to 600° C. The effect of sulfurisation temperature and time on the growth of single phase In_2S_3 and its electrical and optical properties have been investigated. X-ray diffraction studies showed that sulfurisation of indium films at 300° C and above result in single-phase beta-In_2S_3. Low sulfurisation temperature required prolonged annealing after the sulfurisation to obtain single phase β-In_2S_3. The band gaps of the prepared samples were found to increase with the sulfurising temperature upto 400°C and become a constant (~ 2.3eV) for sulfurising temperature above 400°C.

Chapter 4 deals with the preparation of copper indium selenide. $CuInSe_2$ thin films were made by two-stage process consisting of the thermal evaporation of metallic bilayers followed by selenization. In this method, the Cu-In precursors were first prepared by thermal evaporation of In followed by Cu on to glass substrate keeping the substrates at room temperature and its subsequent annealing in vacuum at 153°C for 2 hours to yield $Cu_{11}In_9$ precursors. In the second stage, the precursors were removed from vacuum and exposed to an atmosphere of selenium in a horizontal quartz tube provided with a specially designed furnace, which allowed rapid heating and cooling of samples. N_2 was used as the carrier gas. A systematic study was conducted varying the duration of selenization and the selenization temperature. A direct band gap of 1.05 eV obtained for the $CuInSe_2$ thin films prepared by selenizing at 350°C for 3 hours.

The information gained from the above studies were used to fabricate $CuIn(S_{1-x},Se_x)_2$ thin films as absorber layer for thin film solar cells which is reported in detail in Chapter 5. Although $CuInSe_2$ with the direct band gap of 1.05 eV is well studied for fabrication of thin film solar cell devices, a band gap of above 1.2-1.3 eV is considered optimal for maximizing conversion efficiencies.

Two thermal profiles were used to study the incorporation of sulfur to increase the band gap of $CuInSe_2$ thin films. The thermal profiles were, a) the prepared $CuInSe_2$ thin films (CIS) were annealed in sulfur atmosphere for different duration (post sulfurisation) and b) the sulfur was passed through the reaction vessel during the selenization (co chalcogenisation). From the study it was observed that when the $CuInSe_2$ prepared by two stage process were post sulfurised, the sulfur may be occupying the interstitial positions or forming a $CuInS_2$ phase along with $CuInSe_2$ phase. The present study shows that the sulfurisation of $CuInSe_2$ is not a feasible technique for

the production of $CuIn(Se_{1-x},S_x)_2$ film. The co-chalcogenisation process of Cu/In precursors resulted in $CuIn(Se_{1-x},S_x)_2$ thin films. A band gap of 1.38 eV, which is more close to the band gap of $CuInS_2$, obtained for the $CuIn(Se_{1-x},S_x)_2$.

The sixth and final chapter is about the trials those have been carried out in the laboratory to fabricate $Mo/CuInS_2/CdS/ZnO$ heterojunction. Heterojunction is formed by p-type $CuInS_2$ prepared by two-stage process and n-type CdS buffer layer by CBD. The device was completed by depositing a window layer of high resistive ZnO followed by highly conducting ZnO:Al by RF magnetron sputtering. Even though the open circuit voltage and fill factor of Mo/CIS/ CdS/ZnO/ZnO:Al junction were comparable to the reported values, the efficiency of was very low, which was due to the very low short circuit current. This could be due to differences in spectral absorption in window material. We also tried to fabricate a hybrid solar cell using the semiconductor layers we optimised in our laboratory. The polymer for the fabrication of cell used was poly aniline. Poly aniline (PANI) was made into solution by adding cyclohexanon. A drop of much diluted liquid form of PANI was solution casted on n-type In_2S_3 prepared on ITO coated. Silver was painted as electrodes. The cell structure was $ITO/In_2S_3/PANI/Ag$. Though the cell showed only poor junction behaviour, we hope a better efficiency cell by improving the characteristics of n-type layer and polymer layer. Photovoltaic characteristics are mainly controlled by the electrical properties of the polymer film which depend strongly on the synthesis conditions. So trials can be done using the polymer layers prepared by new coating methods like spin coating etc.

The work presented in this thesis has been published in the form of following papers.

Publications relating to the work presented in this Thesis

1. Growth of $CuInS_2$ thin films by sulphurisation of Cu-In alloys, Aldrin Antony, Asha A.S., **Rahana Yoosuf**, Manoj R., M.K.Jayaraj, Solar Energy Materials and Solar Cells 81 (2004) 407.
2. β-In_2S_3 Thin Films Prepared by The Sulphurisation of Evaporated Indium Films, **Rahana Yoosuf**, **Rahana Yoosuf**, Jerome K. C, Aldrin Antony, Manoj R. and Jayaraj M. K., Materials, Active Devices and Optical Amplifiers, Proc. SPIE Int. Conf. APOC 2003, Wuhan, China, 5280 (2004) 669.
3. Optical and photoelectrical properties of β-In_2S_3 thin films prepared by two stage process, **Rahana Yoosuf**, M.K.Jayaraj , Solar energy materials and solar cells 89(2005) 94
4. Study on Sulfur Diffusion in $CuIn(Se_{1-X}S_x)_2$ Thin Films Using Two Thermal Profiles, **Rahana Yoosuf**, M.K.Jayaraj, Thin Solid Films, 515(15), (2007) 6188.

Papers in International Conferences

1. Growth of $CuInSe_2$ Thin Films By Two-Stage Process **Rahana Yoosuf**, Jincy Jose, R. Ratheesh Kumar, K. Rajeev Kumar, M.K.Jayaraj International confernce on Optoelectronic Materials and Thin films for Advanced Technology (OMTAT 2005), (Kochi, India, October 2005)
2. $CuInS_2$/CdS Solar cell with the Absorber Layer Prepared by Sulphurisation Technique, A.S. Asha, **Rahana Yoosuf**, G.Sukesh, Aldrin Antony and M.K. Jayaraj, 2nd International Conf. on Electrochemical Power Systems (Hyderabad, India, December 2004)
3. Study on Sulfur Diffusion in $CuIn(Se_{1-X}S_x)_2$ Thin Films Using Two Thermal Profiles, **Rahana Yoosuf**, M.K.Jayaraj, The E-MRS 2006 Spring Meeting (E-MRS - IUMRS - ICEM 06) (Nice, France, May 2006)

Papers Presented in National Conferences

1. Improved Adhesion of Copper Indium Sulphide by Gallium Incorporation Asha A. S., **Rahana Yoosuf**, Sukesh G, M. K. Jayaraj, *DAE Solid State Physics Symposium,* India,Vol 49 (2004),p768
2. Growth of Single Phase In_2S_3 Films by Chalcogenisation of Metallic Indium Films, **Rahana Yoosuf**, Aldrin Antony, Manoj R, Mini Krishna, Nisha M and M.K.Jayaraj, *DAE Solid State Physics Symposium,* India,Vol 46 (2003) p.771
3. Preparation and characterization of single phase $CuInS_2$ films by two stage process, Aldrin Antony, M.Gafoor, Asha.A.S, **Rahana Yoosuf** and M.K.Jayaraj, Proc. DAE Solid State Physics Symposium, Chandigarh, India, Vol 45 (2002) p.475.

Chapter 1

Development and Fundamentals of Thin Film Solar Cells

1.1 Introduction

The progress of mankind was always intimately related to the availability of energy. The energy needs of man for his sustenance have been increasing at a rapid rate ever since he came on earth. Primitive man gained energy primarily as food. With the passage of time he began to use the fire, wind and water for his energy demands. He started cultivating land for agriculture and training animals to work for him and thus gave a new dimension to the use of energy. The sun was supplying all the energy needs of him either directly of indirectly and he was using only renewable source of energy.

A turning point was the discovery of steam engine (AD 1700), which started the Industrial Revolution. Man began to use a new source of energy, viz coal in large quantities. The fossil fuel era using non renewable sources began and energy now available in a concentrated form. Nuclear energy came on the scene after the Second World War. Nuclear energy provides a significant but a very small amount of the energy requirements of many countries.

Today every country draws its energy needs from a variety of sources which can be broadly classified as commercial and non commercial. The commercial source includes the fossil fuels (coal, oil and natural gas), hydro electric power and nuclear power, while the non commercial sources include wood, animal wastes and agricultural wastes. In an industrialized country like USA, most of the energy needs are met from commercial sources, while developing countries like India; the use of commercial and non commercial sources is equal.

In the early 1970s, the disruption of oil supplies to the industrialized world spurred to serious consideration of another terrestrial power source. In order to meet the energy requirement of world population with average electricity

supplies of 1 kW capacity per head at present, an average of some 100 GW of new capacity would have to be installed each year. For several reasons neither fossil fuels nor nuclear energy could supply more than a fraction of such a large increase in electricity generation. First of all these resources are fast depleting and the fossil fuel era is gradually coming to an end especially oil and natural gas. As well, if fossil fuel were to supply more than a small part of the required capacity it would cause severe environmental damage. They contribute unpredictable and irreversible climate changes in the near future through the emission of carbon dioxide [1]. The use of nuclear energy on even a fraction of this scale would also have severe environmental consequences and, in view of the continuing political and religious conflicts around the world, would seem likely to lead to widespread proliferation of nuclear weapons.

As an alternative, photovoltaic (PV) power generation has been commenced to receive considerable attention. This trend was reinforced by public controversy over nuclear fission reactors and by a series of accidents in nuclear power stations, especially those of Three Mile Island (in 1979) and Chernobyl (in 1986). Since the beginning of the 1990s, ecological considerations linked with the CO_2/global warming problem have taken over as a main driving force in promoting PV solar energy.

Photovoltaic is the most useful way of utilizing solar energy by directly converting it into electricity. The photovoltaic effect is defined as the generation of an electromotive force as a result of the absorption of ionizing radiation.

Photovoltaic energy not only can help meet the growing worldwide demand for electricity, but it can do so without incurring the high economic and environmental costs of burning fossil fuels and installing power lines. It is the most attractive non conventional energy source of proven reliability from

the micro to the mega watt level. PV technology needed only a simple solid state device for direct room temperature conversion of abundant solar light into electricity. Energy conversion devices which are used to convert sun light to electricity by the use of the photovoltaic effect are called solar cells. They are pollution free hence environment friendly. There are no moving parts. And if the device is correctly encapsulated against the environment, there is nothing to wear out. Photovoltaic systems are modular, and so their electrical power output can be engineered for virtually any application, from low-powered consumer uses-wristwatches, calculators and small battery chargers-to energy-significant requirements such as generating power at electric utility central stations.

The nations especially poor and developing nations with limited conventional power sources, particularly in remote areas, are increasingly turning into PV power for enhancing their development index. Now about 2 GW of solar cells are being used worldwide in a variety of applications, ranging from MW of stand alone /grid connected power stations to several MW of low power electronic devices.

1.2 Outline of Development of Solar Cell

The invention of the p-n junction in 1949 formed the basis of solar cells. The discovery of the photovoltaic effect dates back to 1839 when French physicist Edmond Becquerel found a photo voltage between electrodes in electrolyte solutions [2] while studying the behaviour of solids in electrolytes. He observed that a small voltage and current were produced when metal plates immersed in an electrolyte were exposed to sun light. In 1877 Adams and Smith discovered a similar effect in selenium which is still used today in exposure meters for photography [3]. Later, cuprous oxide also showed a significant light dependent voltage [4]. The technical development

began with the first practical solar cell, diffused silicon p-n junction, developed at Bell Telephone Laboratories by Chapin, Fuller and Pearson in 1954 [5]. Since then the science and technology of PV devices and systems have undergone revolutionary evolutions.

Almost simultaneously, p-Cu_xS/n-CdS was emerged out as a cheaper alternative to silicon solar cell. The photovoltaic effect in Cu-CdS system was discovered by Raynolds *et al* in 1954 [6]. The first thin film Cu_2S/CdS cell [7] was based on rather simple and cheap technology known as clevite process [8] in which several μm thick CdS film was deposited on to a metallized plastic substrate, then an acid etch of the CdS film followed by immersion in hot cuprous chloride solution for few seconds to topotaxially convert the CdS surface to Cu_2S. For a period of almost 20 years this photovoltaic system was the only all –thin film cell available.

At first the research works on PV power technology was mainly aimed on space applications. The builders of space craft required an energy source that was reliable, long lasting and required no maintenance. Solar cells, however, are an ideal choice for this application for they are reliable, maintenance-free and their energy source-sunlight is abundant and virtually everlasting. In 1958, the first practical solar cells were developed for space applications. The satellite Vanguard I was launched in 1958, with six small silicon cell panels, providing about 5 mW of power. More than 1000 satellites using solar cells were utilized during the 1960s and 1970s.

In the middle of 1970s the efforts were made to use the solar cells for terrestrial applications. Since 1975 most of the solar cell market is aimed on the power requirements on earth, although they remain the dominant source of power for space application.

The past two decades have seen substantial progress in the field of PV modules: commercial prices of modules have shown a sustained average reduction of 7.5% per year; during the same time, the worldwide production of modules has increased on average by 18% per year. A solar cell powered plane demonstrated a transcontinental flight across the United States.

Although in PV market can be expected to keep on progressing in the near future, it will take many decades before PV modules can substantially contribute to electricity generation. The reduction in PV module cost progresses with the increase of production, but the world is rapidly reaching a stage where a further decrease in cost is conditional on the global availability of raw materials. Thus, PV technologies that involve the use of lesser quantities of cheaper and less refined input materials are favoured.

Recently some effort has been made to develop flexible solar cells on polyimide and metal foils. Highest efficiencies of 12.8% and 17.6% have been reported for $CuInGaSe_2$ cells on polyimide [9] and metal foils, [10] respectively. Similarly, flexible CdTe solar cells have got an efficiency of 7.8% on metal [11] and 11% on polyimide [12].

1.3 Fundamental Principles of Solar Cell Devices

A PV system consists of

- Solar cell array
- Load leveller
- Storage system
- Tracking system(if needed)

Though solar cell, which converts sunlight directly into electricity, is only a part, it is the basic component of a PV module. To understand the many aspects of solar cell, it is important to realize the fundamentals of how the devices work. Although photovoltaic cells come in a variety of forms, the

most common structure is a semiconductor material into which a large-area diode, or p-n junction, has been formed. Electrical current is taken from the device through a contact on the front n-region that allows the sunlight to enter the solar cell, and a contact on the back that completes the circuit. Figure 1.1 is a schematic depiction of a rudimentary solar cell that shows the important features.

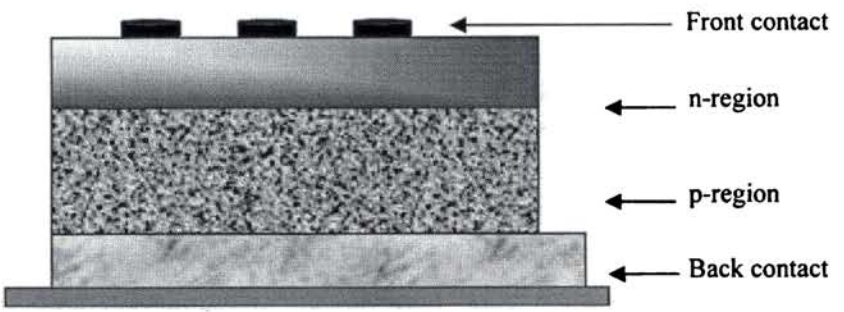

Figure 1.1 The schematic representation of a typical solar cell

In some junctions, a thin insulator film is placed between the two semiconductors or the semiconductor and the metal, thereby forming a semiconductor - insulator - semiconductor or a metal - insulator - semiconductor junction. Moreover, pn-junctions may be classified into homojunctions and heterojunctions according to whether the semiconductor material on one side of the junction is the same as or different from that on the other side. Also liquid-junction solar cells exist where the junction is formed between a semiconductor and a liquid electrolyte.

1.3.1 Electronic Analysis of a pn Junction

The PV effect can be observed in almost any junction of materials that have electrical characteristics. But the best performance has been from cells using semiconductor materials. A solar cell consists of two layers of semiconductor, one p-type and the other n-type, sandwiched together to form

a p-n junction. The fabrication of the p-n junction is the key to successful operation of the photovoltaic device. Before electrical contact is made, the n-type region has an excess of electrons with respect to the p-region and the p-region has an excess of holes with respect to the n-region. After contact, a gradient of concentration of carriers at the junction exist and an equilibrium state is subsequently established. Figure 1.2 shows the diagrammatic formation of a p-n junction.

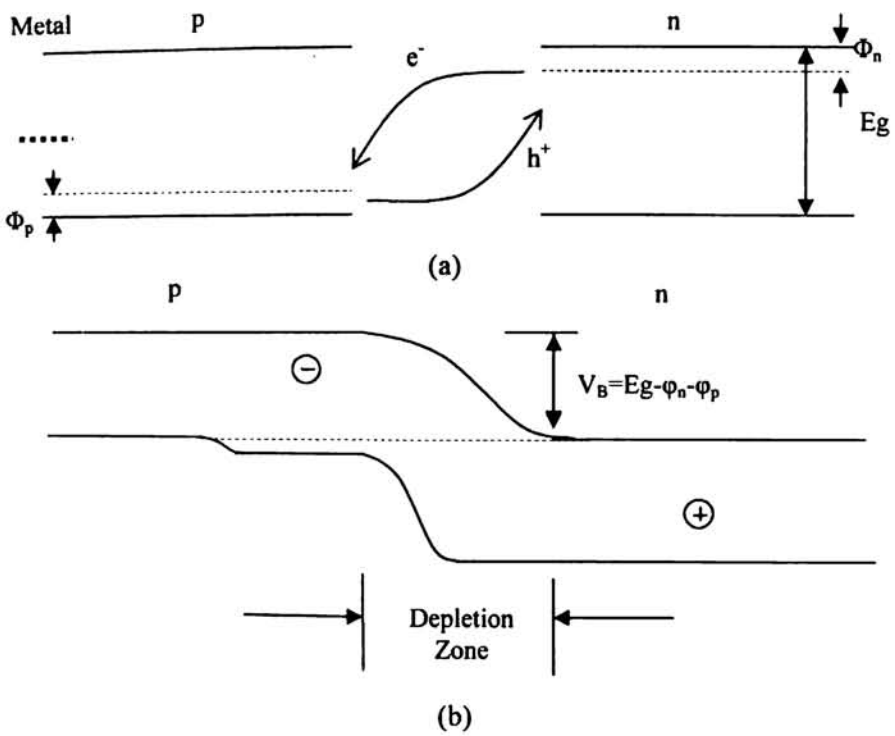

Figure 1.2: a) Diagrammatic formation of a p-n junction. Dotted lines indicate the Fermi levels b) energy level diagram of a p-n junction with ohmic contacts.

When particles of light (photons) are absorbed by the semiconductor, they transfer their energy to some of the semiconductor's electrons, which are then able to move about through the material. For each such negatively charged electron, a corresponding mobile positive charge, called a hole, is

created. In an ordinary semiconductor, these electrons and holes recombine after a short time and their energy is wasted as heat. In a solar cell, the electrons and holes near the pn junction are swept across in opposite directions by the action of the electric field and others diffuse towards the junction to replace them. This separation of charge induces a voltage across the device. By connecting the device to an external circuit, the electrons are able to flow and this flow of electrons is called electricity [13]. The electricity produced by a solar cell is direct current and can be used as such, converted into alternating current, or stored for later use.

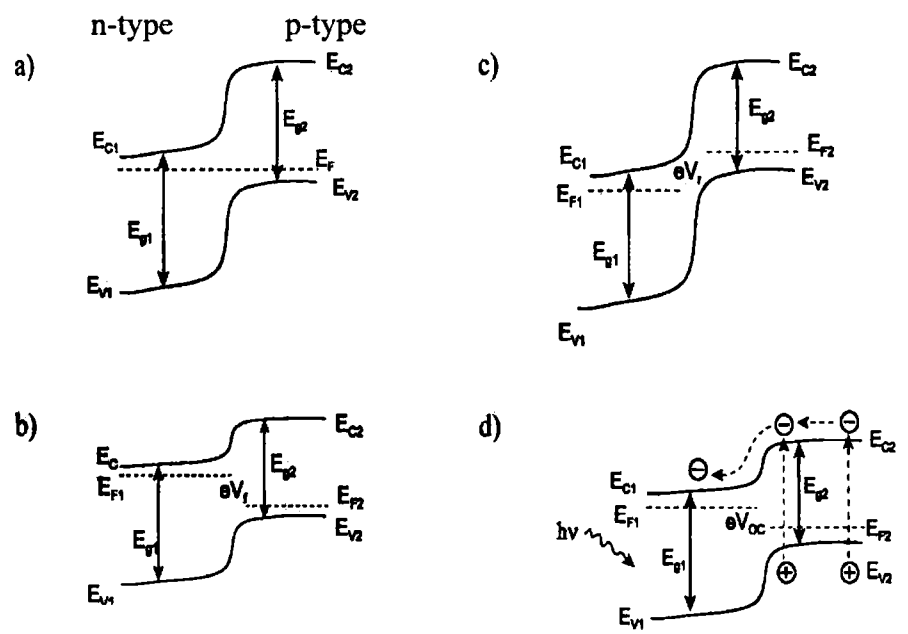

Figure 1.3 Energy band diagram of a p-n heterojunction solar cell. (a) at thermal equilibrium in dark (b) under a forward bias (c) under a reverse bias and (d) under illumination, open circuit conditions.

Figure 1.3 presents a schematic energy band diagram of a pn hetero junction solar cell (a) at thermal equilibrium in dark, (b) under a forward bias, (c) under a reverse bias, and (d) under illumination, open circuit conditions.

Numbers 1 and 2 in figure 1.3 refer to an n-type and a p-type semiconductor, respectively, and E_{ci} and E_{vi} to their conduction and valence bands, respectively. E_{gi} and E_{Fi} are the band gaps and Fermi levels, respectively. In the absence of an applied potential, the Fermi levels of the semiconductors coincide, and there is no current flow. This state is shown in figure1.3a. When a forward bias V_f is applied the Fermi level of the n-type semiconductor is shifted upwards and that of the p-type semiconductor downwards, thus lowering the potential energy barrier of the junction, and facilitating the current flow across it (Fig. 1.3b). The reverse bias V_r (Fig.1.3c) increases the potential barrier and thus impedes the current flow. Illumination of the junction (Fig.1.3d) creates electron-hole pairs, causing an increase in the minority carrier concentration. The potential energy barrier decreases, allowing the current to flow, and an open circuit voltage V_{oc} (photo voltage under open circuit conditions) is generated across the junction.

1.3.2 Power output and Performance efficiency

In its most basic form a solar cell is described by the Shockley model of p-n junction with a current density pre factor J_0 [14].

The current voltage characteristic is given by

$$J_L = J_0[\exp(\frac{Ve}{kT}) - 1] \qquad 1.1$$

Where V is the voltage across the junction and T is the absolute temperature. J_0 is the saturation current or dark current obtained.

When light falls on the junction, electron-hole pairs are created at a constant rate providing an electrical current flow across the junction. The net current is the difference between the normal diode current and light generated current J_L.

An ideal solar cell can be represented by a current source connected in parallel with a rectifying diode as shown in figure 1.4.

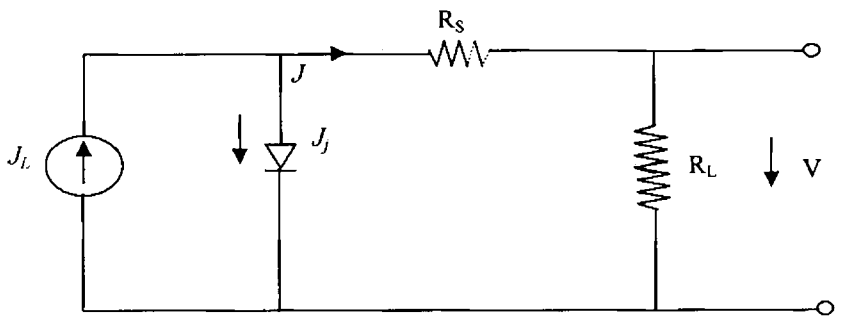

Figure 1.4 Idealized equivalent circuit of a solar cell.

The solar cell may also contain the internal resistance R_S which is mainly due to the high sheer resistance of the diffused layer which is in series with the junction. The light generated current acts as a constant current source supplying the current to either the junction or useful load depending on the junction characteristics and the value of the external load resistance [15].

The net current J is given by

$$J = J_L - J_j = J_0\{\exp[(V + JR_s)e/kT] - 1\} \qquad 1.2$$

The internal voltage drop in a cell can be minimized and for ideal solar cell R_s may be assumed to be zero. The corresponding figure of current voltage characteristics is given in the figure 1.5.

From the figure 1.5 it can be seen that the curve passes through the fourth quadrant so surely the device is power generating. Figure 1.6 is a more clear diagram of the forth quadrant obtained with the rotation of current axis by 180^0 around the voltage axis.

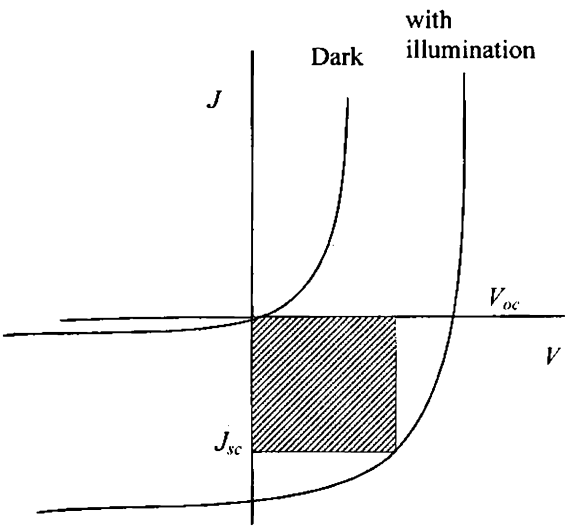

Figure 1.5 Current voltage characteristics of a junction diode in the dark and under illumination

V_{oc} is the maximum voltage obtainable at the load under open circuit conditions of the diode, and J_{sc} is the maximum current through load under short circuit conditions.

In the ideal case, the short circuit current J_{sc} is equal to the photo generated current J_L, and the open circuit voltage V_{oc} is given by

$$V_{OC} = \frac{kT}{e} \ln\left(\frac{J_L}{J_o} + 1\right) \qquad 1.3$$

Since $J_L \gg J_o$

$$V_{OC} = \frac{kt}{e} \ln \frac{J_L}{J_o} \qquad 1.4$$

The power output from the device can be maximised by maximising the area under the curve in figure 1.6.ie, maximising the product $V_{oc} \times J_{sc}$

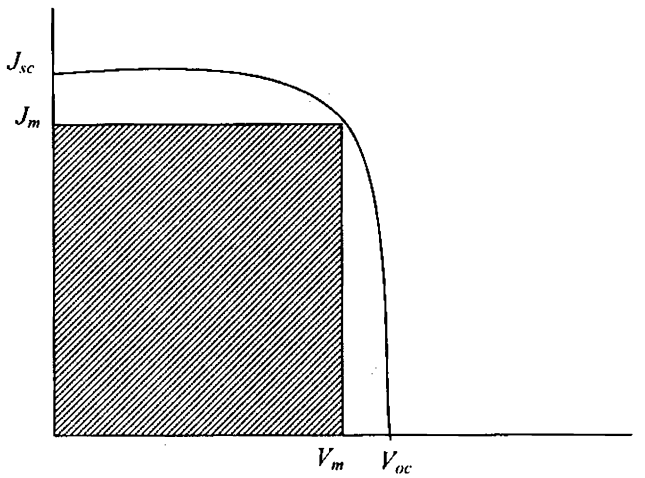

Figure 1.6 I-V characteristics of an illuminated solar cell in the forth quadrant

The cell generates maximum power P_{out} at maximum voltage V_m and maximum current J_m.

$$P_{out} = V_m \times J_m \tag{1.5}$$

The fill factor FF is

$$FF = \frac{J_m V_m}{J_{sc} V_{oc}} = \frac{P_{out}}{J_{sc} V_{oc}} \tag{1.6}$$

The fill factor is used as a measure of how well a junction was made in a cell and how low the series resistance has been made. For practical photovoltaic cells, the fill factor ranges from approximately 0.70 to 0.85.

The conversion efficiency η is simply Pout/Pin. It is considered as the figure of merit for solar cell performance

$$\eta = \frac{P_{out}}{P_{in}} \tag{1.7}$$

$$P_{out} = V_m J_m = FF V_{oc} J_{sc} \tag{1.8}$$

Hence

$$\eta = \frac{FFV_{oc}J_{sc}}{P_{in}} \qquad 1.9$$

The input power P_{in} is the input solar irradiance. This quantity is best measured using a calibrated detector with a similar spectral sensitivity as the device [16].

Because the short-circuit current and open-circuit voltage vary in opposite directions as a function of band gap (I_{sc} decreases with increasing Eg, and V_{oc} increases with increasing Eg) and the fill factor follows V_{oc}, the efficiency will exhibit a maximum value, occurring at a band gap of approximately 1.5 eV. Using reasonable device parameters for single-junction solar cells, one calculates a maximum theoretical efficiency of 29% [17].

For both theoretical and practical reasons, not all of the solar radiation energy falling on a solar cell can be converted into electrical energy. Weak low frequency photons do not possesses sufficient energy to dislodge electrons. Strong, high frequency photons are too energetic, and although they dislodge electrons, some of their energy is left over unused. So, only about 45% of the energy in the solar radiation at sea level is capable of producing electrons and holes.

However actual efficiencies are again much lower due to electrical resistance of the semiconductor materials, the recombination of electron hole pairs and other loss modes such as a part of solar energy is reflected back to the sky, absorbed by non photovoltaic surfaces, or converted to heat. With modules and arrays there are additional losses that result from the mismatch between individual cells in a module and between modules in an array. Thus the best single crystal cells yield efficiencies of about 16 to 20%.

1.4 Complexity of Manufacturing

The cost and complexity of manufacturing may vary across these materials and device structures based on many factors, including deposition in a vacuum environment, amount and type of material utilized, number of steps involved, need to move cells into different deposition chambers or processing steps, and others.

The important steps leading to a the cost-effective manufacture of thin film solar modules are

- Quantitative analysis of processing steps for commercial scale equipment design and operation.
- Device characterization relating the device performance to materials properties and processing conditions.
- Development of alloy materials with different band gap to allow improved device structures for stability and compatibility with module design.
- Development of improved window/heterojunction layers and contacts to improve device performance and reliability.
- Evaluation of cell stability with respect to illumination temperature.

1.5 Types of Solar Cell

Several different semiconductor materials are used to make the layers in different types of solar cells, and each material has its benefits and drawbacks. The first requirement of a material to be suitable for solar cell application is a band gap matching to solar spectrum. The band gap should be between 1.1 and 1.7 eV. The material must also have high motilities and lifetime of charge carriers. Other requirements are (1); direct band structure (2); consisting of readily availability, non-toxicity (3) easy, reproducible

deposition technique, suitable for large area production; (4) good photovoltaic conversion efficiency; and (5) long-term stability.

These conditions are met by many II-VI, III-V, I-III-VI_2 and II-IV-V_2 compounds and silicon. Depending on the material used solar cells can be categorized into three main groups:

- Si- Single crystalline, polycrystalline and amorphous silicon
- III-V Group single crystals
- Polycrystalline thin films

1.5.1 Silicon Solar Cells

i) Single-Crystalline Silicon

Currently, the most widely used semiconductor in solar cells is single-crystal silicon. The advantages of silicon are its mature processing technology, the large abundance of it in the crust of earth (usually obtained from sand SiO_2), and its nontoxicity, which is important factor thinking from the environmental perspective. Today the best single crystal Si solar cells have reached an efficiency of 24.7% [18]. Compared with theoretical maximum value of 30% this performance achievement can be attributed to the substantial understanding of the material properties and improved design of the solar cell. Commercial silicon solar cell modules are available with conversion efficiencies as high as 18%. The major disadvantages of single-crystalline silicon solar cells are the requirements of high grade material and the problems associated with producing single crystals over large areas. Because of the cost involved in producing the bulk material, cells produced by single crystal silicon are prohibitively expensive. But the smallest scale or most specialised applications (such as on calculators and satellites) still rely on single crystal silicon technology. Higher efficiencies have been produced by more elaborate constructions (e.g. multi-quantum wells), but this

advantage has always been more than offset by the resultant increase in cost. Recently, there have been some imaginative attempts to make single crystal ribbon silicon, which is lower in cost than high quality single crystals. However, to date the efficiencies of these apparently low-cost materials have been relatively low.

ii) **Polycrystalline Silicon**

The production of polycrystalline cells is more cost-effective than single-crystalline silicon. Silicon is poured into blocks that are subsequently sawed into plates. During solidification of the material, crystal structures of varying sizes are formed hence the polycrystalline material has a large number of crystallites. These crystallites introduce boundaries and these boundaries obstruct the flow of electrons and encourage them to recombine with holes thereby reducing the power output of the cell [19]. Large grain sizes are required to reduce the negative influence caused by grain boundaries. Another disadvantage is that the cast material must be sliced, however, leading to a loss of about half of the material. Although polycrystalline silicon materials are less efficient than crystalline silicon, they are commercially viable since they are sufficiently cheaper. So research works are going on new innovative ways of minimizing the effects of grain boundaries and on improving the sawing techniques such as multiple-wire saws continue to reduce the loss in producing thinner wafers.

iii) Amorphous Silicon

Amorphous Silicon (a-Si) PV modules were the first thin-film PV modules commercially produced and are presently the only thin-film technology that has had an impact on the overall PV markets. The PV effect in a-Si was observed in 1974 using films deposited by the DC glow discharge of silane (SiH_4) and in both Schottky-barrier and p-i-n device structure [20]. It has a

much higher absorption coefficient over wavelengths of importance in the solar spectrum than crystalline silicon. As a result a much thinner layer of amorphous silicon is sufficient to absorb solar spectrum. The cells are made from layers having a thickness less than 1 μm [15]. However, the efficiencies of these modules have not yet reached levels that were predicted in the 1980's. To a significant degree this is due to the intrinsic degradation of a-Si under illumination. The amount of light-induced degradation can be limited to 20% in modules operating under outdoor conditions. The use of multi-band gap multijunction devices and the use of light-trapping appear to be the most powerful device design techniques to improve stabilized device performance. Presently, cells have stabilized efficiencies of 12.7% and modules of 1 square foot have stabilized efficiencies of over 10% [21].

1.5.2 Group III-V Technology

Photovoltaic technologies based on group III and V elements show very high efficiencies under either normal or concentrated sunlight. Although expensive, their cost can be compensated for by using concentrators, which increase the energy conversion efficiency under higher illumination. Concentrators focus light from a large area to a small area thereby increasing illumination to many times the terrestrial sunlight. The most important solar cells in this category are gallium arsenide (GaAs) and indium phosphide (InP).

i) Gallium Arsenide

Gallium Arsenide (GaAs), a compound semiconductor has been developing synergistically with its use in light emitting diodes, lasers, and other optical devices besides solar cells. It has a direct band gap of 1.43 eV, nearly ideal for single junction solar cells. The absorption coefficient of GaAs is relatively high and causes sufficient absorption of photons in only a few microns of material. It is also very resistant to radiation damage. This, along

with its high efficiency, makes GaAs very desirable for space applications. The most efficient solar cell to date has been based on this material and cells of 25.1% efficiency have already been confirmed [22]. When used in concentrator application, the efficiency increases to 27.6% [23]. The highest theoretical efficiency of 39% is also reported for GaAs solar cells [24] and it can maintain higher theoretical efficiencies at high temperatures. For mass production of GaAs solar cells, gallium element availability and the toxic nature of the arsenic are considered as major limitations of this technology. However its demonstrated high efficiency and its tolerance of higher temperatures make it very attractive for concentration system.

ii) Indium Phosphide

Indium Phosphide (InP) has a direct band gap of 1.34 eV, close to the optimum for solar energy conversion. InP crystals are grown by the Czochraski method at high pressures or by using a liquid encapsulation technique to preserve the stoichiometry. A 21.9% efficient InP crystalline solar cell has already been reported [25]. Homojunction cells are limited by surface recombination, but heterojunctions with good lattice matching and hence buried homojunction or hetero faced junctions are more efficient [26]. In concentration cells, the efficiency was increased to 24.3% [27]. A 31.8% multijunction InP /GaInAs cell has been achieved by Wanless *et al* [28]. The major limitation of this technology is the high cost due to limited resources for indium and purification of phosphorous.

Advantage of III-V materials is that they are less prone to radiation damage and the higher theoretical efficiencies are maintained at high temperatures. The major practical difficulty encountered with these materials is associated with their photon absorption characteristics. If photons have the correct energy to be absorbed, they will be absorbed in a narrow region very close to

the exposed surface. This causes a high internal resistance and consequently increases the resistance loss effect.

1.5.3 Polycrystalline Thin Films

Another promising technology is polycrystalline thin films. Thin film solar cells have several striking advantages over crystalline Si (c-Si) and III-V solar cells because they are not produced from single crystal material. Since they require less material to generate a given amount of power, they make attractive alternatives to single crystalline devices. Among the various kind of thin film solar cell materials, copper indium diselenide ($CuInSe_2$), copper indium disulfide ($CuInS_2$), and copper gallium diselenide ($CuGaSe_2$), are highly appealing since their band gaps are near optimum for absorption of the solar spectrum in space (AM0) and on the surface of Earth (AM1.5).

1.6 Thin Film Photovoltaics

Right from the beginning it has been recognized that cheaper solar cells can be produced only if cheaper and more sparingly used materials and lower cost technologies are utilized. One of the most promising strategies for lowering PV costs is the use of thin film technologies in which the PV materials are deposited onto inexpensive large area substrates such as window glass and flexible substrates. A more economical use of the material would result if a thin film of material could be utilized. The conversion efficiency may be reduced but this would be more than balanced by the gain in power to weight ratio. There is thus a considerable stimulus for the development of commercially successful thin film solar cells.

The development of solar cells entirely based on thin film processes started with the Cu_2S/CdS cell [29]. Even though several pilot productions came into operation but Cu_2S/CdS type solar cells displayed severe stability problems. It was noticed that the degradation of the cells due to the inherent

instability of Cu_2S could not be avoided. So their development was discontinued by the 1980s [30].

A search for more suitable thin film materials revealed copper indium sulphide, cadmium telluride (CdTe) as well as copper indium diselenide ($CuInSe_2$) and its related alloys for the production of low cost thin film solar cells and they have been established as the most promising candidates for the next generation of solar cells.

CdTe is one of the most suitable solar cell materials with a band gap of 1.5 eV at room temperature, which matches the solar spectrum perfectly [31]. This semiconductor has been receiving great attention as a photovoltaic material since 1960s due to their high specific power, i.e. power per weight, on thin and flexible substrates and excellent radiation hardness which make them a promising material for space application [32]. A maximum efficiency 16.5% has been reported for CdTe based small area laboratory devices [33]. Despite of its potential, the utilization is limited by the difficulty of controlling the material properties. It is also difficult to make electrical contact to CdTe, especially to the p-type material.

To respond to the potential demand in the terrestrial power generation market, which required module efficiencies in excess of 15% and low cost of fabrication, research and development efforts shifted gradually to other polycrystalline thin film systems like copper indium selenide/sulfide based solar cells. Polycrystalline thin film solar cells such as $CuInSe_2$ (CIS), Cu (In, Ga)Se_2 (CIGS) compound semiconductors are important for terrestrial applications because of their high efficiency, long-term stable performance and potential for low-cost production. Because of the high absorption coefficient ($\sim 10^5\ cm^{-1}$) a thin layer of ~2 μm is sufficient to absorb the useful part of the spectrum. During the past thirty years the research and

development efforts resulted in a conversion efficiency improvements from 6% to 19.2% [38] for CIS based solar cells.

1.7 I-III-VI_2 Thin Films

A photovoltaic device has to perform two basic functions. The first function is to absorb the incident photons with energy greater than the band gap energy of the material in order to generate electron-hole pairs. The second function is to separate these electron hole pairs in space in order for a current to flow through an external circuit for utilization. So the parameter that depends most strongly on the choice of semiconductor material to fabricate a

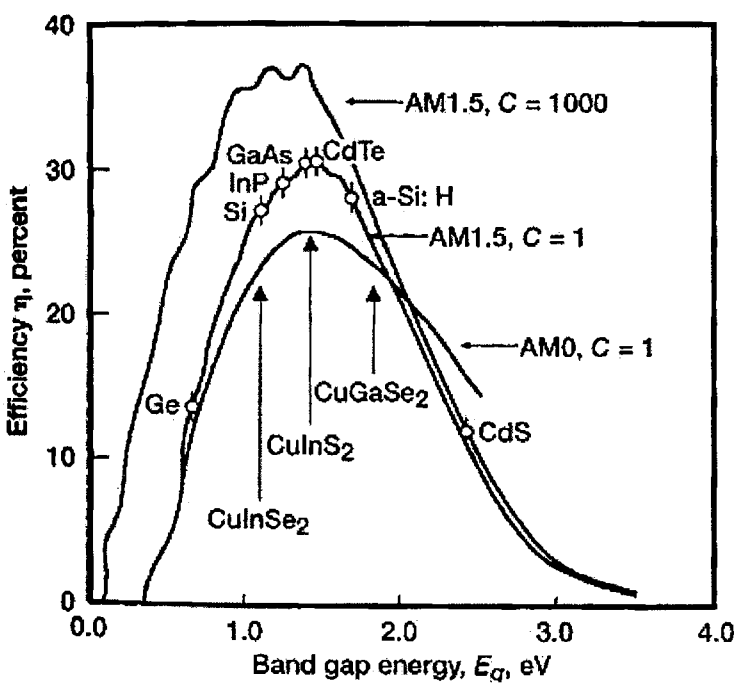

Fig 1.7 Ideal solar cell efficiency as a function of the band gap energy for the spectral distribution AM0 and AM1.5 with a power density of 1sun, and for AM1.5 with 1000 sun.

PV device is the band gap energy. The increase in the band gap will cause a decrease in the saturation current of the solar cell pn junction and as a result

the open circuit voltage increases. Therefore a maximum in the efficiency exists.

Figure 1.7 shows the theoretical efficiencies as a function of band gap [34]. It shows that the optimum band gap occurs between 1.4 and 1.6. The band gap value of the $CuInSe_2$ films can be increased by alloying with Ga to obtain the optimum band gap needed for the high efficiency. $CuInS_2$ have a band gap of 1.53 eV is closely matching the requirements to yield high efficiency.Table 1.1 shows the highest efficiencies produced by the thin film laboratory-scale solar cells of $CuInSe_2$ and its alloys. $CuInSe_2$ based solar cell devices have demonstrated good thermal, environment and electrical stability. Currently, these polycrystalline compound semiconductor solar cells are attracting considerable interest for space applications, because it is proven from the proton and electron irradiation tests that CIS solar cells have proven that their stability against particle irradiations superior to Si or III–V solar cells [35].

Device type	**Area (cm^2)**	**% Efficiency (η)**
$CuInSe_2$/CdS/ZnO	0.263	14.8
Cu(In,Ga)Se_2/CdS/ZnO	0.408	19.2
$CuGaSe_2$/CdS/ZnO	0.38	9.3
$CuInS_2$/CdS/ZnO	0.38	12

Table 1.1 Reported performances of laboratory-scale solar cells based on $CuInSe_2$ and its alloys.

1.8 CIS Based Solar Cells

Copper indium diselenide (CIS) is a more recent thin film PV material and it is the most promising one among the chalcopyrite materials. Conversion efficiencies of between 12 and 15% have already been achieved for devices based on a $CuInSe_2$/CdS/ZnO heterojunction [36]. All thin film CdS/

$CuInSe_2$ cells were fabricated by vacuum evaporation with an efficiency of 6.6% in 1975 by Kazmerski *et al.* [37]. All thin film homojunctions of $CuInS_2$ and $CuInSe_2$ were also fabricated by same group by varying the flux of S or Se during vacuum evaporation [38]. A step forward was marked next by the report of CdS/ $CuInSe_2$ heterojunction with an efficiency of 10% by vacuum evaporation using three source methods. It approached the initial single crystal device in efficiency, by achieving a major increase in the short circuit current to 39 mA/cm^2 [39].

By 1996, several improvement were made including increasing the crystallite size by varying the concentration of copper as the film is deposited with a copper rich layer at bottom, and the introduction of gallium or sulfur to make a larger band gap. These efforts have led to 0.4 cm^2 cell with an efficiency of 17.7% [40]. CIS modules currently on the market reach stable efficiencies of more than 11%.

For large scale production of $CuInSe_2$ solar cells, the availability of indium (In) is an issue. Although it appears that there is a sufficient abundance of In to meet the growing demand of an effective solar cell market, there could be a conflict between supply and demand. Requirements of large amounts of In may be reduced by using thinner layers of $CuInSe_2$ or by using $CuInGaSe_2$ in which about 25% of the In is replaced by Ga.

The introduction of Ga also increases the relatively low band gap 1.04 eV of $CuInSe_2$ to better match the solar spectrum. The flexibility of the material system allows in principle the band gap variation from 1.04 eV of $CuInSe_2$ via 1.53 eV of $CuInS_2$ and 1.68 eV of $CuGaSe_2$ to 2.43 eV of $CuGaS_2$ [41]. Gallium incorporation is also believed to improve adhesion between the CIS and the molybdenum electrical back contact [42] and also increases the open-circuit voltage of the cell. Solar cells based on $CuInSe_2$ have been made at the Institute of Energy Conversion (IEC) and elsewhere with band

gaps of about 1.2 eV through the addition of Ga, leading to efficiencies greater than 15%. $Cu(In,Ga)Se_2$ solar cells yield a conversion efficiencies of 19.2% [33].

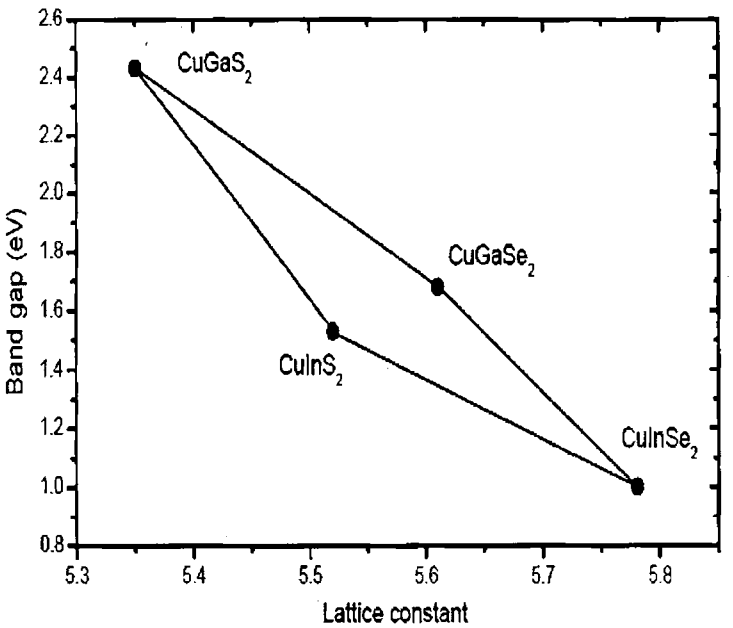

Figure 1.8 Band gap versus lattice constant for various chalcopyrite semiconductors.

There have been attempts to modify the band gap of $CuInSe_2$ to better suit the solar spectrum also alloying of $CuInSe_2$ with $CuInS_2$, i.e. the formation of the quaternary alloy $CuIn(Se_{1-x}S_x)_2$ [43]. $CuInS_2$ has a band gap of about 1.55 eV and the band gap of $CuIn(Se1\text{-}x,Sx)_2$ ranges from 1.0 to 1.55 eV, depending on the amount of S in the film. The structural and optical properties of such films are gaining importance in view of the intensive interest in the opto-electronic field. Significant increases in device performance has been reported [44] with the explanation of reduction of the density of deep trap states in the absorber film which reduces recombination in the space charge region.

Recent trends in $CuInSe_2$ research and development focus on these high band gap chalcopyrite alloys. The high flexibility in the optical band gap of these materials is illustrated in figure 1.8.

1.9 Configurations for CIS Solar Cells

1.9.1 Substrate Solar Cells

Thin film solar cells with CIS absorber layers are mostly grown in the substrate configuration. A schematic representation of a substrate solar cell is presented in figure 1.9.

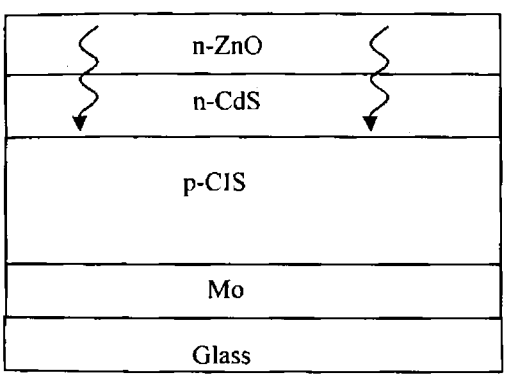

Figure 1.9 Typical Structure of a substrate $CuInSe_2$ based solar cells

The growth sequence starts with the deposition of a metallic contact on the glass substrate. The commonly used substrate for this device is molybdenum coated soda-lime glass. The Mo layer acts as the ohmic back contact to the cell and also improves the adhesion between the glass substrates and the active layers. Also Mo does not chemically interfere with the growing film at the processing temperatures [45]. If the Mo layer is deposited under sub-optimized conditions, it exhibits either tensile or compression stresses which contribute to the commonly observed peeling of $CuInSe_2$ films at the $Mo/CuInSe_2$ interfaces.

The second step is the growth of the p-type absorber layer. This can be done by co evaporation from elemental sources or by the deposition of metal precursor layers and subsequent selenization. The best performance is achieved if the heterostructure is continued with CdS buffer layer grown by a chemical bath process [46]. The CdS buffer layer is lattice and electronically matched to the CIS absorber film. It is also reported that these buffer layers passivate the grain boundaries of the polycrystalline $CuInSe_2$ absorber films, resulting in high open circuit voltages. Alternate materials and deposition methods like In_2S_3 [47], $In(OH)_xS_y$ [48], $(In,Ga)_xSe_y$ [49], and ZnSe [50] have also been resulted in reasonably good efficiency.

Finally, the transparent front contact is deposited. Usually it consists of two layers; one is undoped ZnO for band matching, the second is doped ZnO layer for good conductivity. ZnO is the ideal window material due to its wide band gap (3.2 eV), high temperature stability and the fact that it can be doped in any desired order. The layers are usually grown by sputtering or chemical vapour deposition. The combination of buffer and front contact is frequently referred to as window layer.

The solar cell structure is completed by the evaporation of 1-2 μm thick Al grid contacts onto the ZnO window layer. In order to reduce resistive losses, a 50 nm thick Ni layer can be included between the ZnO window layer and the Al grid contacts. $Cu(In,Ga)Se_2$ solar cells with substrate structure yield conversion efficiencies of up 18.8% [51].

1.9.2 Superstrate Solar Cells

The front wall or superstrate solar cell refers to a configuration where the glass substrate is not only used as mechanical support but also as part of the transparent encapsulation. This configuration is commonly used for solar cells based on CdTe and a-Si absorber layers and was also successfully employed for solar cells with $Cu(In,Ga)Se_2$ absorber layers [52,53]. The

highest reported efficiency of $Cu(In,Ga)Se_2$ superstrate solar cells is 12.8% [54]. An efficiency of 10.2% has been reported for cells with extrinsic Na doping [55].

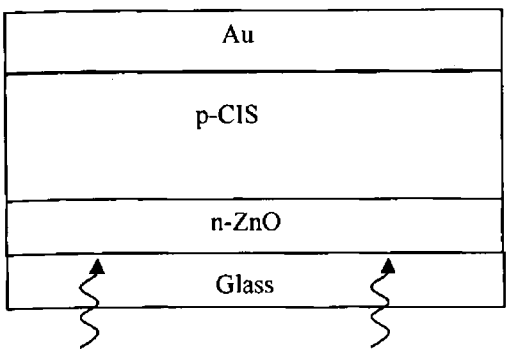

Figure 1.10 Typical Structure of a superstrate $CuInSe_2$ based solar cells

A schematic drawing of the superstrate configuration is shown in figure 1.10. The growth sequence for superstrate solar cells starts with the deposition of the transparent front contact on glass, followed by a ZnO buffer layer and the growth of the absorber layer. Finally, a metal layer is applied for the ohmic back contact. The superstrate configuration offers some technological advantages; the substrate glass acts as reliable encapsulation against environmental impacts and no second glass is needed on the back. Rather, any low cost encapsulation can be applied because it needs not to be transparent. This facilitates production and lowers the overall cost.

1.10. Future of Solar Cells

Recent developments suggest that photovoltaic technology may soon be playing a much larger role in our lives. While efficiencies have been improved, the cost of the solar cells themselves has steadily fallen in recent

years with increasing mass production and should continue to do so over the coming decade.

Advances in nanotechnology have opened new perspectives in low-cost thin film processing. In combination with the established conventional techniques of chalcogenisation these methods allow solar cell production [56] without the requirement of expensive vacuum deposition systems.

The organic photovoltaics which use the advantage of conjugated organic polymers to conduct electricity also offer the possibility of low cost fabrication of large area solar cell. Aside from possible economic advantage, organic solar materials also possess low specific weight and are mechanically flexible.

Development of systems technology and integration of solar cells into building materials such as roof tiles is also reducing the overall system costs and making them more attractive to buyers. Rooftop photovoltaic installations, both by public institutions and by individual citizens, are becoming more and more common worldwide. These changes should have a significant impact on reducing the emission of greenhouse gases and other pollutants, and will take the world one step closer to a cleaner energy future.

1.11 Objective of This Research Work

While the increasing demand for energy creates a boom of PV industry in global market, its widespread use is still hindered by its high costs. Benefiting from the inherent advantages to thin film PV will require breakthroughs in reducing manufacturing costs, primarily by improving yields and increasing throughput. A critical requirement is the accessibility of an easily scalable deposition processes for the active layers in order to reduce process complexity and costs of solar. Attention will therefore be focused on the development of a relatively low cost easily scalable two stage

deposition technique, to produce uniform coatings of thin films on large area substrates. Two-stage process consists of the deposition of Cu-In precursors with industrial growth processes in the first step followed by their sulfurisation/ selenization using H_2S gas/Se vapour. Two stage process has been optimised for producing single phase, p-type $CuInSe_2$, $CuIn(Se_{1-x}S_x)_2$ and n-type In_2S_3 thin films. However, the material quality of the absorber films is critically related to the chalcogenisation parameters (i.e. reaction temperature and duration) and the metallic precursor formation steps. Against this background, the present study systematically quantifies the influence of the above referred to parameters on the material quality of the semiconductor thin films.

References

[1] H. J. Moller, *Semiconductors for Solar Cells*, Artech House Inc., London (1993)1.

[2] A. E. Becquerel and C. R. Hebd Seanc. *Acad. Sci.* **9** (1839) 145.

[3] C. E. Fritts, *Lumiere Electr.* **15** (1985) 226.

[4] W. Schottky, *Z Phys.* **11** (1930) 460.

[5] D. M Chapin, C. S. Fuller and G. L. Pearson, *J. Appl. Phys.*, **25** (1956) 676.

[6] D.C Raynolds, G.Leies, L.L. Antes and R.E. Marburger, *Phys. Rev.* **96** (1954) 533.

[7] K. L. Chopra, P. D. Paulson and V. Dutta, *Prog Photovolt: Res. Appl.* **12** (2004) 69.

[8] P. K. Bhatt, S. R. Das, D. K. Pandya and K. L. Chopra, *Solar Energy Materials* **1** (1979) 215.

[9] A. N. Tiwari, M. Krejci, F.J. Haug and H. Zogg *Prog. in Photovoltaics: Research and Applications* **7** (1999) 393.

[10] J.R Tuttle, A. Szalaj and J. Keane. *Proc. of the 28th IEEE PV Specialists Conference*, Anchorage (2000) 1042.

[11] I. Matulionis, S. Han, J. A. Drayton, K. J. Price and A. D. Compaan, *Proc. of the MRS Spring Meeting*, San Francisco,H8 (2001) 1

[12] A. Romeo, M. Arnold, D. L. Batzner and H. Zogg, *Proc. of PV in Europe from PV Technology to Energy Solutions*, Rome, (2002) 377.

[13] A. Shah, P. Torres, R. Tscharner, N. Wyrsch and H. Keppner, *Science* **285** (1999) 692.

[14] W. Shockley, *Bell System Technical Journal*, **28** (1949) 435.

[15] Shockley and Quieisser, *J. Appl. Phys.* **51** (1961) 4494.

[16] G. P. Smestad, *Optoelectronic of Solar Cells*, SPIE Press, Washington (2002) 41.

[17] H. J. Hovel, *Semiconductors and Semimetals*, Academic Press, New York (1975) 132.

[18] M. A. Green, K. Emery, D. L. King, S. Ifari, and W. Warta, Prog. Photovoltaics Res. Appl. **9** (2001) 49.

[19] R. H. Bube, *Photovoltaic Materials*, Imperial College Press, London (1998)57.

[20] D. E. Carlson, US. *Patent,* 4,064,521(1977).

[21] M.A. Green and K. Emery, *Prog. PV Research and Applications* **1** (1993) 225.

[22] S. M. Vernon, V.E Haven, L. M. Geoffrey and M.M. Sanfacon *Proc.22nd IEEE PV Specialist Conference*, Las Vegas, USA (1991) 353.

[23] R. H. Bube, *Photovoltaic Materials*, Imperial Collage Press, London, (1998) 116.

[24] C. J. Keavney, V. E. Haven and S. M. Vernon, *Proc. 21st IEEE PV Specialists Conference*, Kissiminee, USA (1990) 141.

[25] J. S. Ward, M. W. Wanlass, T. J. Coutts, K. A. Emery and C. R. Osterward, *Pro.22nd IEEE PV Specialist Conference,* Las Vegas, USA, (1991) 365.

[26] V. V. Galavanov, R. M. Kundulkov and D. N. Nasledov, *Sov. Phys. Solid State* **8** (1967) 2723.

[27] M. W. Wanlass, T. J. Coutts, J. S Ward, K. A. Emery, T. A Gessert and C. R. Osterward, *Pro. 21st IEEE PV Specialists Conference*, Kissiminee, USA (1990) 38.

[28] R.W. Birkmire and E. Eser, *Annu. Rev. Mater. Sci.* **27** (1997) 625.

[29] H. W. Schock and F. Pfister, *Proc. of the 16th European PV Conference,* Glasgow (2000) 270.

[30] D. Bonnet and P. Meyers, *J. Mater. Research* **13** (1998) 2740.

[31] H. J. Moller, *Semiconductors for Solar Cells*, Rtech. House Inc., London (1993) 286.

[32] X. Wu, J. C Kane, R. G. Dhere, C. DeHart, D. S Albin, T. A Gessert, D. H. Levi and P. Sheldon. *Proc. of the 17th European PV Solar Energy Conference and Exhibition*, Munich, (2002) 995.

[33] K. Ramanathan, M. A. Contreras, C. L. Perkins, S. Asher, F. S. Hasoon, J. Keane, D.Young, M. Romero, W. Metzger, R. Noufi, J.Ward, and A. Duda, *Prog. Photovolt: Res. Appl.* **11**, (2003) 225.

[34] S.M. Sze, *Physics of Semiconductor Devices*, Wiley & Sons, New York (1981) 790.

[35] R. A. Mickelsen in: *Proc. 18th IEEE PV Spec. Conf.* Kissimime, USA (1985) 1069.

[36] S Verma, N Orbey, R. W. Birkmie and T. W. F Russel., *Prog. PV Research and Applications* **4** (1996) 341.

[37] L. L. Kazmerski, M. S. Ayyagari and G.A. Sanborn, *J. Appl. Phys*, **46** (1975) 4865.

[38] L. L. Kazmerski and G. A. Sanborn, *J.Appl.Phys*, **48** (1977) 3178.

[39] R. Amichelson and W. S Chen, *Proc, 15th IEEE PV Specialist Conference,* IEEE Publishing, New York (1981) 800.

[40] J. R. Tuttle, J. S. Ward, A. Duda, T. A. Berens, M.A. Contreras and K.R. Ramanathan, *Proc. Material Research Society*, San Franscisco (1996) 143.

[41] R. W. Birkmire, *Solar Energy Mater. Solar Cells* **65** (2001) 17.

[42] C. L Jensen, D. E. Tarrant, J. H. Ermer and G. A. Pollock, *Pro. 23rd IEEE PV Specialists Conference*, Louisville USA (1993) 577.

[43] M. A, Contreras, B. Eggas, K. Ramanathan, J. Hilter, A. Swartzlander, F. Hasson and R. Noufi, *Prog. in Photovoltaics* **7**, (1999) 311.

[44] F. J. Haug, *Development of Cu(In,Ga)Se_2 Superstrate Thin Film Solar Cells*, PhD Thesis, Dipl. Phys. Universit at Ulm, (2001) .

[45] C. J. Sheppard, V. Alberts, and W. J. Bekker, *Phys. Stat. Solidi* (A) **201** (2004) 2234.

[46] V. Probst, W.Stetter, W.Riedl, H.Vogt, M.Wendl, H.Calwer, S.Zweigart, B.Freienftein and H.Cerva, *Thin Solid Films* **387**, (2001) 262.

[47] A. Rockett, A. Elfotouh, D. Albin, M. Bode, R. Klenk, T. C Lommasson, T.W. F Russell, R. D Tomlinson, J Tuttle, L. Stolt, T. Walter and T.M. Peterson, *Thin Solid Films* **237** (1994) 1.

[48] M. A. Contreras, B. Egaas, K. Ramanathan, J. Hiltner, A. Swartslander, F. Hasoon, and R. Noufi, *Prog. in PV Research and Applications*, 7 (1999) 311.

[49] S. Belgacem, M. Amlouk and R. Bennaceur, *Rev. Phys. Appl.* **25** (1990) 1213.

[50] D. Hariskos, R. Herberholz, M. Ruckh, U. Ruhle, R. Schaffler, and H. W. Schock, *Proc.of 13th European PV Solar Energy Conference*, Nice (1995) 1995

[51] J. R. Tuttle, T. A. Berens, J. Keane, K. R. Ramanathan, J. Granata, R. N. Battacharaya, H. Wiesner, M. A. Contreras, and R. Noufi, *Proc.of 25th IEEE PV Specialists Conference*, Washington D. C (1996) 797.

[52] A. Bauknecht, U. Blieske, T. Kampschulte, A. Ennaoui, V. Nadenau, H. W Schock, A. N. Tiwari, M. Krejci, S. Duchemin, M. C. Artaud, L. M. Smith, S. Rushworth, J. Sollner and M.C Steiner, *Proc. of 2nd World Conference on PV Solar Energy Production*, Vienna (1998) 2436.

[53] R. Klenk, R. Mauch, R. Schaffler, D. Schmid and H. W. Schock, *in Proceedings 22nd IEEE Photovoltaic Specialists Conference*, Las Vegas (1991)1071.

[54] T. Negami, M. Nishitani, T. Wada and T. Hirao, *Proc. of 11th European PV Solar Energy Conference,* Montreux, (1992) 783.

[55] T. Nakada, T. Kume and A. Kunoika, *Solar Energy Mater. Solar Cells*, **50** (1998) 97.

[56] M. Kaelin, D. Rudmann, F. Kurdesau, T. Meyer, H. Zogg and A. N. Tiwari, *Thin Solid Films*, **431-432** (2003) 58.

Bibliography

[1] S. P. Sukhatme, *Solar Energy*, Tata McGraw Hill, Delhi (1997).

[2] M. A. Green, *Solar Cells-Operating Principles*, Technology, and System Applications, Prentice-Hall, Englewood Cliffs, New Jersey (1982).

[3] Shah, P. Torres, R. Tscharner, N. Wyrsch and H. Keppner, *Science* **285** (1999) 692.

[4] E. Martinot, A. Chaurey, D. Lew, J. R. Moreira and N. Wamukonya, *Annual Review of Energy and the Environment* **27** (2002).

[5] K. L. Chopra, P. D. Paulson and V. Dutta, *Prog Photovolt: Res. Appl.* **12** (2004).

[6] H. W. Schock and F. Pfister, *Proc. of the 16th European PV Conference,* Glasgow (2000).

[7] L.D. Partain, *Solar Cells and Their Applications*, John Wiley and Sons Inc., New York (1995) 600.

Chapter 2

Deposition and Characterization Techniques for Thin Films

An understanding of the fundamental properties of the thin films at various stages of preparation is an important prerequisite for the production of device quality films and those properties depend strongly on synthesis conditions. Film properties rely on its thickness, composition and structure and on how the film interacts with its environment: light, electric and magnetic fields, chemicals, mechanical force, heat etc. The deposition technique employed for the growth of thin films and various characterisation tools used for the study of the films during deposition and after film formation is given in this chapter.

1 Introduction

The research in photovoltaics is focused on making solar cells cheaper and/or more efficient, so that they can more effectively compete with other energy sources. One way of doing this is to develop cheaper methods of obtaining sufficiently pure material that is apt for photovoltaic conversion. Another approach is to significantly reduce the amount of raw material used in the manufacture of solar cells. The various thin-film technologies currently being developed make use of this approach to reduce the cost of electricity from solar cells. Thin film solar cells use less than 1% of the raw material compared to wafer based solar cells, leading to a significant price drop per k Wh.

2.2 Thin Film Deposition

Thin-film deposition is any technique for depositing a thin film of material onto a substrate or onto previously deposited layers. Thin is a relative term, but most deposition techniques allow layer thickness to be controlled within a few tens of nanometres, and some like molecular beam epitaxy allows single layers of atoms to be deposited at a time.

Deposition techniques fall into two broad categories, depending on whether the process is primarily chemical or physical.

2.3 Chemical Deposition

Here, a fluid precursor undergoes a chemical change at a solid surface, leaving a solid layer. An everyday example is the formation of soot on a cool object when it is placed inside a flame. Since the fluid surrounds the solid object, deposition happens on every surface, with little regard to direction; thin films from chemical deposition techniques tend to be conformal, rather than directional.

Chemical deposition is further categorized by the phase of the precursor. Plating relies on liquid precursors, often a solution of water with a salt of the metal to be deposited. The most commercially important process is electroplating. It was not commonly used in semiconductor processing for many years, but has seen revival with more widespread use of chemical-mechanical polishing techniques. Chemical vapor deposition (CVD) generally uses a gas-phase precursor, often a halide or hydride of the element to be deposited. In the case of metal organic chemical vapor deposition (MOCVD), an organometallic gas is used. Commercial techniques often use very low pressures of precursor gas. Plasma enhanced CVD uses an ionized vapor, or plasma, as a precursor.

2.4 Physical Deposition

Physical deposition uses mechanical or thermodynamic means to produce a thin film of solid. An everyday example is the formation of frost. Since most engineering materials are held together by relatively high energies, commercial physical deposition systems require a low-pressure vapor environment to function properly and most can be classified as physical vapor deposition.

2.4.1 Physical Vapor Deposition

Physical vapor deposition (PVD) is a technique used to deposit thin films of various materials onto various surfaces. The material to be deposited is placed in an energetic, entropic environment. A cooler surface is kept facing this source which draws energy from the particles those escape from the material surface, as they arrive, allowing them to form a solid layer. The whole system is kept in a vacuum deposition chamber, to allow the particles to travel as freely as possible. Since particles tend to follow a straight path, films deposited by physical means are commonly directional, rather than

conformal. Physical vapor deposition methods are clean, dry vacuum deposition methods in which the coating is deposited over the entire object simultaneously, rather than in localized areas.

Various physical depositions include sputtering, pulsed laser deposition (PLD) and evaporation. Sputtering relies on a plasma to knock material from a target. Noble gases like argon are usually used for plasma. The target can be kept at a relatively low temperature, since the process is not one of evaporation. This makes sputtering one of the most flexible deposition techniques. It is especially useful for compounds or mixtures, where different components would otherwise tend to evaporate at different rates. PLD systems work by an ablation process. Pulses of focused laser light vaporize the surface of the target material and convert it to plasma; this plasma usually reverts to a gas before it reaches the substrate. Evaporation is a very simple and convenient method and is the most widely used technique. Sufficient amount of heat is given to the evaporant to attain the vapour pressure necessary for evaporation. Then the evaporated material is allowed to condense on a substrate kept at a suitable temperature.

The preparation of the precursor films described in this thesis work were performed by thermal evaporation by resistive heating,

2.5 Thermal Evaporation

Evaporation involves two basic processes: evaporation and condensation. A hot source material evaporates and condenses on the substrate.

Evaporation takes place in a vacuum. Vapours other than the source material are almost entirely removed before the process begins. In high vacuum with a long mean free path, evaporated particles can travel directly to the substrate without colliding with the background gas. At a typical pressure of 10^{-4} Pa, a 0.4 nm particle has a mean free path of 60 m.

Hot objects in the evaporation chamber, such as heating filaments, produce unwanted vapours that limit the quality of the vacuum. Evaporated atoms that collide with foreign particles may react with them; for example, if aluminium is deposited in the presence of oxygen, it will form aluminium oxide. They also reduce the amount of vapor that reaches the substrate.

Evaporated materials deposit non uniformly if the substrate has a rough surface. Because the evaporated material falls on the substrate mostly from a single direction, protruding features block the evaporated material from some areas. This phenomenon is called shadowing or step coverage. When evaporation is performed in poor vacuum or close to atmospheric pressure, the resulting deposition is generally non-uniform and may not be continuous or smooth film. Rather, the deposition will appear fuzzy or cloudy. Only materials with a much higher vapor pressure than the heating element can be deposited without contamination of the film.

The evaporation system includes an energy source besides vacuum pump which evaporates the material to be deposited.

Many different energy sources exist. In the thermal method, the source material is placed in a crucible, which is radially heated by an electric filament, while in the electron-beam method, the source is heated by an electron beam with energy up to 15 K eV. In flash evaporation, a fine wire of source material is fed continuously onto a hot ceramic bar, and evaporates on contact. Resistive evaporation is carried out by passing a large current through a wire or foil of the material that is to be deposited.

2.5.1 Comparison to Other Deposition Methods

Evaporation has a better step coverage than the other alternative methods, such as sputtering and chemical vapor deposition. This may be an advantage or disadvantage, depending on the desired result. Deposition by sputtering is

slower than evaporation. Sputtering uses plasma, which produces many high-speed atoms that bombard the substrate and may damage it. Evaporated atoms have a Maxwellian energy distribution, determined by the temperature of the source, which reduces the number of high-speed atoms.

2.6 Other Deposition Processes

There are some other methods outside these two categories, based on a mixture of chemical and physical means:

- In *reactive sputtering*, a small amount of some non-noble gas such as oxygen or nitrogen is mixed with the plasma-forming gas. When material is sputtered from the target, it reacts with this gas and a different material is deposited on the substrate. i.e. an oxide or nitride of the target material.
- In *topotaxy*, a specialized technique similar to epitaxy, thin film crystal growth occurs in three dimensions due to the crystal structure similarities (either heterotopotaxy or homotopotaxy) between the substrate crystal and the growing thin film material.
- *Two stage process*, a cost effective technique consisting of the preparation of precursor film by any of the method like sputtering, thermal evaporation, followed by the chalcogenisation of these samples.

2.7 Two Stage Process

The major concerns related to the preparation of thin films in high production level are poor material utilization and the difficulty of obtaining uniform material fluxes over large area substrates. Attention will therefore be focused on the development of a relatively easily scalable two stage

deposition technique, to produce uniform coatings of thin films on large area substrates.

Two stage processes is a simple method for the preparation of chalcogenide and selenide thin films. This method has been effectively employed to produce high efficiency solar cells.

As the name indicates the two stage processes consists of two steps; 1) preparation of the precursor, 2) chalcogenisation of the precursor. Strength of two-stage approaches arises from the fact that they can utilize various deposition techniques (sputtering, thermal evaporation, screen printing and so on) in the precursor stage.

We have used the two stage processes to prepare copper indium selenide ($CuInSe_2$), copper indium sulfur selenide ($CuIn(Se_{1-x}S_x)_2$, and indium sulfide thin films. During the first step of the two stage process, a metal film containing (Cu and In (and /or Ga) or In only), are sequentially deposited, according to the final compound to be obtained are prepared by vacuum processes (thermal evaporation). During the second step of the process, the precursors are reacted with selenium or sulfur or in a mixture of sulfur and selenium atmosphere in order to form the ternary compound semiconductors. The final quality of the films formed depends on this chalcogenisation process as well as the structural properties of the precursor film before the chalcogenisation stage.

In our work of preparing $CuInSe_2$, copper and indium layers are deposited on glass substrates by thermal evaporation. The Cu-In bi-layer is annealed in vacuum to form the copper indium alloy ($Cu_{11}In_9$). This alloy was then selenized at various temperatures to form $CuInSe_2$ thin films. For post sulfurisation, the $CuInSe_2$ obtained as above were allowed to remain in sulfur atmosphere for some time. The $CuIn(Se_{1-x}S_x)_2$ thin films were

prepared by annealing the $Cu_{11}In_9$ alloy in a combined atmosphere of sulfur and selenium. For indium sulfide preparation indium is first deposited by thermal evaporation and then this metallic film is exposed to H_2S atmosphere to get In_2S_3 thin films of desired property. In the preparation of $CuInSe_2$ and $CuIn(Se_{1-x}S_x)_2$ thin films a very thin layer of gallium was coated prior to indium coating in the first stage of two stage process (the precursor preparation), for better adhesion of the final film to the substrate. Details of thermal cycles used for chalcogenisation and the conditions are described in the respective sections of film growth.

2.7.1 Sulfurisation Set up

Sulfurisation was carried out in a specially designed set up as shown in figure. The set up consists of a reaction vessel made of quartz, temperature controlled heater and the sulfurisation source. H_2S was used as the sulfurising agent, which was prepared using a Kipp's apparatus by the reaction between dilute hydrochloric acid and ferrous sulfide. The sulfurisation temperature was varied from 250^0 C to 400^0 C. The schematic diagram of the set up used for sulfurisation is shown in figure 2.1.

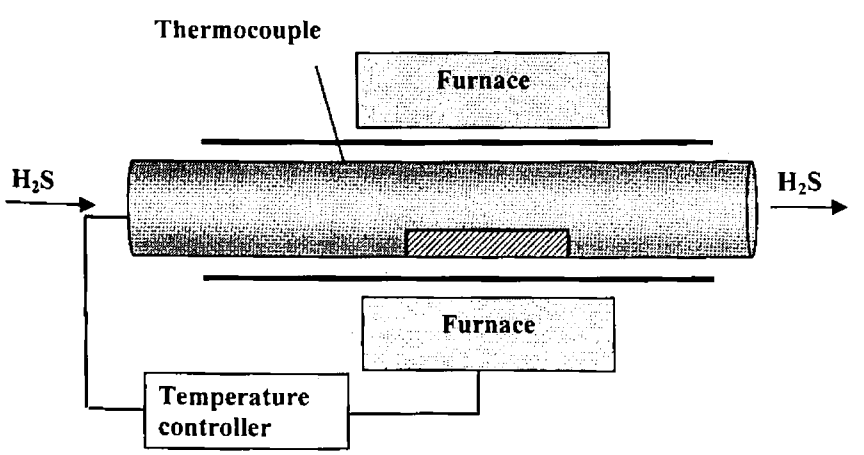

Figure 2.1 Schematic diagram of Sulfurisation Set up

2.7.2 Selenization Set up

Selenization was carried out in a specially designed apparatus consisting of a double walled quartz tube and a split furnace which allowed rapid heating and cooling of the samples. Selenium shots were used as the selenium source since H_2Se gas is highly toxic. The unreacted selenium is condensed on the water cooled end of the quartz tube. Any trace of Se escaping the furnace is dissolved in carbon di sulfide. The nitrogen gas was flowed from the selenium source region to the substrate region to carry the selenium vapor. The selenization temperature was varied from 250^0 C to 400^0 C. A Proportional Integral Derivative (PID) controller was used to maintain different thermal cycles. The photograph of the selenization set up fabricated in our lab is shown in figure (Fig. 2.2).

For co chalcogenisation and post sulfurisation a mixture of selenium and sulfur atmosphere were used. Selenium atmosphere was created as explained previously. With this arrangement H_2S is allowed to pass during the selenization for co chalcogenisation. To carry out the post sulfurisation the $CuInSe_2$ samples prepared by selenization process were allowed to sulfurise for different duration.

Figure 2.2 The photograph of selenization set up

2.7.3 Substrate Cleaning

The chemical cleanliness of the glass substrate, prior to growth, directly influences the material properties of the deposited films. Scratches on the glass have an adverse effect on the structural properties of the thin films, while the presence of contaminants normally results in films with poor adhesion properties. Commercially available microscopic glass slides (7.5 cm × 2.5 cm) and quartz substrates were used as substrate. To eliminate visible impurities the slides were washed with a commercially available soap solution and then with distilled water. To eliminate organic impurities they were kept in freshly prepared chromic acid for 20 minutes. Then these slides were washed in a current of distilled water and dried.

2.8 Characterisation of the Thin Films Prepared

The optimization of the preparation conditions is the main task in order to get device quality films. This has to be carried out on the basis of detailed structural, compositional, morphological, optical and electrical properties of the films obtained at different growth conditions. In this work, the analysis of the thin films prepared was done during deposition and after film formation. The following section deals with the various characterisation tools used for the study.

2.8.1 Thin film thickness

i) Quartz Crystal Microbalance

A quartz crystal microbalance (QCM) measures mass by measuring the change in frequency of a piezoelectric quartz crystal when it is disturbed by the addition of a small mass of any other tiny object intended to be measured. Frequency measurements are easily made to high precision:

hence, it is easy to measure small masses. Correlation between mass and frequency is achieved by means of the Sauerbrey equation [1].

In this in-situ method, thickness measurement depends on the oscillation of a quartz crystal when excited and the frequency of its oscillation depends on its thickness as given by the relation [2],

$$f = \frac{v}{2d} = \frac{N}{t}(nmkc/\sec) \qquad 2.1$$

where, v is the velocity of the transverse elastic waves normal to the crystal plate, d is the thickness of the crystal and N is the frequency constant depending on the nature of the crystal.

When a film of thickness t is deposited on the quartz plate, the mass of the crystal is changed. The corresponding change in the frequency of the crystal can be utilised to find the average thickness of the film deposited.

$$t = \frac{\Delta f}{C\sigma} \qquad 2.2$$

where, σ is the density of the deposited film and $C = \frac{f^2}{N\rho}$ (ρ is the density of the quartz crystal) is called the sensitivity for mass determination which is a constant of the crystal used. The QCM used in our lab was Model C200 in which the changes in the resonant frequency of the quartz crystal oscillator with the film deposition are calibrated to give the deposition rate and the thickness of the film. The quartz thickness monitor was used during the deposition of Ga, In and Cu layers.

ii) Stylus Thickness Profiler

The thickness of the films obtained after two stage process is measured using stylus thickness profiler (Vecco Dektak 6M Stylus Profiler). In principle this method consists of measuring the mechanical movement of a stylus as it

traverses a film-substrate step. The diamond stylus has a tip radius of 0.0001 inch, and bears on the specimen being measured with a force of about 0.1 gm. The stylus traverses a substrate film step, and the vertical motion of the stylus relative to a reference plane is converted to an electrical signal. This signal is amplified and recorded on rectilinear paper. Thus, a profile graph is produced which represent a cross section of film step as well as substrate surface irregularities. The schematic diagram illustrating the determination of thickness of thin films using stylus profiler is given in figure 2.3

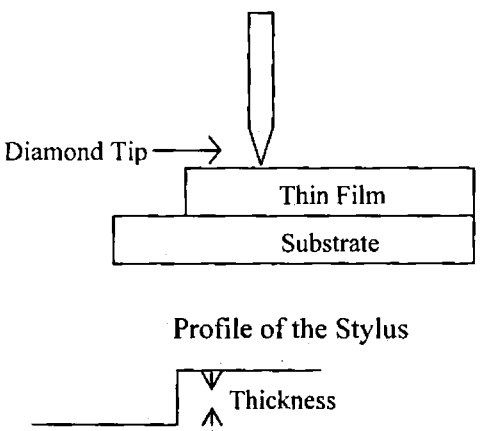

Figure 2.3 Schematic diagram illustrating the determination of the thin film thickness with Stylus Profiler

2.8.2 Structural Characterisations

i) X- Ray Diffraction (XRD) Technique

Solid matter can be described as 1) amorphous: The atoms are arranged in a random way 2) crystalline: The atoms are arranged in a regular pattern, and there is as smallest volume element that by repetition in three dimensions describes the crystal. This smallest volume element is called a unit cell. The dimensions of the unit cell are described by three axes: a, b, c and the angles between them alpha, beta, and gamma.

About 95% of all solid materials can be described as crystalline. When X-rays interact with a crystalline substance (Phase), one gets a diffraction pattern. This x-ray diffraction pattern is like a fingerprint of the substance. The powder diffraction method is thus ideally suited for characterization and identification of polycrystalline phases by a match procedure [3]. Furthermore, the areas under the peak are related to the amount of each phase present in the sample.

The basic law involved in the diffraction method of structural analysis is the Bragg's law. When monochromatic X-rays impinge upon the atoms in a crystal lattice, each atom acts as a source of scattering. The crystal lattice acts as series of parallel reflecting planes. The intensity of the reflected beam at certain angles will be maximum when the path difference between two reflected waves from two different planes is an integral multiple of λ. This condition is called Bragg's law and is given by the relation,

$$2dSin\theta = n\lambda \qquad 2.3$$

where n is the order of diffraction, λ is the wavelength of the X-rays, d is the spacing between consecutive parallel planes and θ is the glancing angle [4].

X-ray diffraction studies give a whole range of information about the crystal structure, orientation, average crystalline size and stress in the films. Experimentally obtained diffraction patterns of the sample are compared with the standard Powder Diffraction Files published by the International Centre for Diffraction Data (ICDD). International Center Diffraction Data (ICDD) or formerly known as (JCPDS) Joint Committee on Powder Diffraction Standards is the organization that maintains the data base of inorganic and organic spectra.

The average grain size of the film can be calculated using the Scherrer's formula [5],

$$d = \frac{0.9\lambda}{\beta Cos\theta} \qquad 2.4$$

where, λ is the wavelength of the X-ray and β is the full width at half maximum intensity in radians.

The lattice parameter values for different crystallographic systems can be calculated from the following equations using these hkl parameters and the interplanar spacing d.

Cubic system, $$\frac{1}{d^2} = \frac{h^2 + k^2 + l^2}{a^2} \qquad 2.5$$

Tetragonal system, $$\frac{1}{d^2} = \frac{h^2 + k^2}{a^2} + \frac{l^2}{c^2} \qquad 2.6$$

Hexagonal system, $$\frac{1}{d^2} = \frac{4}{3}\left(\frac{h^2 + hk + k^2}{a^2}\right) + \frac{l^2}{c^2} \qquad 2.7$$

The particular advantage of X-ray diffraction analysis is that it discloses the presence of a substance and not in terms of its constituent chemical elements. Diffraction analysis is useful whenever it is necessary to know the state of chemical combination of the elements involved or the particular phase in which they are present. Compared with ordinary chemical analysis the diffraction method has the advantage that it is much faster, requires only very small sample and is non destructive.

X-ray diffraction measurements of the different films were done using Rigaku automated X-ray diffractometer. The filtered copper Kα (λ=1.5418A^0) radiation was used for recording the diffraction pattern.

ii) Scanning Electron Microscopy

Scanning electron microscopy (SEM) is used for inspecting topographies of specimens at very high magnifications using equipment called the scanning electron microscope. There are many advantages in using the SEM instead of a light microscope. The SEM has a large depth of field which allows a large amount of the sample to be in focus at one time. The SEM also produces images of high resolution. The combination of higher magnification, larger depth of focus, greater resolution makes the SEM one of the most heavily used instrument in current research field. SEM inspection is often used in the analysis of cracks and fracture surfaces, bond failures, and physical defects on the die or package surface.

During SEM inspection, a beam of electrons is focused on a spot of the specimen, resulting in the transfer of energy to the spot (Fig. 2.4). These bombarding electrons, also referred to as primary electrons, dislodge electrons from the specimen itself. The dislodged electrons, also known as secondary electrons, are attracted and collected by a positively biased grid or detector, and then translated into a signal.

To produce the SEM image, the electron beam is swept across the area being inspected, producing many such signals. These signals are then amplified, analyzed, and translated into images of the topography being inspected. The electron beam typically has an energy ranging from a few hundred eV to 50 keV.

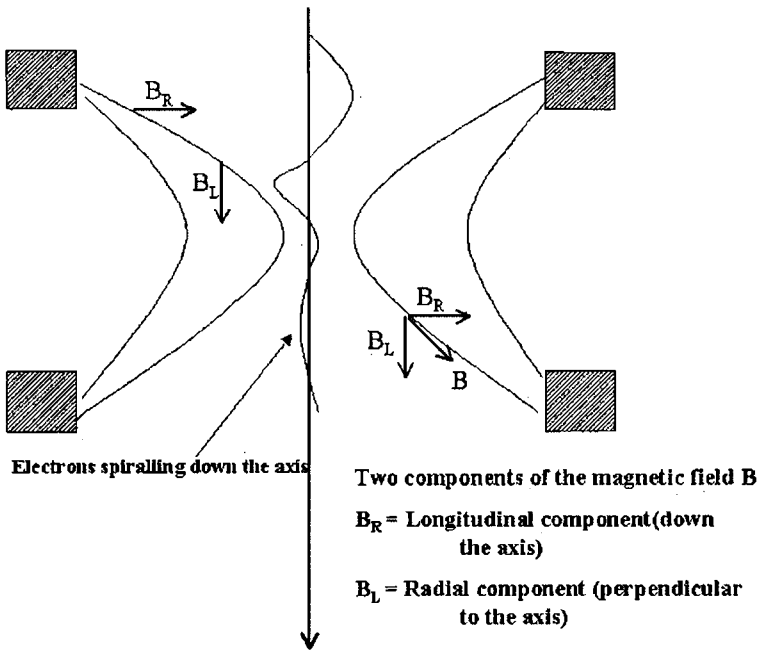

Figure 2.4 The focusing of electrons in SEM

A SEM may be equipped with an Energy Dispersive X-ray (EDX) analysis system to enable it to perform compositional analysis on specimens.

iii) Energy Dispersive X-ray Analysis

EDX Analysis stands for Energy Dispersive X-ray analysis. It is a technique used for identifying materials and contaminants, as well as estimating their relative concentrations on the surface of the specimen. The EDX analysis system works as an integrated feature of SEM, and can not operate on its own without the latter.

During EDX Analysis, the specimen is bombarded with an electron beam inside the scanning electron microscope. The energy of the beam is typically in the range 10-20keV. The bombarding electrons collide with the specimen electrons, knocking some of them off in the process. A position vacated by

an ejected inner shell electron is eventually occupied by a higher-energy electron from an outer shell giving up some of its energy as X-ray.

The amount of energy released by the transferring electron depends on which shell it is transferring from, as well as which shell it is transferring to. Furthermore, the atom of every element releases X-rays with unique amounts of energy during this transferring process. Thus, by measuring the amounts of energy present in the X-rays being released by a specimen during electron beam bombardment, the identity of the atom from which the X-ray was emitted can be established. The X-rays are generated in a region about 2 microns in depth, and thus EDX is not a surface science technique.

The output of an EDX analysis is an EDX spectrum. An EDX spectrum normally displays peaks corresponding to the energy levels for which the most X-rays had been received. Each of these peaks is unique to an atom, and therefore corresponds to a single element. The higher a peak in a spectrum, the more concentrated the element is in the specimen.

2.8.3 Optical Characterisations

The knowledge of the optical property of any type of PV sample either under collimated light incident at variable angles, or under diffuse light, nevertheless, would greatly contribute to the comprehension of its electrical performances when it is exposed outdoors to the solar irradiation.

The spectrophotometers enable the measurement of optical constants like the absorption coefficient, band gap, spectral reflectance and transmittance of any prototype sample, of small dimensions (few square centimetres), under a collimated light beam incident at a fixed angle.

i) Absorption coefficient and Band gap

The absorption coefficient of a solar cell depends on two factors: the material making up the cell, and the wavelength or energy of the light being absorbed. Solar cell material should have an abrupt edge in its absorption coefficient. The reason is that light whose energy is below the material's band gap cannot free an electron and it isn't absorbed. A small absorption coefficient means that light is not readily absorbed by the material.

The band gap Eg of a semiconductor material is the minimum energy needed to move an electron from its bound state within an atom to a free state, where the electron can be involved in conduction. The lower energy level of a semiconductor is called the valence band and the higher energy level where an electron is free to roam is called the conduction band. The band gap is the energy difference between the conduction band and valence band.

When the energy of the incident photon ($h\nu$) is larger than the band gap energy the excitation of electrons from the valence band to the empty states of the conduction band occurs. The light falling on the material is then absorbed. Electron hole pairs are created depending on the number of incident photons $S_0(\nu)$ (per unit area, unit time and unit energy). The frequency ν and wavelength λ of the incident photon are related by the equation

$$\lambda\ [\mu m] = c/\nu = 1.24/h\nu \qquad 2.8$$

where c is the speed of light.

The photon flux $S(x,\nu)$ decreases exponentially inside the material according to the relation

$$S(x,\nu) = S_0(\nu) \exp(-\alpha x) \qquad 2.9$$

where, the absorption coefficient, ($\alpha(\nu) = 4\pi k\upsilon/c$) is determined by the absorption process in semiconductors and k is the extinction coefficient [6].

The absorption coefficient $\alpha(\nu)$ depends on the band structure of the semiconductor. In direct band gap semiconductors where the minimum of the conduction band and the maximum of the valence band occur for the same wave vector in the Brillouin zone, the absorption coefficient α_d as a function of the frequency ν is given by the relation [7],

$$\alpha_d(\nu) = \frac{\alpha_0 (h\nu - Eg)^{1/2}}{h\nu} \qquad 2.10$$

where E_g is the band gap energy of the material and α_o is a constant.

In indirect band gap semiconductors, the absorption coefficient for allowed transition takes the form

$$\alpha_{in}(\nu) = \frac{(h\nu - Egi \pm Ep)^2}{\exp(Ep/KT) - 1} \qquad 2.11$$

where $\pm E_p$ is the absorbed or emitted phonon energy, K is the Boltzmann constant, T is the temperature, E_{gi} is the indirect band gap energy.

So for direct transition (2.9), we have

$$(\alpha h\nu)^2 = \alpha_0 h\nu - \alpha_0 E_g \qquad 2.12$$

Therefore, a plot of $(\alpha h\nu)^2$ vs $h\nu$ will be a straight line for direct band gap materials. The intercept of the curve to the photon energy axis gives the band gap (E_g) of the material.

The absorption spectra of the samples were taken using JASCO V570 UV-VIS- NIR spectrophotometer. It measures the intensity of light passing through a sample (I), and compares it to the intensity of light before it passes through the sample (I_o). The ratio I / I_o is called the transmittance, and is

usually expressed as a percentage (%T). The absorbance, A, is based on the transmittance:

$A = -\log(\%T)$

The absorption coefficient (α) was calculated from the absorbance. Finally the band gap of the material is found out from the plot $(\alpha h\nu)^2$ vs $h\nu$.

2.8.4 Electrical Characterisations

i) Resistivity by Two Probe Method

The resistivity of the films was determined by the two-probe method with the electrodes in planar geometry. Evaporated indium layers or high conducting silver paste was used as the electrodes. The current voltage measurements were carried out using a Keithley's source measure unit (Model SMU236). The resistivity (ρ) of the films is calculated applying ohm's law, by the relation $\rho = RA/L$. Where R is the resistance obtained from current- voltage characteristic curves. 'A' is the area of the film in planar geometry which is given by the product of the film thickness and the width of the film. L is the spacing between the electrodes.

ii) Temperature Dependence of Conductivity

The temperature dependence of conductivity was measured by measuring the current voltage (I-V characteristics) varying temperature of the specimen from 20 K to 500 K. Keithley's source measure unit (Model SMU236) and liquid helium cryostat having automated temperature controller (Model Lakeshore 321) was used to carry out the I-V characteristics. Liquid helium was used to cool the samples to 20 K. The specimen temperature was raised to 500 K using heaters. The voltage is kept constant and the variation of current with temperature is noted.

The activation energy is calculated from the arrhenious plot, which allows determining the time and temperature relationship of a process.

Thermally excited reactions are described by

$$\sigma = \sigma_0 \exp(-\frac{E_a}{kT}) \qquad 2.13$$

where E_a is the activation energy [8].

An arrhenious plot of this equation is a plot of log σ over 1/kT which gives a straight line. The slope of this line yields the activation energy.

References

[1] G. Sauerbrey, *Z. Physik*, **155** (1959) 206.

[2] L. I. Maissel and R. Glang, *Handbook of Thin film Technology*, Mc Graw Hill Book Company, New York (1983) 1-108.

[3] C. Surayanarayana and M. G. Norton, *X Ray Diffraction - a Practical Approach*, Plenum Press, New York (1998) p.6.

[4] C. Kittel, *Introduction to Solid State Physics*, 7th edition, Wiley Eastern Limited, Paris (1996) p.29.

[5] B. D. Cullity and S. R. Stock, *Elements of X ray diffraction*, 3rd edition, New Jersey, Prentice Hall (2001) p.388.

[6] H. J. Moller, *Semiconductors for Solar Cells*, Artech. House Inc., London (1993) p.12.

[7] J. Bardeen, F. J. Blatt and L.H. Hall, *Proceedings of Photoconductivity Conf.* (1954, Atlantic City), (Eds) R. Breckenridze, B. Russel and T. Hahn, J. Wiley and Chapman and Hall, New York (1956) p.146.

[8] N. F. Mott, *Metal Insulator Transitions*, 2nd edition, Taylor & Francis, London (1990) p.52.

Bibliography

[1] K. L. Chopra, *Thin Film Phenomena*, Robert E. Krieger Publishing Co. Inc., New York, 1979.

[2] R. W. Berry, *Thin Film Technology*, Van Nostrand Reinhold Company, New York, 1968.

[3] L. I. Maissel and R. Glang, *Handbook of Thin film Technology*, Mc Graw Hill Book Company, New York, 1983.

[4] L. Holland, Vacuum *Deposition of Thin films*, John Wiley & Sons Inc., New York, 1956.

[5] C. M. Van Atta and M. Hablanian, *Vacuum and Vacuum Technology*, *Encyclopedia of Physics* VCH Publishers Inc, New York, 1991.

[6] C. Jaeger Richard, *Introduction to Microelectronic Fabrication*, Upper Saddle River: Prentice Hall, New Jersey, 2002.

[7] M. Marudachalan, Processing, Structure and diffusion in $CuInxGa_{1-x}Se_2$ thin films for solar cells, Ph.D. thesis, University of Delaware, 1996.

[8] H. J. Moller, *Semiconductors for Solar Cells*, Rtech. House Inc., London, 1993.

[9] P. E. J Flewitt and R. K. Wild, *Physical Methods for Materials Characterisation*, 2nd edition, Institute of Physics Publishing, Bristol, 2003.

[10] D. J. O' Connor, B.A. Sexton, R. St. C. Smart, *Surface Analysis Methods in Material Science*, Springer-Verlag, Berlin-Heidelberg, 1992.

[11] H. H. Willared, L. L. Merit Jr, J. A. Dean, F. A. Settle Jr, *Instrumental Methods of Analysis*, 7th edition, CBS publishers, New Delhi, 1986.

Chapter 3

Growth of β - Indium Sulfide Buffer Layer by Two Stage Process

In photovoltaic thin film cells, the rectifying contact is between p-type absorber layer and the n-type buffer layer. Maintaining a high-quality pn junction was observed to be a critical factor for device efficiency. The transport properties of heterojunctions strongly depend on interface characteristics such as potential barrier height, interface state and band discontinuities. The aim of the buffer layer is to realize the junction with absorber.

The essential characteristics of a typical buffer layer are, it should

- *be n-type for carrier separation,*
- *be resistive with a high coverage efficiency*
- *act as physical barrier against short circuits between the electrodes of the cell*

3.1 Introduction

The semiconducting compounds of $A_2^{III} B_3^{VI}$ family, where A is In or Ga and B is S or Se have attracted particular interest in recent years due to their promising technological applications as buffer layer in solar cells. Indium sulfide (In_2S_3) can be used as an effective replacement for CdS in $Cu(In,Ga)Se_2$ based solar cells [1]. Though the highest conversion efficiency in thin film solar cells has been reported for $Cu(In,Ga)Se_2$ with a CdS buffer layer, there is great importance in replacing CdS with cadmium free buffer layer, for environmental reasons and possible gains in efficiency associated with an increase of the short circuit current. To avoid toxic heavy-metal Cd containing waste in the module production, a Cd free, less toxic buffer layer is desirable. Wide band gap (>2.5 eV) of In_2S_3 thin films suggests it can act as a better buffer layer with improved light emission in the blue region than CdS having band gap 2.4 eV. It is reported that $Cu(In,Ga)Se_2$ solar cell prepared with chemical bath deposited In_2S_3 as a buffer layer has efficiencies (16.4%) near to those obtained by device made with a standard CdS buffer layer [2]. The ternary indium sulfide compounds like $CuInS_2$ with an improved photosensitivity and $In_{2-x}Ga_xS_3$ offering a possibility to tailor the band gap are attractive materials for photovoltaic and optoelectronic devices [3]. In_2S_3 thin films can also be used as the precursor for the preparation of $CuInS_2$, which is one of the most widely used absorber layer in solar cells [4]. In the present work, the preparation and characterization of indium sulfide thin films as buffer layers for solar cell application is described.

3.2 Material Properties of In_2S_3

3.2.1 Crystallographic structure

Indium Sulfide (In_2S_3) is a kind of III_2- VI_3 materials which crystallize in cubic or hexagonal closed packed structure, same as II-VI compounds upon the replacement of the divalent cation by the trivalent In. As one third of the cation site remains empty, it causes a defect structure [5]. According to the Joint Committee on Powder Diffraction Standards (JCPDS), three major crystal modifications are known for In_2S_3 [6-10]. The low temperature metastable α form has a cubic structure with the lattice constant *a* of 5.358 A°. It is a cubic closed packed structure of sulfur, where 70% of the In atoms are randomly distributed on octahedral sites and the rest remain in tetrahedral sites [11]. α form transforms irreversibly at 360°C to the β form having a defect spinal lattice (*a* =10.73 A°) in which eight of the tetrahedral sites are occupied by In, where as four are randomly left empty [12]. Thus the chemical formula of β-In_2S_3 could be written as $[In(t)_{2/3}\square_{1/3}]$ $In_2(o)S_4$ where (t),(o) and □ represent tetrahedral, octahedral and vacant sites respectively. Under certain conditions, a high ordering of this vacancy at the tetrahedral sites occurs, establishing a tetragonal super cell containing spinel blocks along the c-axis [13-14]. This phase transition from the tetragonal structure to the less ordered β form takes place at 420°C [11, 15]. In the temperature range between 750 and 800°C the β In_2S_3 is reversibly transformed to γ In_2S_3, which has a layered structure with a hexagonal unit cell (*a* =3.85 A°, *c* =9.15 A°.) Of the three modifications, β–In_2S_3 is the stable form with tetragonal structure [16]. Besides these there is a high pressure ε phase, which is rhombohedral (a=6.0561 A° and c=17.5 A°) [17].

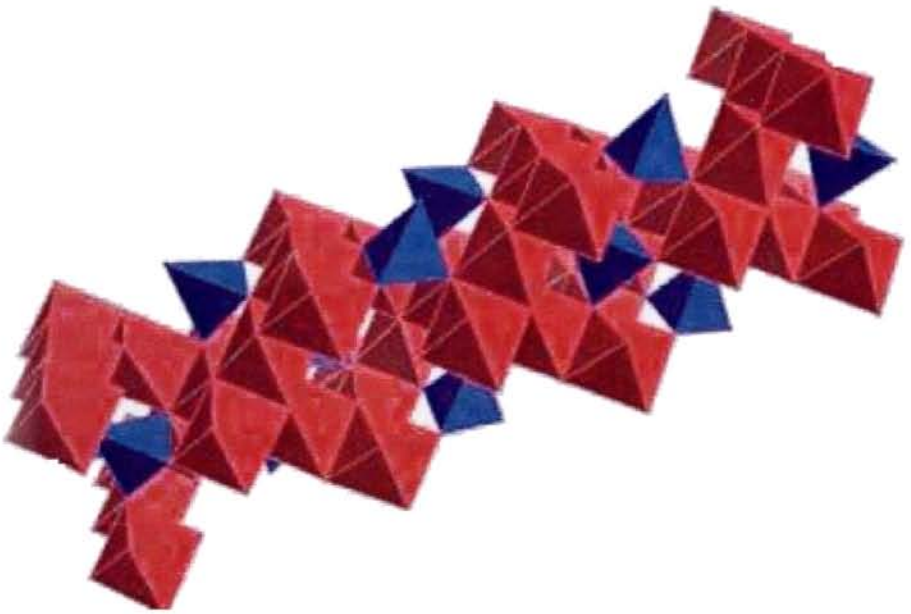

Figure 3.1 Structure of β-Indium Sulfide

The structure of the β modification is related to the spinel lattice. The cation vacancies are randomly located on either the octahedral sites only or on both types of sites. A model of ordered vacancies within a super structure of tetragonal symmetry was proposed by Rooymans [18]. The unit cell consists of three spinel cubes stacked along the c-axis. By rotating the a-and b-axis through 45° a smaller unit cell can be obtained. which belongs to a body centered tetragonal Bravis-lattice with the parameters: a = b = 7.62A° and c = 32.32 A°. This reduced unit cell contains 24-spinel type octahedral sites, which are all occupied by indium atoms. Of the 12 tetrahedral sites, normally occupied in the spinel, only 8 are occupied by indium whereas 4 remain empty (Fig.3.1). These 4 vacancies per unit cell are ordered along a fourfold screw axis of symbol 4_1 parallel to the c-axis. The ordered modification can therefore be interpreted as a

quazi-ternary compound consisting of In, S and vacancies or even as a quasi-quaternary one, when the difference between two types of the cation sites is taken into account.

3.2.2 Optical Properties

Most of the group II–VI materials are direct band gap semiconductors with high optical absorption and emission coefficients (the exceptions are HgSe and HgTe which are semimetals). β–In_2S_3 is an n–type semiconductor with a direct band gap of 2 to 2.3 e V [19, 20]. These values are too small for an application as buffer layer in solar cells. Several values grater than 2.3 eV have also been reported in literature. The In_2S_3 films deposited by Atomic Layer Epitaxy (ALE) [21] show a band gap of 3.3 eV, which is reduced to 2.25 eV on annealing. Barreau *et al* has studied a widening in band gap by the increase in oxygen content in the prepared film [22]. In another work Barreau observed the increase in band gap is also due to sodium content in the film. Their explanation is that sodium increases the ionicity of the tetrahedral cationic sulfur bonds which increases the optical band gap [23]. The blue shift of the optical transmission has been explained by Kim *et al* [24] with the interpretation that the broadening is due to excess of sulfur in the film. Yoshida *et al* and Yasaki *et al* have explained the broadening of optical band gap of the In_2S_3 by quantum size effect [14, 25]. Band tails observed in the optical spectra of vacuum deposited In_2S_3 thin films after the air annealing. It could be considered as films defects created by the thermal evaporation process [26]. The broadening or shift of the short wavelength absorption of In_2S_3 thin films were also explained by the presence of secondary phases and disordered structure [27].

3.2.3 Electrical Properties

Electrical studies on single crystals of In_2S_3 grown by chemical vapor transport and freeze gradient technique show a resistivity 30–1000 Ωcm. The 3% excess sulfur incorporation in these crystals increases the resistivity to 20 KΩ-cm [22]. The same results were observed by Rehwald and Harbeke [28]. Their experiments also showed that the annealing of In_2S_3 samples in air or vacuum at temperatures around 150°C for 2 hours results in a decrease of resistivity by more than an order of magnitude. Bessergenev *et al* have studied the effect of the substitution of sulfur by oxygen in the β–In_2S_3 films, which induces an increase in conductivity [29]. Conductivity is found to be increase with sodium content. When sodium is introduced in the crystalline matrix, it creates a disorder by the non periodic occupation of the tetrahedral sites and it can explain the increase of electrical conductivity [29]. Barreau *et al* showed that when the sodium content increases after particular value, it tends to total filling of the tetrahedral sites, leading to a perfectly ordered material having a very low electrical conductivity [30]. The introduction of oxygen in the thin films can also increase the conductivity by approximately two orders. The introduction of oxygen in the thin films can modify the properties of grain boundaries, which induce an increase in conductivity of the films [22].

3.2.4 Morphological Properties

Sulfur composition in excess of the stoichiometric value in spray pyrolysed In_2S_3 films causes an increase in *a* and *c* parameters [24]. The surface studies show that In_2S_3 prepared by chemical bath deposition at room temperature has a cauliflower-like morphology while films deposited at higher temperature resulted in fibrous structure [31]. Yahmadia *et al* observed some fibre structure along

with large lumps due to the presence of In_6S_7 phase [32]. Yoshida *et al* have reported a significant variation in surface morphology with the reaction temperature [33].

3.3 Processing Techniques for Indium Sulfide Thin Films

A wide range of preparation methods exist to grow In_2S_3 thin films. The deposition method has generally a large impact on the resulting film properties as well as on the production costs. In_2S_3 thin films are currently being deposited using both wet and dry processes. Prominent among them are Low Pressure Metal-Organic Chemical Vapour Deposition (MOVCD) [34], Atomic Layer Chemical Deposition (ALCVD) [1], Spray Pyrolysis [35,36] Chemical Bath Deposition (CBD) [37], Atomic Layer Epitaxy (ALE) [3,38,39], photochemical deposition [40], annealing of elemental layers [41], evaporating metal onto molybdenite [42], and Physical Vapor Deposition (PVD) [23,43], sulfurisation of metallic electroplated indium [44] etc.

CBD is relatively inexpensive, simple and convenient for large area deposition [45]. Using this method, deposition of In_2S_3 thin films from a bath containing indium salt and thioacetamide as sulfide ion source has been reported [46,47]. The CIGS based solar cell prepared with CBD In_2S_3 as a buffer layer have reached the efficiencies (15.7%) [48].

Attempts have been made to deposit In_2S_3 thin films by using successive ionic layer adsorption and reaction (SILAR) method [49].This method is mainly based on immersion of the substrate into separate cation and anion precursor solutions and rinsing between every immersion with ion exchanged water.

ALCVD is based on the surface reaction of the precursors. Main advantage is it allows the deposition of highly homogenous thin films and layer thickness growth control. A solar conversion efficiency of 13.5% has been obtained on small area device with indium sulfide buffer layer by ALCVD [21]. Naghavi *et al.* [2] recently demonstrated an efficiency of 16.4%, which is the record for CIGS using indium sulfide. They employed an atomic layer deposition (ALCVD) process using indium acetylacetonate and hydrogen sulfide (H_2S) for In_2S_3 window layer synthesis, with best results obtained at 220^0C substrate temperature. Although ALCVD has produced the best devices to date, the deposition rate is slow and the reagents are expensive.

With respect to industrial integration, the high vacuum techniques are most attractive. Researchers have examined PVD by sequentially evaporating indium and elemental sulfur [3, 11]. Its main advantage is easy control over growth rate through its various preparative parameters. However, an additional annealing step was required to form high-quality indium sulfide. Annealing temperature is a critical constraint on In_2S_3 window layer deposition, as excessive temperature results in copper diffusion and decreased solar cell performance [50, 51].

In the present investigation we aimed to combine high vacuum evaporation with rapid thermal processing (RTP) for chalcogenisation. The precursor preparation by vacuum evaporation followed by chalcogenisation called the two-step processes are pursued due to their superior potential for industrial production. By the introduction of rapid thermal processing the annealing time could be reduced from 3 h to 45 minutes.

The chalcogenisation was carried out at various annealing temperatures ranging from 250^0 C to 600^0 C in the presence of H_2S which resulted in the sulfurisation

of indium film to yield indium sulfide. The In_2S_3 film characterization including structural, optical, and electrical and composition is presented.

3.4 Experimental Details

Thin films of Indium were coated on the glass and amorphous silica substrates by the vacuum thermal evaporation technique. High purity Indium (99.999%) was evaporated from molybdenum boat at a pressure of 3×10^{-5} m bar. Thickness of indium layer 4000 A^0 was monitored using a quartz digital thickness monitor. The deposition rate was around 1 A° per second.

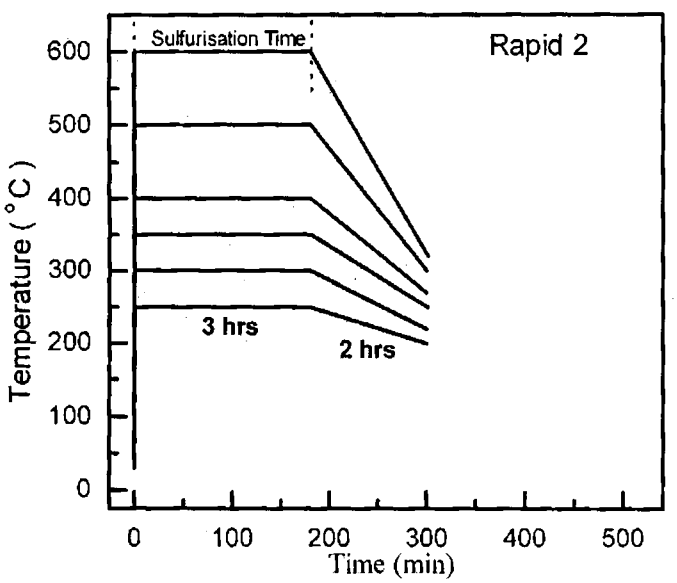

Figure 3.2. The thermal cycle used for Rapid 2 process.

Indium films prepared at room temperature were found to be less adhesive. A substrate temperature of 75° C was maintained during indium deposition for better adhesion. The sulfurisation was done at different temperatures. Initially, the In_2S_3 films were prepared by heating the indium films from room temperature to

set temperature under H_2S atmosphere. It took around 30-45 minutes to reach the set temperature. The slow heating of indium films to set temperature resulted in the evaporation of indium and hence the films obtained were very thin. To minimize the indium loss, the metallic precursors were introduced rapidly into the furnace in the presence of H_2S, which has already attained the set temperature, and the sulfurisation was carried out for 3 hrs. After the sulfurisation samples were allowed to remain in the furnace itself till it cools to room temperature which took around nine hours. This cycle was named as Rapid 9. Rapid indicates the fast heating rate (30 to 70 sec to reach the set temperature) and the 9 indicates the removal of samples after 9 hours. In an another thermal cycle named Rapid 2 the samples were allowed to cool naturally for 2 hours in the furnace after 3 hours sulfurisation and then they were taken out from the surface which prevented the large loss of indium during the cooling to room temperature. This thermal circle is represented graphically in figure 3.2. The sulfurisation carried out for different temperatures varying from 250^{0}C to 600^{0}C.

In both experiments the obtained films were considerably thinner than assumed. Also, since the main aim of the two stage process is making the cost of fabrication less, another thermal cycle was tried to make the time consumption less. In this thermal cycle the metallic precursors were introduced rapidly into the furnace at the set temperature in the presence of H_2S. The duration of sulfurisation was varied from 10 minutes to 3 hours keeping the sulfurisation temperature at 300°C. The samples were rapidly withdrawn form the furnace to minimize the indium loss. The sulfurisation of indium films for 45 minutes and above resulted in single phase β-In_2S_3. The thickness of the films found decreases with the increase in sulfurisation time. So further chalcogenisation experiments were carried out keeping the sulfurisation time constant for 45

minutes but for various sulfurisation temperatures ranging from 250°C to 600°C. This thermal cycle was named Rapid 45 since sulfurisation duration was fixed as 45 minutes. The numeric (Rapid 45) here indicate sulfurisation time and the cooling and heating by introducing and removing the samples from the furnace, whereas in Rapid 2 and Rapid 9 the numeric indicates the natural cooling time of the samples within the furnace.

The thickness of the In_2S_3 was measured by using gravimetric method using a sensitive microbalance. Precursor indium film thickness was measured using a quartz thickness monitor. The In_2S_3 films were further characterized by studying the structural, morphological, optical and electrical properties by X-ray diffractometer, Scanning Electron Microscopy (SEM), UV-VIS-NIR spectrophotometer and I-V measurement system respectively. The crystal structure, lattice strain, lattice parameters, absorption coefficient, conductivity, band gap and resistivity were obtained from these studies. Composition of the films was analysed using Energy Dispersive X-ray analysis (EDX). For electrical characterisation two silver electrodes in planar geometry were used as electrodes.

3.5 Results and Discussions

3.5.1 Crystal structure and composition

The X-Ray diffraction patterns of In_2S_3 films prepared in different processes were analyzed. It has been observed from XRD that there is no formation of indium oxide in the films. The XRD spectra of samples prepared by the Rapid 2 Process are shown in figure 3.3.

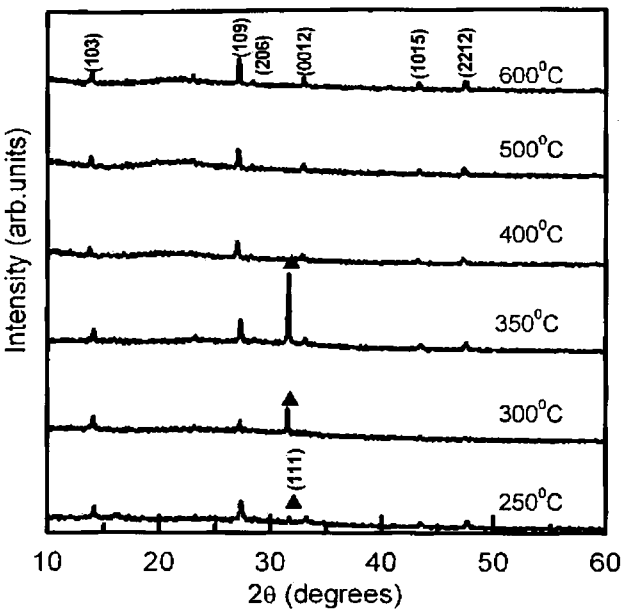

Figure 3.3 XRD pattern of β–In_2S_3 films prepared in Rapid 2 process at different sulfurising temperature. (▲ indicate the (111) peak of InS phase).

The XRD spectra show the presence of InS peak (111) along with In_2S_3 phase for lower sulfurisation temperature (<400°C). As the sulfurisation temperature is increased it has been observed that the intensity of (111) plane corresponding to InS phase along with the other In_2S_3 diffraction peak increases. The films obtained were a mixture of InS and In_2S_3 upto a sulfurisation temperature of 350°C. No peaks corresponding to InS was observed when the sulfurisation was carried at 400°C and above. Single phase In_2S_3 was obtained by Rapid 2 process when the temperature was 400°C and above.

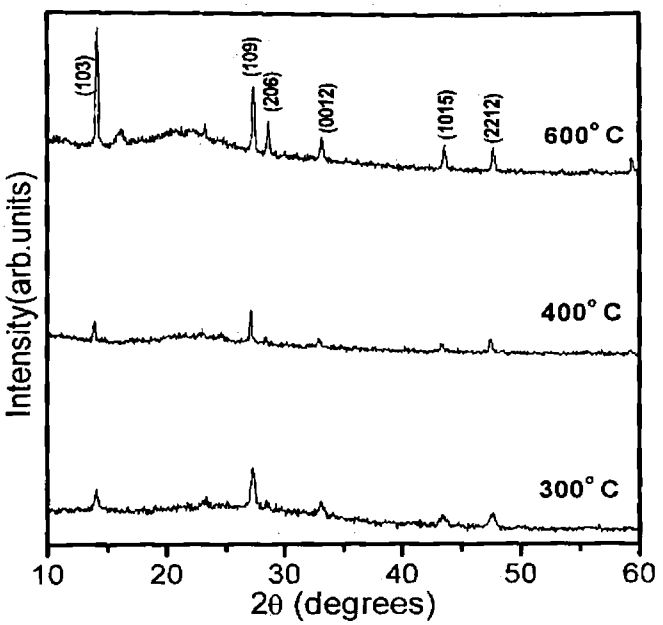

Figure 3.4 XRD pattern of β–In_2S_3 films prepared in Rapid 9 process at different sulfurising temperature.

Figure 3.4 is the XRD spectra of films prepared under Process Rapid 9. Contrary to Rapid 2 process Rapid 9 shows single phase In_2S_3 even at low sulfurisation temperature. The slow cooling to room temperature in Rapid 9 process might be giving sufficient time for conversion of InS phase to In_2S_3. The InS initially formed at low sulfurisation temperature (as evident in the XRD of Rapid 2 process) [52] is being converted to In_2S_3 on the prolonged annealing when the samples are allowed to cool to room temperature in the furnace.

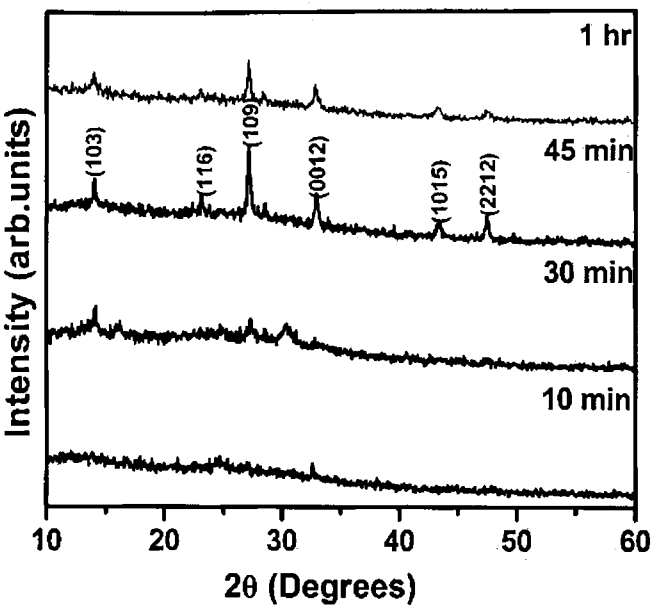

Figure 3.5 X-ray diffraction pattern of β–In_2S_3 prepared by the sulfurisation of indium films for different time duration at 300^{0}C.

The crystallinity of the films was also studied for the Rapid 45 samples. The sulfurisation of the indium films at 300^{0}C in H_2S atmosphere for 10 minutes yielded only a single (0012) peak of β-In_2S_3 and showed poor crystallinity (Fig.3.5). The films obtained by 30-minutes sulfurisation at 300^{0}C showed two major diffraction peaks (109) and (103) of β- In_2S_3 along with (111) peak of InS phase. This may be because the duration of sulfurisation was insufficient for the complete conversion of InS to In_2S_3. Another diffraction peak (003) corresponding to In_6S_7 was also present, but it disappeared on annealing the samples in air for 30 minutes.

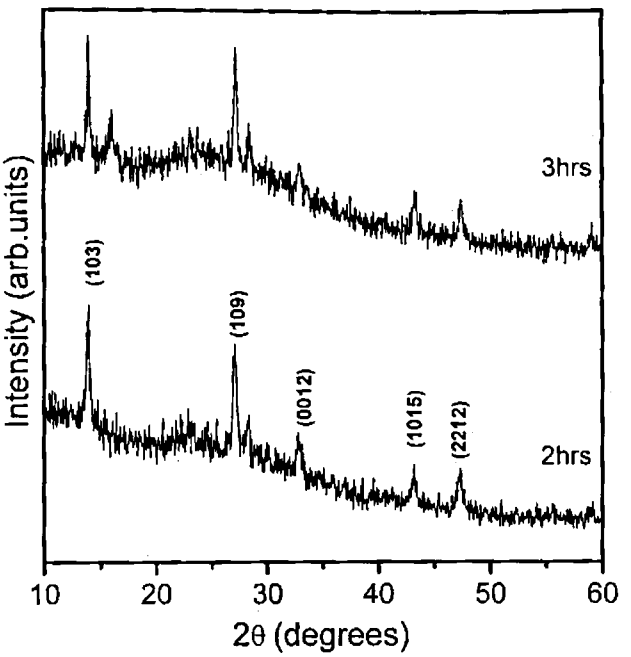

Figure 3.6 X-ray diffraction pattern of β–In_2S_3 prepared by the sulfurisation of indium films for 2 hours and 3 hours duration at 300°C.

Single phase In_2S_3 was obtained when the sulfurisation time was 45 minutes at 300°C. For the films obtained by the sulfurisation for 45 minutes and 1 hour showed the prominent peak corresponding to (109) plane of In_2S_3 while the films sulfurised for 2 hours and 3 hours showed the preferred orientation of (103) plane (Fig. 3.6). However no peaks corresponding to InS or any other impurity phase was observed when the sulfurisation time was 45 minutes and above. Hence for further studies varying sulfurisation temperature, the sulfurisation time was fixed as 45 minutes.

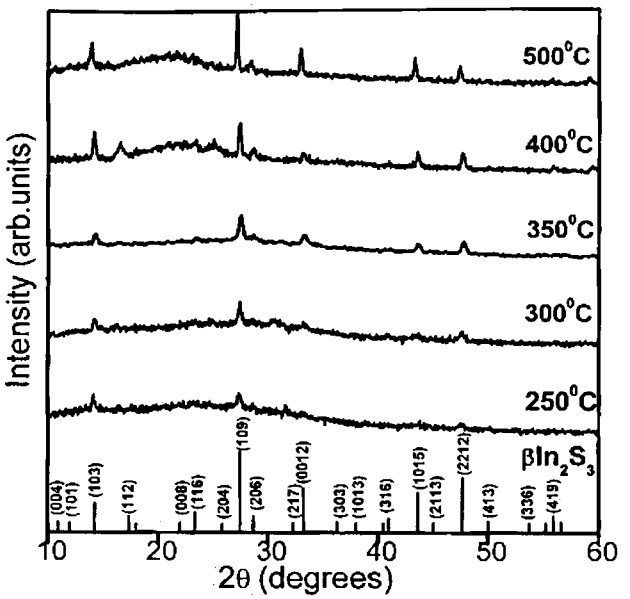

Figure 3.7 X-ray diffraction pattern of β–In_2S_3 prepared by the sulfurisation of indium films at various temperatures for 45 minutes.

The XRD pattern of In_2S_3 films prepared at different sulfurisation temperature for 45 minutes is shown in figure 3.7. X-ray diffraction studies show that sulfurisation of indium films at 300°C and above result in single-phase β- In_2S_3. When the films were sulfurised at 600° C, highly oriented In_2S_3 films were obtained (Fig. 3.8).

These films show (h 0 3h) peaks with small value of Full Width at Half Maximum for (103) peak (FWHM=0.264). These films show only (h 0 3h) reflections while the other films, which were prepared at lower sulfurisation temperature showed an orientation along (109) plane.

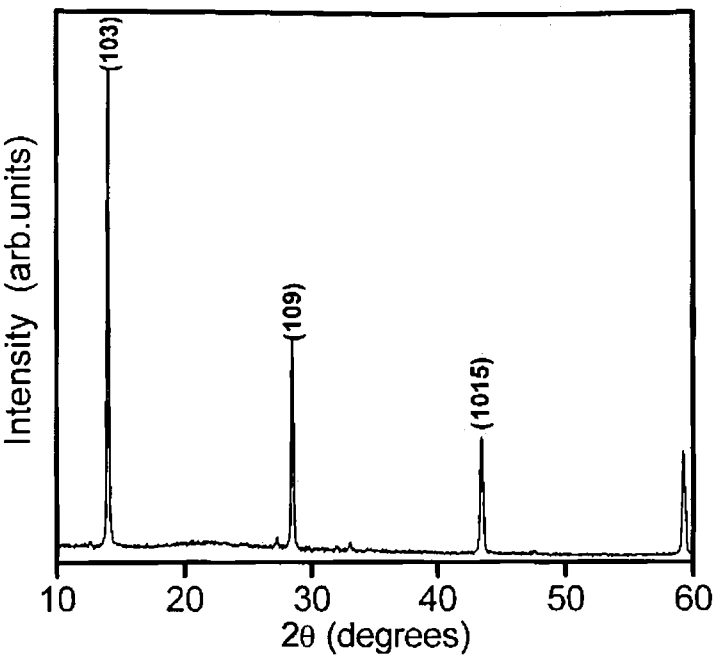

Figure 3.8 X-ray diffraction pattern of β–In_2S_3 prepared by the sulfurisation of indium films at 600^{0}C for 45 minutes.

Grain size of the indium sulfide thin films were calculated using the Scherrer's formula $t = 0.9\lambda/(\beta \cos\theta)$ where λ is the wavelength of the X-rays used, β is the full width at half maximum (FWHM) in radians for a particular peak and θ is the Bragg angle [53]. The grain size was found to be in the range of 20-30 nm irrespective of the process adopted for the sulfurisation. The lattice constants of the films were calculated and the calculated values of a and c (a = 7.8 A^0 and c = 32.61 A^0) are comparable with values for β-In_2S_3 crystals (a = 7.619 A^0 and c = 32.329 A^0) [7]. However the lattice parameters for the film are found to be slightly higher than that of the crystals. This may be due to excess sulfur (as

shown by EDX) percent in the films, which occupy the interstitial position of defect spinal structure causing lattice expansion.

S/In ratio of the prepared films has been calculated by the EDX measurement. All the films prepared have been found to have excess sulfur. It is observed that S/In ratio increases with increase of sulfurisation temperature upto 400° C and then it decreases (Fig. 3.9). The film sulfurised at 350°C has an S/In ratio 1.58 that is nearly stoichiometric.

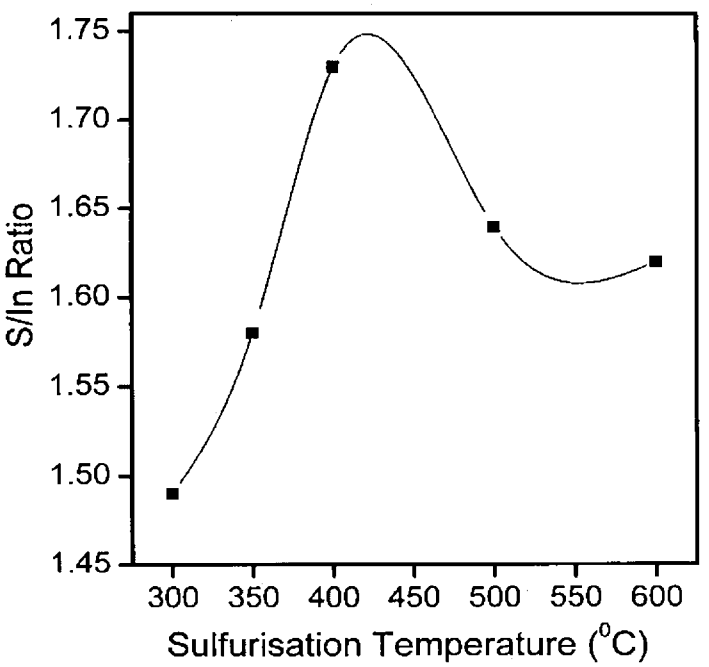

Figure 3.9: Variation of S/In ratio of In_2S_3 films with sulfurisation temperature.

The morphology of the indium sulfide thin films was examined by the Scanning Electron Microscope (SEM). The visual appearance suggests an outer rough surface of spherically structured grains for films sulfurised below 400°C for

the films prepared by rapid 2 and 9 cycles. The higher sulfurisation temperature (>400^{0}C) resulted in randomly distributed needle like particles covering the whole film surface (Fig. 3.10). Also the surfaces are found to be

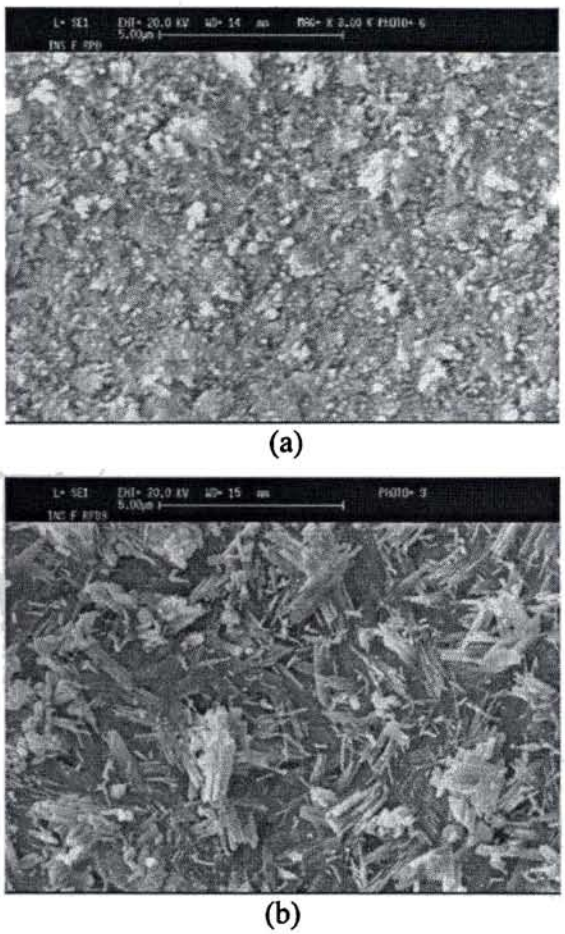

Figure 3.10 Surface SEM of β-In_2S_3 thin films sulfurised at 600^0 C
a) Rapid 2 process, b) Rapid 9 process

more orderly and closely packed for samples that were cooled to room temperature (9 hours) in the furnace itself. The grains are seen as spherically

structured for the films prepared by rapid 45 also, when the sulfurisation temperature is 350° C. As the sulfurisation temperature increases to 400° C the surfaces are found to be more orderly and closely packed (Fig. 3.11).

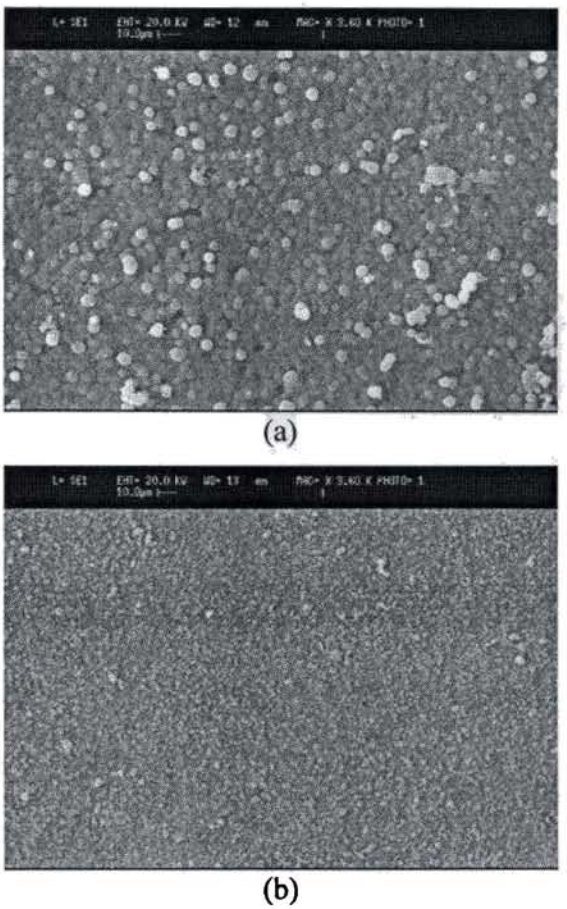

Figure 3.11 Surface SEM of β-In_2S_3 thin films prepared by Rapid 45 process , a) sulfurised 350^0 C b) sulfurised at 400^0 C

Films obtained are found to be formed of clusters when the sulfurisation temperatures are 500°C and 600°C (Fig. 3.12).

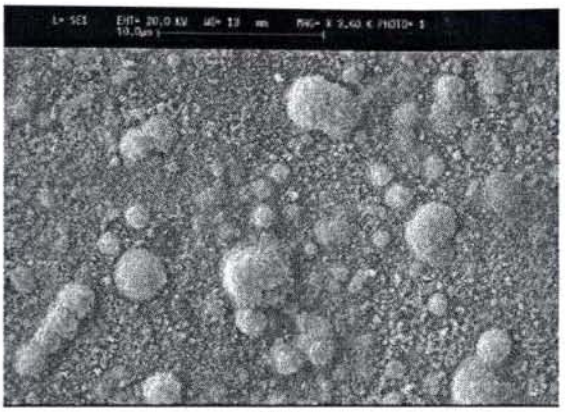

(a)

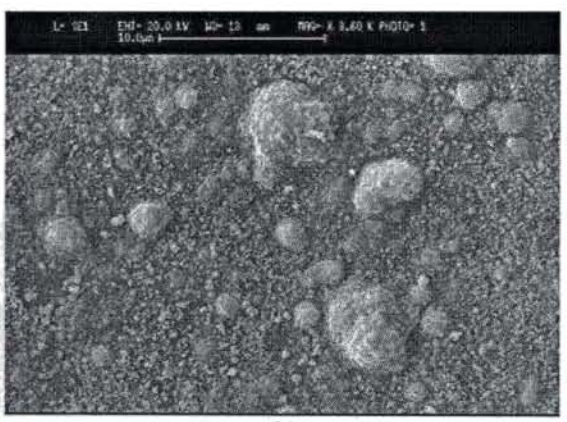

(b)

Figure 3.12 SEM micrographs of β-In_2S_3 thin films prepared by Rapid 45 process , a) sulfurised at 500^{0}C b) sulfurised at 600^{0}C.

3.5.2 Optical Characterizations

The optical energy gaps of β–In_2S_3 thin films were obtained from the optical transmission spectra in the wavelength range 300 to 2000 nm. The absorption

coefficient α was deduced from the transmission spectra using the relation $I = I_o e^{-\alpha t}$ where 't' is the thickness of the film.

The absorption edge of the β–In_2S_3 was examined using the relation given by Bardeen et.al [54]. The coefficient α is related to the incident photon energy hν as $\alpha h\nu = \beta(h\nu - E_g)^n$, where E_g is the energy gap and n=1/2 for direct transition. Figure 3.13 shows the plot of $(\alpha h\nu)^2$ as a function of the photon energy for the films sulfurised at different temperature for 45 minutes. The intercept of the linear portion on the energy axis at $(\alpha h\nu)^2$ eaqual to zero gives the band gap energy.

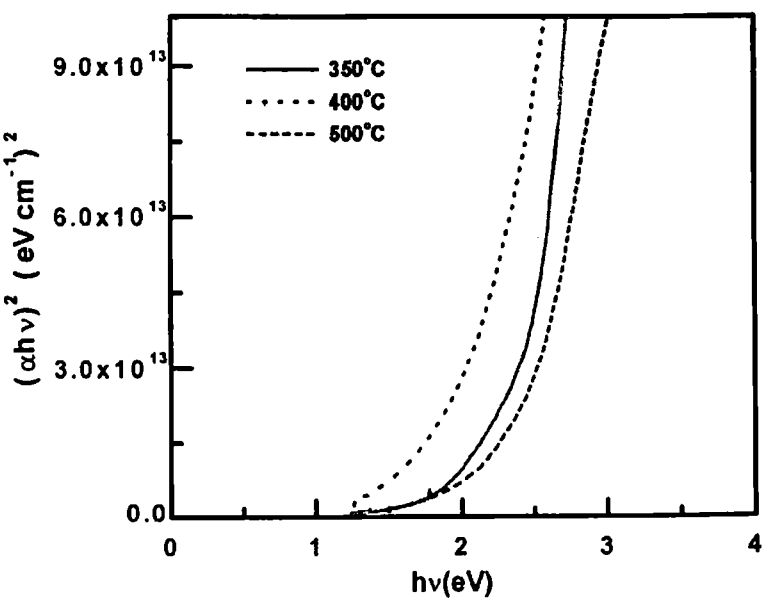

Figure 3.13 The plot of $(\alpha h\nu)^2$ vs the photon energy for β–In_2S_3 films prepared by Rapid 45 process at different temperatures.

The optical band gap measurements show that the sulfurisation temperature affects the band gap values of the films. Asikainen *et al* has reported the dependence of optical properties of β-In_2S_3 on the sulfurising parameter [3]. In

the present study the band gap of In_2S_3 films are found to be in the range of 2.37 to 2.58 eV, which depends on the sulfurisation temperature. The films sulfurised at 350°C which was nearly stoichiometric exhibit the higher band gap 2.58 eV. For the films sulfurised at 400^0 C and above the band gap is around 2.4 eV (Fig. 3.14), which agrees very well with values reported for β- In_2S_3 films prepared by SILAR technique [48].

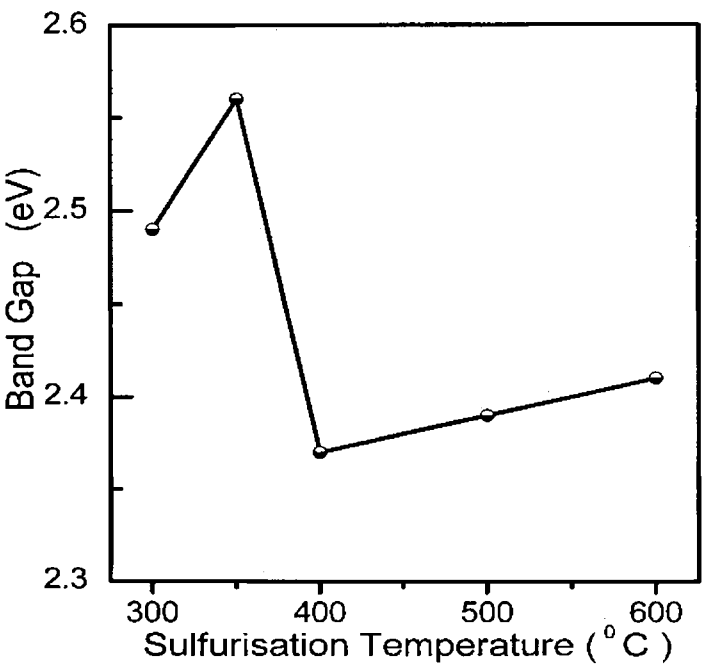

Figure 3.14 Variation of band gap of In_2S_3 films with sulfurisation temperature.

The optical band gap value of the films of In_2S_3 reported in the literature varied from 2 to 2.4 eV. Higher value of band gap (> 2.5eV) has also been reported. This broadening of band gap in In_2S_3 films has been explained with the help of different phenomenon. Kim et. al interpreted the band gap broadening of their thin films by the presence of excess sulfur in the bulk [24]. Other possibility for

band gap broadening can be attributed to the partial substitution of oxygen for sulfur to form $In_2S_{3-x}O_x$ [22]. Their study of the optical properties has shown that the band gap is higher than that of β- In_2S_3 when they contain oxygen. In the present study the possibility of the presence of traces of oxygen cannot be ruled out, however no oxides were detected by XRD or in the EDX spectra. The higher resistivity of the films also suggests the absence of oxygen impurities in the films. Another reason reported in the literature for the band gap broadening of the β- In_2S_3 thin films is on the basis of quantum size effect [25]. Yoshida *et al* have shown that the grain size has an influence on the band gap [14]. Though the average grain size of the films in the present study obtained from the XRD data are ~ 22 nm for a sulfurisation temperature below 400°C and ~30 nm at 400°C and above, the variation of the band gap of the films with sulfurisation temperature may be attributed to the quantum size effect. The sulfurisation at temperature 400°C and above causes an increase in the grain size to 30 nm and have the band gap lower compared to films sulfurised below 400°C. Similar observation of variation of band gap on annealing has been reported by Yousfi *et al* [21].

Table 3.1 Variation of thickness with sulfurisation time

Sulfurisation time	Thickness(nm)
10 minutes	546.61
45 minutes	527.1
I hour	471.2
2hour	451.4
3hour	419.5

The thickness of the In_2S_3 films were measured gravimetrically and it was observed that the thickness of films decreased with increase in the duration of sulfurisation time. The variation of thickness with the sulfurisation time is shown in the table 3.1.

3.5.3 Electrical characterizations

i. Resistivity by two probe method

Resistivity of the samples was calculated from the slope of the current voltage characteristics. The voltage was varied from 0 to 10 V and the corresponding current through the film was noted. A thin layer of silver was used as the electrode. The linear behavior of the I-V curve confirmed that silver forms an ohmic contact with the thin films.

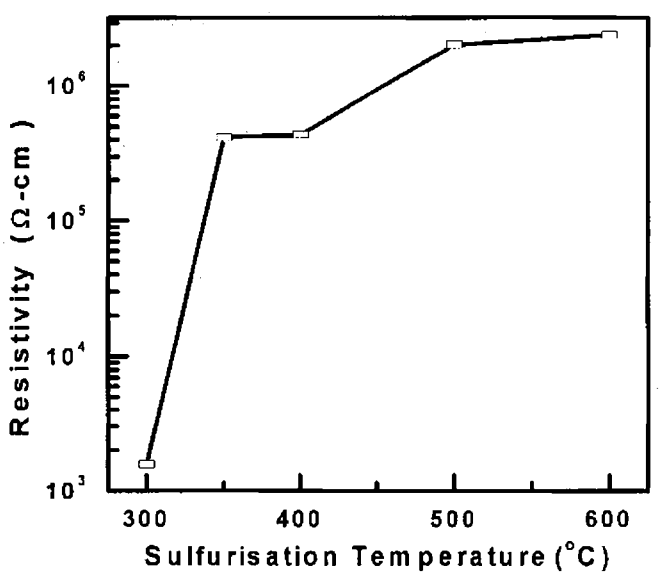

Figure 3.15 The plot of Resistivity (ρ) vs. Sulfurisation Temperature.

The resistivity (ρ) of In_2S_3 films is found to increase with sulfurisation temperature (Fig.3.15). The low resistivity values of In_2S_3 films prepared below 400°C may be due to the presence of impurity phases or incompletion of sulfurisation. At higher sulfurisation temperature the resistivity of β-In_2S_3 films are in the range of 10^6 Ω cm. Similar values have been obtained for ALE grown In_2S_3 films [3].

ii. Temperature Dependence of the Conductivity

The temperature dependence of the conductivity of the films was studied by measuring the variation in current I through samples at different temperatures ranging of 100K to 500K for a constant applied voltage of 12 V.

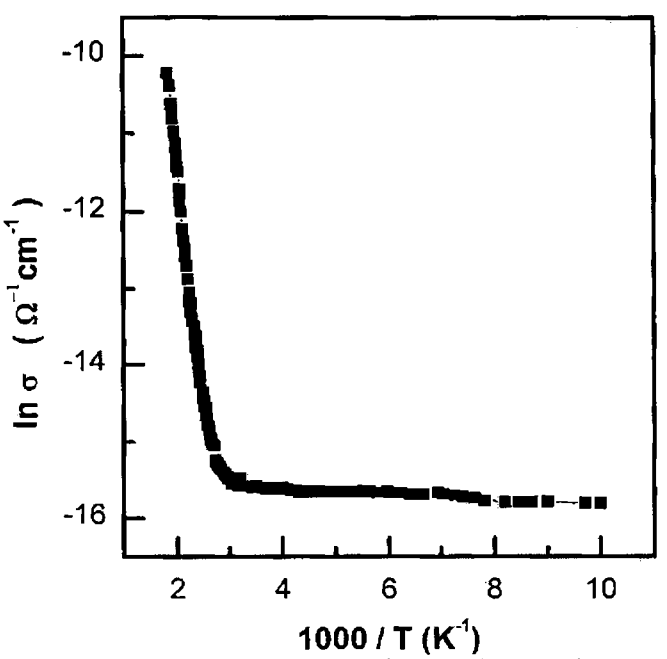

Figure 3.16: Temperature dependence of the conductivity for the films sulfurised at 500°

The conductivity is found to increase very slowly with temperatures in the low temperature range, but shows a rather sharp increase in the high temperature region. This is the typical behavior of a classical broad gap semiconductor. The plot of 10^3/T Vs ln σ is shown in figure 3.16.

The value of the activation energy E_a is evaluated from the plot $ln(\sigma)$ vs 1000/T using the relation [55]

$$\sigma = \sigma_0 \exp(-\frac{E_a}{kT})$$

where T is the absolute temperature and k is Boltzmann's constant.

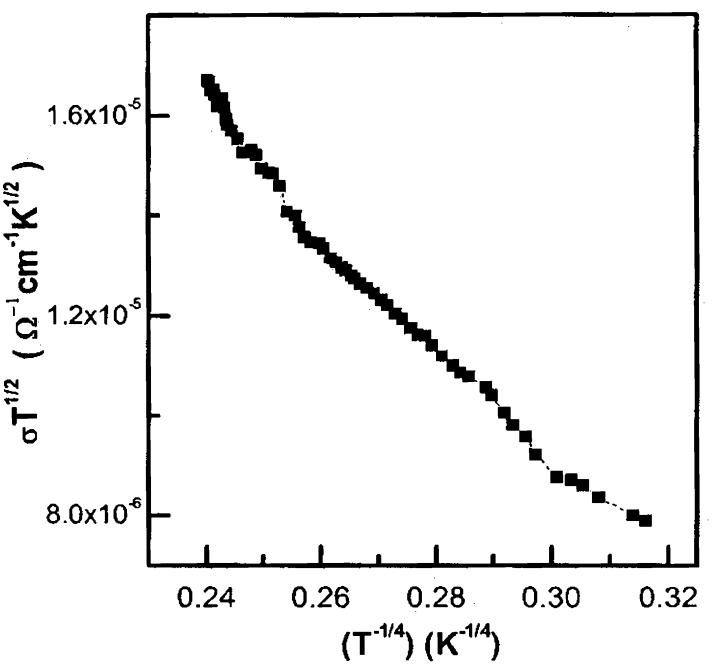

Figure 3.17: The plot of ln ($\sigma T^{1/2}$) vs $T^{(-1/4)}$ in the temperature range 100K to 300 K

The temperature dependence of the conductivity showed two distinct activation regions, a high temperature region above 150°C with an activation energy 0.6 eV and a lower temperature region with activation energy 0.3 eV. All the β-In_2S_3 films showed the same general trend, the change from low to high activation energy is a gradual one. The ln (σ) Vs 1000/T plot is not a well fit by a straight line.

The ln ($\sigma T^{1/2}$) Vs $T^{-1/4}$ plot is more close to a straight line (Fig.3.17) suggesting a variable range hopping in more appropriate [56].

iii. Photosensitivity

Figure 3.18 shows the variation of photosensitivity with the sulfurisation temperature. Photosensitivity ($\frac{I_L - I_D}{I_D}$) is the ratio of the difference between the illuminated current and dark current to the dark current. I_L is the current through the sample under illumination; I_D is the dark current. The measurement was carried out using Source Measure Unit. The samples were illuminated using tungsten halogen lamp. It is observed that photosensitivity increased with sulfurisation temperature. Maximum photo response was obtained for the highly oriented In_2S_3 films prepared by sulfurisation at 600 ° C. The increase in the photosensitivity can be attributed to the improvement in crystallinity with increase in sulfurisation temperature as indicated by XRD (Fig. 3.7 and Fig. 3.8).

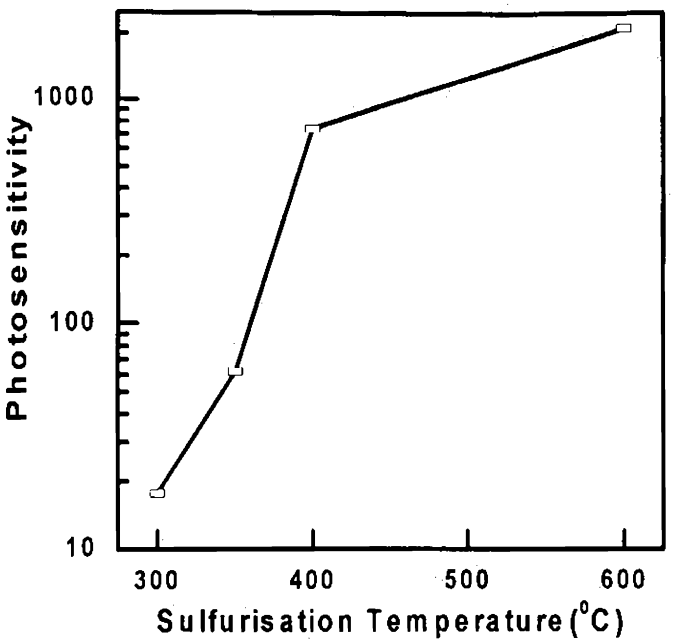

Figure 3.18: The variation of photosensitivity of In_2S_3 films with sulfurisation temperature

The type of carriers responsible for conduction in In_2S_3 films has been determined by the hot probe method and found to be n-type.

3.6 Conclusions

Single phase β-In_2S_3 thin films can be obtained by sulfurising the indium films above 300°C for 45 minutes. Low sulfurisation temperature requires prolonged annealing after the sulfurisation to obtain single phase β-In_2S_3. The slow cooling of the samples sulfurised at high temperature resulted in very smooth and closely packed surface. But considering the time consumption factor and the loss of indium by long duration of process, it can be concluded that the 45 minutes is the optimum duration of sulfurisation for the fabrication of a cost effective buffer layer for solar cell. The

thickness of the In_2S_3 films decreases with increase in sulfurisation time. The resistivity of β-In_2S_3 was found to increase from 10^2 to 10^6 Ω cm with the increase in the sulfurisation temperature. The maximum band gap of 2.58 eV was obtained for the β-In_2S_3 sample sulfurised at 350°C, which is nearly stoichiometric. This wider band gap, n type β-In_2S_3 can be used as an alternative to toxic CdS as window layer in photovoltaics. The β-In_2S_3 thin films can be used as the precursor for the preparation of $CuInS_2$.

References

[1] S. Spiering, D. Hariskose, M. Powalla, N. Naghavi and D. Lincot, *Thin Solid Films* **431-432**, (2003) 359.

[2] N. Naghavi, S. Spiering, M. Powalla, B. Cavana and D. Lincot, *Prog. Photovolt: Res. Appl.* **11** (2003) 437.

[3] T.Asikainen, M. Ritala and M. Leskela, Appl. Sur. Sci. **82/83** (1994) 122.

[4] T. Sakata, *Electro chem.solid letters* **3** (2000) 189.

[5] R. S. Becker, T. Zheng, J. Elton and M. Saeki, *Sol. Ener. Mater.***13** (1986) 97.

[6] Joint Committee on Powder Diffraction Standards ,Card 5-731

[7] Joint Committee on Powder Diffraction Standards ,Card 32-456

[8] Joint Committee on Powder Diffraction Standards ,Card 25-390

[9] Joint Committee on Powder Diffraction Standards ,Card 33-623

[10] H. Habin and W. Klinger, Anorg .Allg. Chem. **97**(1949) 260.

[11] R. Diehl and R. Nitsche, J. Cryst. Growth **20** (1973) 38.

[12] K. Kambas, A Anagnosto Poulose, S. Ves, B. Ploss and J. Spyridelis, *Phys. Stat. Solidi. (b)***127** (1985) 201.

[13] K. Kambas, J. Spyridelis and M. Balkanskr, *Phys. Stat. Solidi. (b)* **105** (1981) 291.

[14] T. Yoshida, K. Yamaguchi, H. Toyoda, K. Akao, T. Sugiura and H. Minoura, *Proc. of Electrochem. Soc*, Electrochemical Society, Pennington, NJ **97-20** (1997) 37.

[15] J. M. Gilles, H. Hatwell, G. Offergeld and J. Van Cakenberghe, *Phys. Stat. Sol.* **2** (1962) K73.

[16] W. Rehwald and G. Harbeke, *J. Phys. Chem. Solids* **26** (1965) 1309.

[17] G. S. D King *Acta Cryst.* **15** (1962) 512.

[18] C. J. M. Rooymans, *J. Inorg. Nucl .Chem* **11** (1959) 78.

[19] J. George, K.S Joseph, B. Pradeep and T.I. Palson, *Phys. Stat. Solidi. A* **106** (1998) 123.

[20] G. Kaitev, V. Dvoinine, A. Oustiantseva, M. Bieliaieva and L. Skorniakov, *Neorg. Mater.* **12** (1976)1760.

[21] E. B. Yousfi, B. Weinberger, F. Donsanti, P. Cowache and D. Lincot, *Thin Solid Films* **387** (2001) 29.

[22] N. Barreau, S. Marsillac, Dalbertini and J. C. Bernede, *Thin Solid Films* **403-404** (2002) 331.

[23] N. Barreau, J. C. Bernede and S. Marsillac, *Journal of Crystal Growth* **241** (2002) 51.

[24] W. T. Kim and C. D. Kim, *J.Appl.Phy.***60** (1986) 2631.

[25] Y. Yasaki, N.Csonoyama and T.Sakata, *J. Electroanal.Chem.***469** (1999) 215.

[26] A. Timoumi, H. Bouzouita, M. Kanzari and B. Rezig, *Thin Solid Films* **480–481** (2005) 124.

[27] N. Kamaoun, R. Bennaceur, M. Amlouk, S. Belgacem, N. Mliki, J.M. Frigerio and M.L. Theye, *Phys. Stat. Sol (A)* **169** (1998) 97.

[28] W. Rehwald and G. Harbeke, *J. Phys. Chem. Solids* **26** (1965) 1309.

[29] V.G. Bessergenev, E. N. Ivanova, Yu. A. Kovalevskaya, S.A. Gromilov, V. Nkirichenko and S. V. Larinov, I*norg. Mater.***32** (1996) 592.

[30] N. Barreau, J. C. Bernede, S. Marsillac, C. Amory and W. N. Shafarman, *Thin Solid Films* **431-432** (2003) 326.

[31] K. Yamaguchi, T. Yoshida and H. Minoura, *Thin Solid Films* **431-432** (2003) 354.

[32] B. Yahmadia, N. Kamouna, , R. Bennaceura, M. Mnarib, M. Dachraouib and K. Abdelkrim, *Thin Solid Films* **473** (2005) 201.

[33] T. Yoshida, K. Yamaguchi, H. Toyoda, K. Akao, T. Sugiura and H. Minoura, *Proc. of Electrochem. Soc* (Photoelectrochemistry), Electrochemical Society, Pennigton, NJ, **97-20** (1997) 37.

[34] Paul O'brien and D. J. Otway, J. R. Walsh, *Thin Solid Films* **315** (1998) 57.

[35] L. Bhira, H. E. Essaidi, S. Belgacem, G. Couturier, J. Salardenne, N. Barreaux and J.C Bernede, *Phys. Stat. Solidi* **181** (2000) 427.

[36] T. T. John, S. Bini, Y. Kashibaba, T. Abe, Y. Yasuhiro, C. S. Kartha and K.P. Vijayakumar, *Semicond. Sci. Technol.* **18** (2003) 1.

[37] N. Barreau, J. C. Bernade, H. El. Maliki, S. Marsillac, X. Castel and J. Pinel, *Solid State Commun.* **122** (2002) 445.

[38] E. B. Yousfi, J.Fouache, D.Lincot, *Appl .Surf. Sci.* **153**(2000) 223.

[39] E. B Yousfi, T. Asikainen, V. Pietu, P. Cowache, M. Powalla and D. Lincot, *Thin Solid Films* **361-362** (2000) 183.

[40] R. Kumaresan, M. Ichimura, N. Sato and P. Ramasay, *Materials Science and Engineering* **B96** (2002) 37.

[41] N. Barreau, S. Marsillac and J.C Bernede, *Vacuum* **569** (2000) 101.

[42] C. Kaito, A. Ito, S. Kimura, Y. Kimura, Y. Saito and T. Nakada, *Journal of Crystal Growth* **218** (2000) 259.

[43] N. Barreau, S. Marsillac, J. C. Bernede, T. Ben. Nasrallah and S. Belgacem, *Phys. Stat. Solidi.* **184** (2001) 179.

[44] J. Herrero and J. Ortega, *Solar Energy Materials* **17** (1988) 357.

[45] J. C. Bernede, N. Barreau S. Marsillac and L. Assman, *Appl. Surf. Sci.* **195** (2002) 222.

[46] D. Hariskose, R. Herberhots, M. Ruckh, U. Ruhle, R. Schaffler and H. W. Schock, *13th European PV Solar Energy Conference* (Epsec), Nice, (1995).

[47] G. A. Kitaev, V. J. Duoinin, A. V. Ustyantseva, M. N. Belyaeva and G. Skorgakw, *Neorg.Mater.* **12** (1976) 1760.

[48] D. Braunger, D. Hariskos, T. Waltre and H.W. Schock, *Sol. Energy Mater. Sol. Cells*, **40** (1996) 97

[49] R.S. Mane and C. D. Lokhande, *Mater. Chem. Phys.* **78** (2002) 15.

[50] S. Gall, N. Barreau, S. Harel, J.C. Berne'De and J. Kessler, *Thin Solid Films* **480-481** (2005) 138.

[51] S. Spiering, A. Eicke, D. Hariskos, M. Powalla, N. Naghavi and D. Lincot, *Thin Solid Films* **451–452** (2004) 562.

[52] Joint Committee on Powder Diffraction Standards, Card 190588

[53] B. D. Cullity and S. R. Stock, *Elements of X-Ray Diffraction*, Printice Hall, N.J. (2001) p.388.

[54] J. Bardeen, F. J. Blatt, and L. H. Hall, *Proc.of Conference on Photoconductivity,* New York, Wiley, (1956) p.146.

[55] C. Guillen and J. Herrero, *J. Appl.Phys.* **71** (1992) 5479.

[56] N. F. Mott, *Metal Insulator Transitions,* 2nd edition, Taylor & Francis, London (1990) p.52.

Chapter 4

Preparation and Characterisation of Copper Indium Selenide Absorber Layer

The key component of the solar cell is the polycrystalline absorber film. The heterojunction is formed between the p-type absorber film and the n-type layer. The efficiency of a solar cell depends mainly on the amount of incident light absorbed by the material. This device characteristic is determined by the crystal structure and characteristics of the absorber layer.

The essential characteristics of a typical absorber layer are, it should

- *Be p-type*
- *Possess high absorption coefficient*
- *Have good carrier life time*
- *Have direct band gap*
- *Be non toxic*

4.1 Introduction

Current emphasis in photovoltaic is directed towards the development of high performance inexpensive solar cells that can serve in the long term as viable alternatives to the single crystal silicon technology. Foremost among those materials that have emerged as leading candidates are the I-III-VI_2 and II-IV-V_2 group semiconductors based solar cells. Of the I-III-VI_2 group that are of particular interest are $CuInX_2$ (X = S, Se, Te). Among the variety of $CuInX_2$ materials interest in $CuInSe_2$ (CIS) dates back to the work of Wagner *et al* [1]. It has proven to be a promising absorber material for high efficiency photovoltaic devices since it possesses the following useful properties (*i*) it has a direct band gap about 1.02 eV at room temperature, which is in the energy range for optimum solar conversion;(*ii*) it can be doped easily either n or p type by varying the Cu/In ratio and thus permits the formation of homo junctions and several types of hetero junctions; and (*iii*) it has high quantum efficiency and good thermal stability [2]. But the photovoltaic interest in $CuInSe_2$ and related compounds is mainly due to the extremely high absorption coefficient, possessed by these materials (Fig. 4.1). This high value of α (10^5 cm^{-1}) implies that 99% of the incoming photons are absorbed within the first micrometer of the material. As a result, only about 1μm of this material is required to effectively absorb all the incoming photons and hence reduce the consumption of raw materials. The material properties can be varied by replacing part of the indium by gallium and/or part of the selenium by sulfur to form $Cu(In,Ga)(S,Se)_2$ [3].

Interest in CIS based solar cells considerably increased with the report of 10% efficient cells in 1982 by three source evaporation [4]. Conversion efficiencies

higher than 19.2% have been achieved using these materials [5] until this date. CIS-based solar cells are very stable, and thus their operational lifetimes are long. CIS-based thin films can be prepared both from gas and liquid phases by a variety of methods.

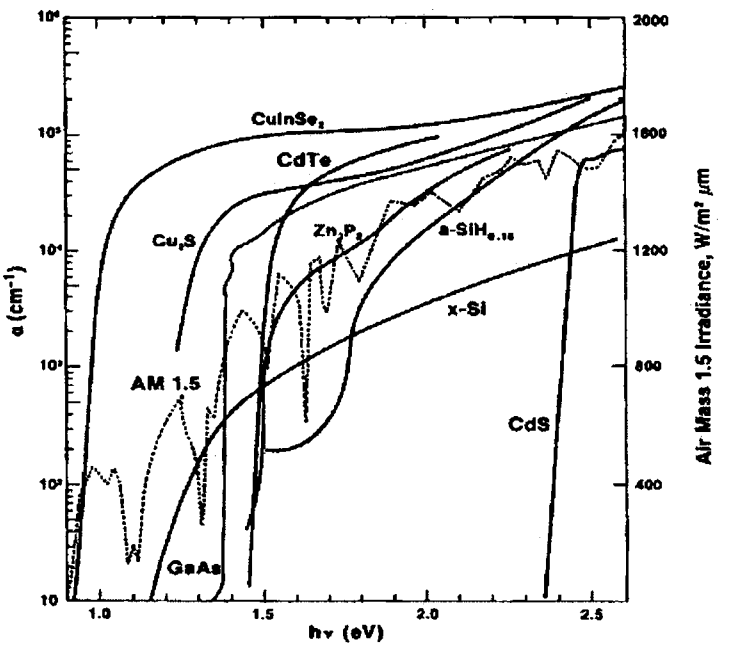

Figure 4.1 Absorption spectrum of $CuInSe_2$ compared with other photovoltaic semiconductors [6].

4.2 Material Properties of $CuInSe_2$

4.2.1 Crystallographic Structure

$CuInSe_2$ is a member of the family of I-III-VI_2 (ABX_2) chalcopyrite semiconductors. The ABX_2 chalcopyrite crystal structure resembles the zinc-blende structure in that each of the two cations A and B are coordinated tetrahedrally by four anions X (Fig. 4.2), but the anion is coordinated by 2A+2B,

with generally dissimilar neighbourhood bond lengths $R_{AX} \neq R_{BX}$. The unit cell is thus tetragonal [7]. The primitive cell for this structure is made up of eight tetrahedrons with shared vertices, so that the whole cell is just two stacked cubic structures. By convention, the short edge is labelled *a* and the long edge is labelled *c*.

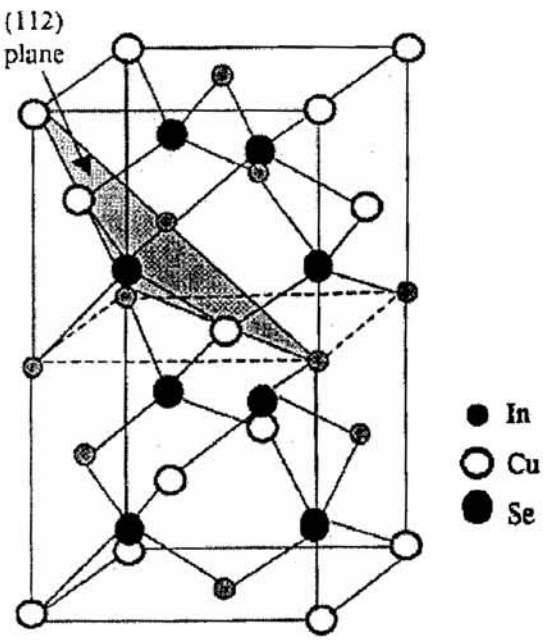

Figure 4.2 Chalcopyrite crystal structure

In $CuInSe_2$, each group I (Cu) or group III (In) atom has four bonds to the group VI atom (Se). In turn each Se atom has two bonds to Cu and two to In. The tetrahedral structure becomes distorted due to differing bond strength between I-VI and III-VI atoms. Hence the ratio of the lattice constant c/a is not exactly two. It varies from 2.01 to 1.96. For $CuInSe_2$, the lattice parameters are, a = 0.5789 nm and c = 1.162 nm. The different bond strengths make the anion (Se)

to adopt an equilibrium position close to any one pair of the cation than to other, causing anion displacement and the unequal bond length.

4.2.2 Phase Diagram

The phase diagrams of $CuInSe_2$ have been extensively investigated by Godecke et.al. [8]. The phases for the Cu-In-Se system are represented either by ternary phase diagrams or pseudo binary phase diagrams. Pseudo binary representations were chosen to simplify presentation, since the system in question tends to exist along pseudo binary tie lines. The figure 4.3 shows the pseudo binary phase diagram for the Cu-In-Se system.

According to this phase diagram, four different phases are likely to occur in this ternary system. They are: the alpha phase ($CuInSe_2$), the beta phase ($CuIn_3Se_5$), the delta phase (the high temperature sphalerite phase) and $Cu_{2-y}Se$. The phase adjacent to the alpha phase has a similar structure. The beta phase is actually a defect chalcopyrite phase build by ordered arrays of defect pairs.

At room temperature alpha phase extend from a Cu content of 22% to 24.5%. Thus the range of copper percentage for a single phase $CuInSe_2$ is very small not even 25% of Cu. For efficient thin film solar cells the Cu content varies between 22 and 24%. This range lies within the single phase region of the alpha phase at the temperature 500 – 550°C. At room temperature it lies in the alpha + beta region. Thus there is a tendency for phase separation in $CuInSe_2$ after deposition.

Although phase diagram shows a relatively small range for single phase $CuInSe_2$, the partial replacement of In with Ga as well as the use of Na containing

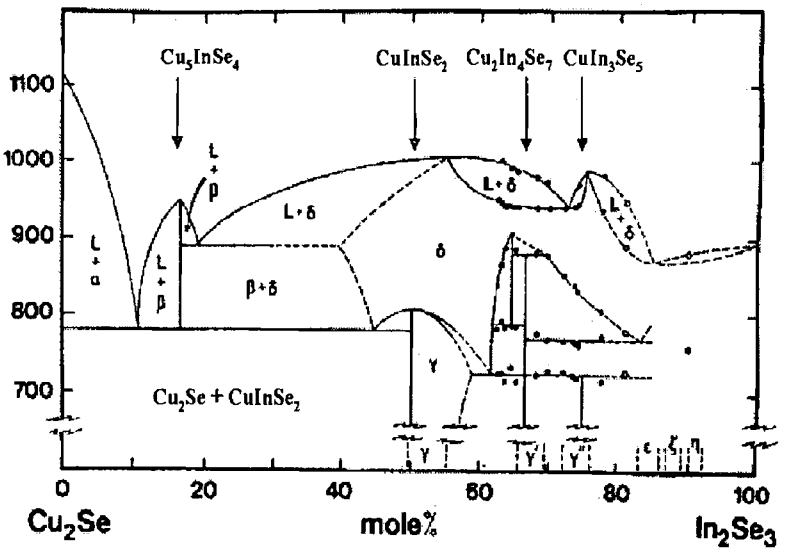

Figure 4.3 Cu_2Se-In_2Se_3 pseudobinary phase diagram[9].

substrates considerably widens the single phase region. The Ga is able to diffuse by a vacancy mechanism through either Cu or In vacancies, the addition of Ga to pure $CuInSe_2$ increases the band gap [10].

4.2.3 Optical and Electrical Properties

The performance characteristics of polycrystalline $CuInSe_2$ materials are highly dependent on their stoichiometric composition, defect chemistry and structure which in turn are strongly related to the film growth parameters. They are also critically influenced by the presence of secondary phases in the bulk of the material. The following sections deal with how these parameters affects the properties of $CuInSe_2$ thin films.

$CuInSe_2$ thin films possess band gap energy equal to 1.1 eV. Early measurements of the band gap of single crystalline $CuInSe_2$ exhibited nominal

disagreements [11], suggesting a value in the range of 1.02 to 1.04 eV [12]. Optical characterisation of polycrystalline $CuInSe_2$ absorber films, suitable for devices, almost always indicates a significantly lower effective band gap of approximately 0.9 eV [13]. These variations in the optical properties of $CuInSe_2$ materials are a direct consequence of variations in stoichiometry. Intragranular vacancies have also been shown to affect the optical band gap [14].

The studies of Rockett *et al* [15] have shown the presence of secondary phases and segregated layers on the surface of polycrystalline films grown by physical vapor deposition changes the conductivity in the order of magnitude. The presence of secondary phases at grain boundaries also causes sub band gap absorption [16]. It has been reported that an addition absorption other than the main absorption edge [17] due to the secondary impurity phases such as Cu_xS contribute at energies below band gap as well as transitions from acceptor levels to the conduction band.

The variation of absorption coefficient with the In/Cu ratio has been studied [18]. The indium rich films had high energy gaps. They explained it as, when In/Cu ratio increases, indium occupies some of the copper sites, resulting antisite defects. Since the size of the indium atom is larger than that of copper, this effect would lead into an increase in band gap. There is also report that, the samples having lower In/Cu ratio would absorb low energy photons more effectively than those having higher In/Cu ratio [19].

Electrical properties of $CuInSe_2$ thin film depend strongly upon the stoichiometry, preparation methods, and substrate temperature during deposition of the films. When the Se content is low, the films show p-type and low conductivity for high Cu/In ratio, and n-type and high conductivity for low

Cu/In ratio. For high Se content, the film show p-type but larger conductivity for high Cu/In ratio, while n-type and smaller conductivity for low Cu/In ratio [20]. The resistivity of $CuInSe_2$ can be varied from 10^{-2} to 10^4 Ω cm depending on the Cu/In ratio and the preparation conditions [21]. In situ conductivity measurements during the growth of $CuInSe_2$ films have been carried out by Alt *et al* [22]. It was found from the σ vs. 1/T plot that for In rich films, a formation of band bending occurs at grain boundaries.

4.2.4 Effect of Temperature

The formation of a thin p-type $MoSe_2$ layer between the Mo and the absorber that occurs during the absorber preparation at sufficiently high temperatures [23, 24] is found beneficial for the cell performance for several reasons. First, it forms a proper ohmic back contact. The Mo/$CuInGaSe_2$ contact without the $MoSe_2$ layer is not ohmic but a Schottky type contact that causes resistive losses [25]. The second advantageous consequence of the $MoSe_2$ interface layer is improved adhesion of the absorber to the Mo back contact. Another advantage is, since the band gap of $MoSe_2$ is wider (about 1.4 eV) than that of a typical $CuInSe_2$ absorber, it reduces recombination at the back contact, providing simultaneously a low-resistivity contact for holes [26]. The $MoSe_2$ layer also prevents further reactions between $CuInGaSe_2$ and Mo.

A moderate inter diffusion of CdS and $CuInSe_2$, which occurs to some extent at high annealing temperature [27] is potentially beneficial to the cell performance.

Guillen and Herrero have identified a variable range hopping conduction mechanism taking place at very low temperatures and a thermally activated conductivity over the grain boundaries at temperatures close to the room

temperature. The heat treatment of the films involves an increase in the conductivity and a decrease in the thermal activation energy [28].

A detailed study on phases formed during the production of $CuInSe_2$ grown by reacting the stalked layers of Cu, In and Se were carried out by Sachan *et al* [29]. They obtained the elemental phases of In and Se with the phases of $CuSe_2$ and $Cu_{11}In_9$ for low reaction temperature. But temperature above 215° C the peak corresponding to Se was observed in the XRD pattern. At temperature 235° C and above $CuInSe_2$ appeared as the main peak in the XRD pattern and single phase $CuInSe_2$ obtained at reaction temperature of 400° C.

Detailed study on the evaporation temperature on properties of the film prepared by vacuum evaporation was explained in the work of Isomura *et al* [30]. For application as an absorber layer in a high efficiency solar cell, a $CuInSe_2$ film needs to have a long diffusion length and long minority carrier life time. Large grain size, uniform morphology and non existence of a second phase are required for this purpose. Kim *et al* have reported that the film obtained by selenization of Cu/In precursors at low vacuum satisfied these conditions [31].

4.3 Various Deposition Methods for $CuInSe_2$ Thin Film Preparation

The success of photovoltaic energy conversion depends on the availability of low cost, large area solar cell modules. Recent progress was achieved by the systematic investigations and optimization of the basic production processes of different technologies. Varieties of methods have been experimented to grow $CuInSe_2$ thin films like molecular beam epitaxy [32], flash evaporation [33], multi-source evaporation [34], single-source evaporation [35], RF sputtering [36],

spray pyrolysis [37, 38], electrodeposition [39], and selenization of metallic film [40-45].

$CuInSe_2$ film formation can be divided mainly into two major categories (1) those where Se is incorporated with the metals during material delivery (2) processes where the metals are delivered separately from Se. Co evaporation, electrodeposition, sputtering etc are included in the first category while the second one indicates the two stage process which involves deposition of the precursor metal and subsequent reaction with selenium to produce $CuInSe_2$.

Sputtering offers simple and flexible control over film stoichiometry. Characterisation of $CuInSe_2$ films prepared by sputtering has been reported by He *et al* [46].

On the basis of economic considerations, preparation of $CuInSe_2$ by electrodeposition seems attractive. Electrodeposition of CIS-based thin films has been studied extensively by several groups [47, 48] since 1983 when Bhattacharya published the first paper on one-step electrodeposition of $CuInSe_2$ thin films [49]. The films prepared by this method in general revealed a microcrystalline or amorphous phase with widely differing stoichiometry. The studies of Chaure and co workers showed that the conversion from p type to n type conductivity varies as deposition cathodic voltage increased from low to high values [50].

Vacuum deposition has its merit of simplicity of preparation. Evaporation processes can be applied to $CuInSe_2$ growth. Evaporation by two sources, evaporation by three sources and the two stage process are the some of the thermal evaporation techniques used for the growth of $CuInSe_2$ thin films. The two stage process and the evaporation by three sources have certain advantages

over other techniques in terms of stoichiometry control, hence preferred nowadays. The most successful absorber deposition method for high efficiency small-area devices seems to be the three-stage co evaporation of $CuInSe_2$ from elemental sources in the presence of excess Se vapor [51]. However, poor material utilization and the difficulty of obtaining uniform material fluxes over large area substrates are some of the concerns related to scaling this method to a high production level [52]. So recent research are going on the development of a relatively easily scalable two stage deposition technique, to produce uniform coatings of thin films on large area substrates.

The two stage process which includes the selenization of precursors such as Cu/In alloy [53] also offers great advantages in terms of low cost of production. This technology forms the basis for commercial products now being developed by Siemens Solar Technologies. The potentials for large area compositional uniformity and control of the ratio of Cu/In by thermal evaporation followed by selenization results in $CuInSe_2$ films suitable for solar cell application [54].

A solar cell fabricated with absorber layer grown by two stage process has attained an efficiency of 9.8% [55]. For the production of $CuInSe_2$ by two stage method, the detailed investigations of phase formation process in Cu-In bilayers have been reported in literature. Cu-In alloys are known to exist in different phases and compositions ranging from pure copper to pure indium [56]. The deposition of single phase precursor is not possible by sequential evaporation of the metals. The heating up of the film is necessary for diffusion reactions leading to the formation of $CuIn_2$, $Cu_{11}In_9$ and at higher temperature Cu_7In_3 [57].

4.4 Experimental Details

$CuInSe_2$ thin films were made by cost effective two stage process. Two stage process involves deposition of Cu-In precursors in the first step followed by their selenization using H_2Se gas or Se vapour in the second stage. In this technique, both steps, the precursor preparation and the selenization, are important for the quality and the adherence of the $CuInSe_2$ film onto substrate. Selenization of the Cu-In precursors have utilized H_2Se gas or Se vapour. The use of H_2Se gas has been considered environmentally unfriendly due to its toxic nature [58]. In addition, there are problems relating to rapid volume expansion leading to poor adhesion of the film onto the Mo back contact, and In loss resulting from the complexity of reaction kinetics that is the interdiffusion of intermediate phases which leading to poor quality films. Hence, in this work, selenization was achieved using elemental Se.

4.4.1 Preparation of $Cu_{11}In_9$ Alloy

For the preparation of the $CuInSe_2$ (CIS) by two-stage process, the first step is the preparation of $Cu_{11}In_9$ precursors. It is achieved by the annealing of Cu-In bilayers in vacuum. Cu-In bilayer was deposited on glass and Mo substrates by thermal evaporation in high vacuum chamber at a pressure of $3x10^{-6}$ mbar. High purity metals of copper (99.99%) and indium (99.999%) were evaporated from molybdenum boats. The thickness of the In layer was maintained at 400 nm and that of Cu layer varied to obtain various Cu/In ratios. Both depositions were carried out at room temperature. The deposition rate and thickness of individual layers were carefully controlled and measured using an oscillatory quartz crystal monitor located at a position close to the substrate. The film obtained after

selenization was found to be less adhesive. So for better adhesion of CIS, a thin layer of gallium of thickness 10 nm was deposited prior to indium deposition.

The Cu-In bilayer thin films thus prepared were annealed at different temperatures varying from 153^{0}C to 200^{0}C in high vacuum of 3×10^{-6} mbar for 2 hours. The optimum temperature found was 153^0 C. The choice of this temperature is based on the phase diagram (Fig. 4.4) of Cu-In by Subramanian *et al* [59]. The annealing temperature below 153° C resulted in incomplete reaction while temperature above 153°C resulted in loss of indium.

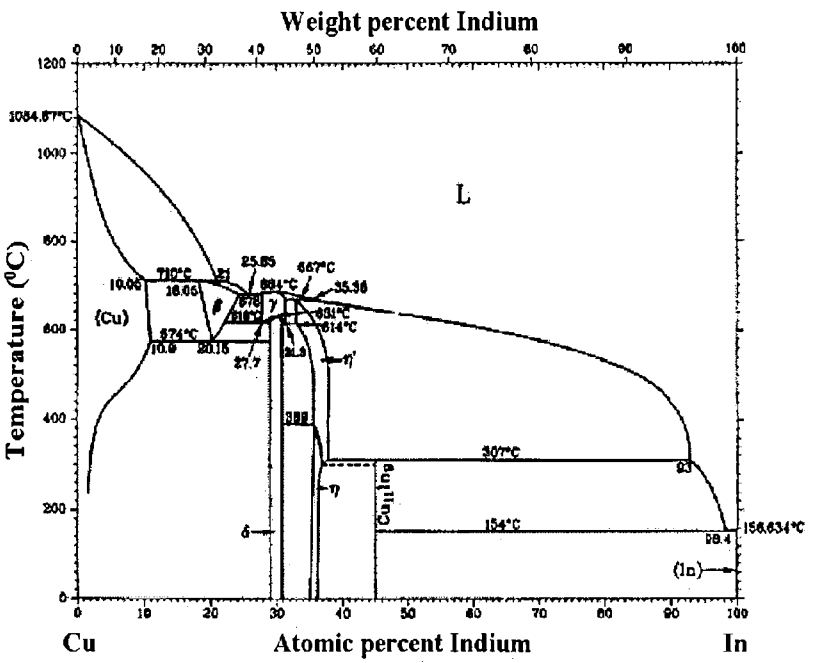

Figure 4.4 Cu-In binary phase diagram

4.4.2 Chalcogenisation

In the second stage, the precursors were removed from vacuum and exposed to an atmosphere of selenium using N_2 as carrier gas in a horizontal quartz tube provided with a specially designed furnace, which allowed rapid heating and cooling of samples. A thermal cycle consisting of rapid heating and cooling of samples was selected for selenization since the slow heating and cooling cycle had been resulted in indium loss. The Se granules were used as the selenium source since the H_2Se gas is toxic. The Se granules were heated separately and N_2 gas is passed through the chamber to carry the selenium vapour to the reaction zone. The complete details of the selenization system are described in the chapter 2. The selenization was carried out for different duration such as 1, 2 and 3 hours. The structural studies were performed for optimising the reactive annealing time for the formation of single phase $CuInSe_2$ film. After optimising the duration of selenization, studies on the effect of annealing temperature were studied. The selenization temperature at the reaction zone was varied from 250° C to 400° C. The other parameters like duration of selenization and heating profiles were kept constant. The temperature was monitored by a thermocouple attached to the furnace. After optimising the selenization temperature and duration of selenization as 350° C and 3 hours respectively, the experiments were repeated using precursor of various Cu/In ratios.

Crystallinity of the prepared alloys and films were measured using X-ray diffractometer with Cu-K_α radiation. The surface morphology and composition of the films were evaluated using the scanning electron microscopy (SEM) technique and energy dispersive X-ray spectroscopy (EDX) respectively. Optical transmittance measurements have been performed using UV-VIS-NIR

spectrophotometer. The electrical properties of the films were investigated by current–voltage measurements.

4.5 Results and Discussions

4.5.1 Structural Characterisations

Structural characterisation of the Cu-In precursors was carried out using XRD. The Cu-In alloy deposited over glass, molybdenum and the gallium coated molybdenum substrates were analysed.

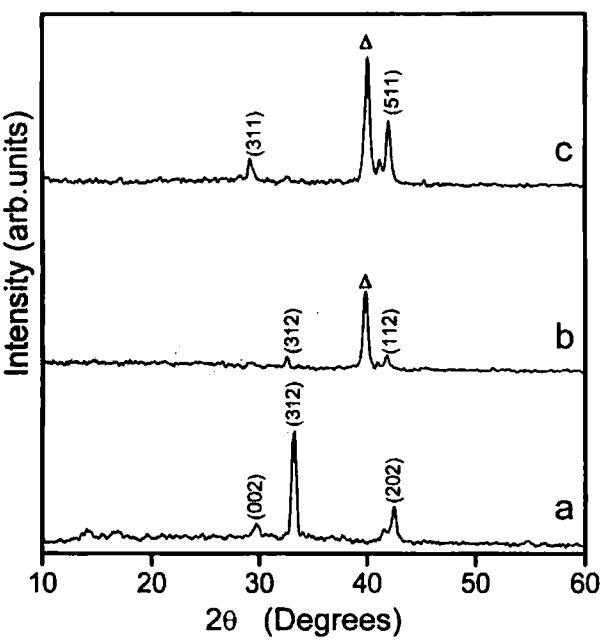

Figure 4.5 XRD patterns of the Cu-In precursor layer coated over (a) glass, (b) Molybdenum and (c) Gallium coated over Molybdenum substrates. Δ Indicates (110) peak of Molybdenum substrate.

Figure 4.5 shows the XRD pattern of the Cu-In precursor layer grown over glass, molybdenum and gallium coated molybdenum substrates. All the major

peaks can be indexed to that of $Cu_{11}In_9$ which indicating a good mixing of elemental species. For Cu-In deposited over glass the main reflection was from (312) plane. For Cu-In grown over Mo the grains were randomly oriented showing reflections from (312) and (112) planes. When a thin layer of gallium was introduced between Molybdenum and Cu-In layer, major reflection peak in the XRD was that from (511) plane of $Cu_{11}In_9$ alloy.

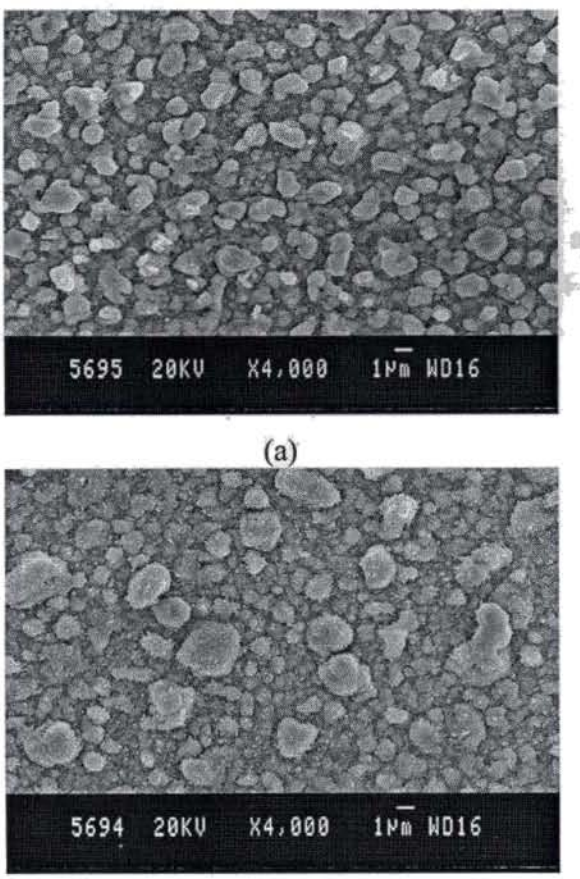

Figure 4.6 Surface morphologies of (a) Mo/CuIn, (b) Mo/Ga/CuIn

The SEM results shows that the CuIn alloy on Mo are consisted of a smooth surface. The size and number of particles changed when gallium layer is introduced prior to the Cu and In bilayers (Fig. 4.6).

The XRD patterns of samples selenized at 350° C for different duration of 1, 2 and 3 hours are studied in detail (Fig. 4.7). It is known from the studies performed by Agnihotri *et al*, Szot *et al* and Don *et al* that the diffraction patterns of $CuInSe_2$ polycrystalline thin films having chalcopyrite structure have peaks at 26.6, 27.8, 35.6, 42, 44.4, 52.5, and 71 for 2θ and these peaks correspond respectively to the reflections from the (112), (211), (105)/(203), (220)/(224), (116)/(312), and (316) planes [60-62]. It was seen from the diffraction pattern of sample selenized for 3 hours that the peaks 27, 35.85, 42.15, 44.45, 52.75 and 71.7 were observed here too. The other samples formed by selenization for 1 hour and 2 hours also showed similar XRD spectra. But for the samples selenized for 1 hour, some peaks of $Cu_{11}In_9$ and In_2Se_3 binary peak were identified in addition to $CuInSe_2$ phase. When the duration of selenization was increased to 2 hours, then the In_2Se_3 peak was not and $CuInSe_2$ peak (200) was observed. Single-phase $CuInSe_2$ thin films were obtained for samples selenized for 3 hours at 350° C. In all the three cases, the dominant peak corresponds to (112) plane of $CuInSe_2$. From these results it was concluded that the $CuInSe_2$ films formed by selenization of metallic precursors had the chalcopyrite structure. The presence of Cu/In alloy and In_2Se_3 phases in the samples selenized for 1 hour and 2 hours indicates that for short duration the reaction is incomplete. The optimized selenization duration was 3 hours to obtain crystalline single phase $CuInSe_2$ film.

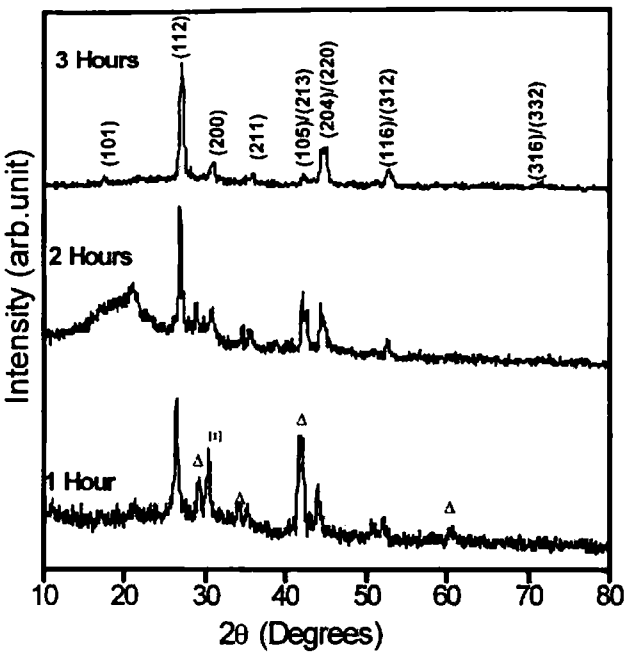

Figure 4.7 The XRD pattern of CIS film prepared from $Cu_{11}In_9$ precursors selenized at 350^{0}C for different duration. (Δ and Ξ indicate the XRD pattern corresponding to $Cu_{11}In_9$ and In_2Se_3 phases respectively).

The experiment carried out by varying the selenization temperature but for fixed duration of 3 hours. Figure 4.8 – 4.11 shows the XRD pattern of films prepared for different selenization temperature ranging from 250°C to 400°C.

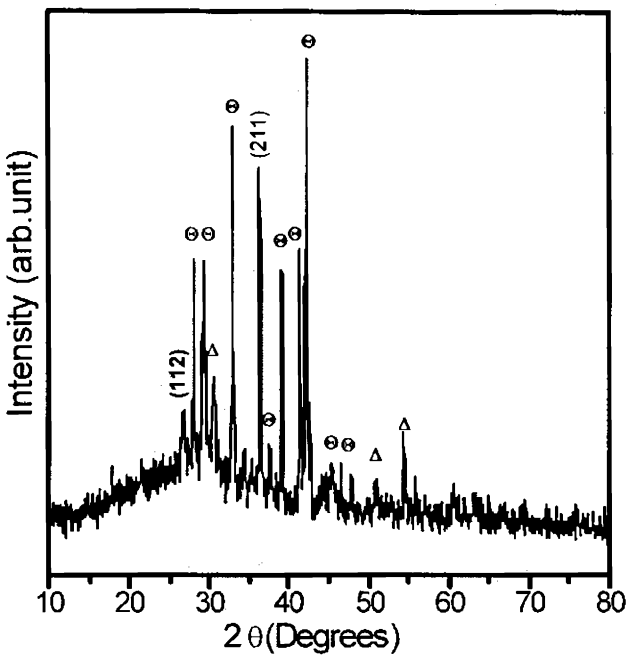

Figure 4.8 XRD pattern of CIS film grown from $Cu_{11}In_9$ precursors selenized at 250° C. (Θ and Δ indicate the XRD pattern corresponding to $Cu_{11}In_9$ and In_2Se_3 phases respectively).

Even at the selenization temperature as low as of 250° C $CuInSe_2$ peaks were detected. But binary phases like $Cu_{11}In_9$ and In_2Se_3 were also present (Fig. 4.8). An identical sample selenized at 300° C showed $Cu_{11}In_9$ phase, along with $CuInSe_2$. The presence of other binary phases like Cu_3Se_2 and In_2Se_3 were also detected (Fig. 4.9). This might be due to the fact that at 300°C the precursor starts to decompose and indium is free to evolve as In_2Se_3 and Cu_3Se_2 [63]. The lower selenium vapor pressure and the higher temperature might be favouring the growth of binary phases of selenium.

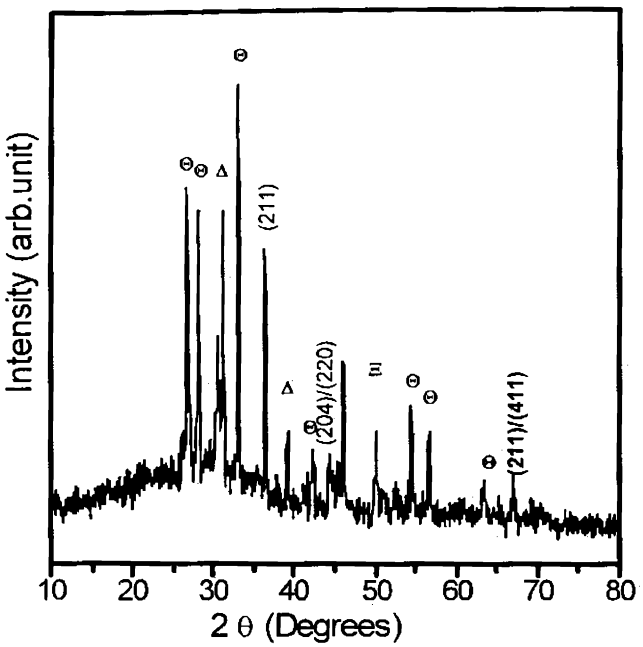

Figure 4.9 XRD pattern of the CIS film prepared from $Cu_{11}In_9$ precursors selenized at 300° C. (Θ, Δ and Ξ indicate the XRD pattern corresponding to $Cu_{11}In_9$ In_2Se_3 and Cu_3Se_2 phases respectively).

The samples selenized at 350^0 C resulted in crystalline quality material with no detectable evidence of secondary phases (Fig. 4.10).

The main reflection corresponds to that from (112) plane; which are closed packed planes in the chalcopyrite lattice. The usual growth direction of thin films is perpendicular to these planes [64].

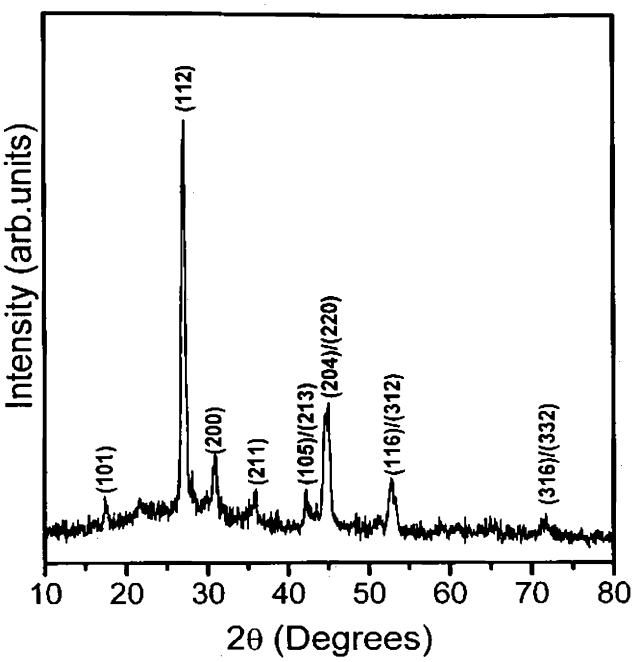

Figure 4.10 XRD pattern of the CIS film prepared from $Cu_{11}In_9$ precursors selenized at 350° C.

When selenization temperature was raised to 400° C, some impurity phases such as Cu_3Se_2, In_2Se_3, $CuSe_2$ were detected in X-ray diffraction patterns (Fig. 4.11). The presence of binary phases Cu_3Se_2, In_2Se_3 and $CuSe_2$ can be attributed to the segregation of In away and Cu towards the upper part of the layer at such a high temperature [65]. The optimum selenization temperature for the formation of single phase $CuInSe_2$ is found to be 350° C. Binary phases coexist at above and below this selenization temperature.

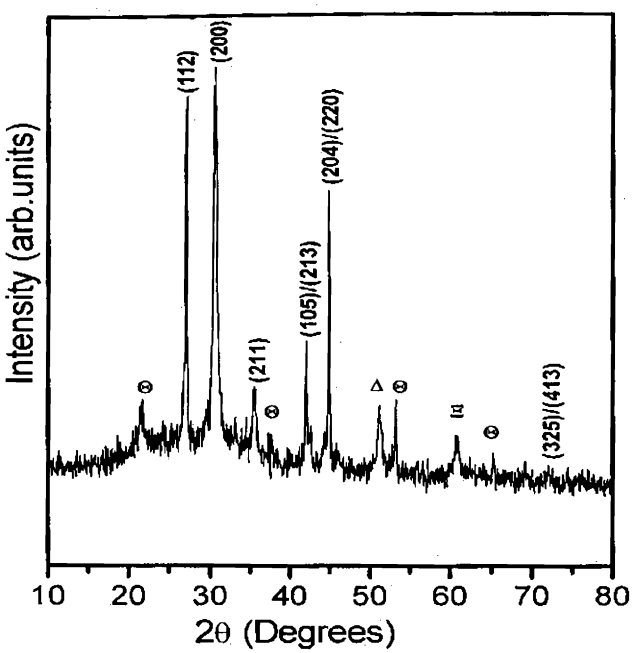

Figure 4.11 XRD pattern of CIS film prepared from $Cu_{11}In_9$ precursors selenized at 400° C. (Θ, Δ and Ξ indicate the XRD pattern corresponding to Cu_3Se_2, In_2Se_3 and $CuSe_2$ phases respectively).

SEM and EDX studies showed that the sample with nearly stoichiometric starting precursors (Cu/In =1.041) are homogeneous with round shaped structures. The films which are Cu rich samples (Cu/In=1.2) were characterised by poor morphological properties, having no apparent grain

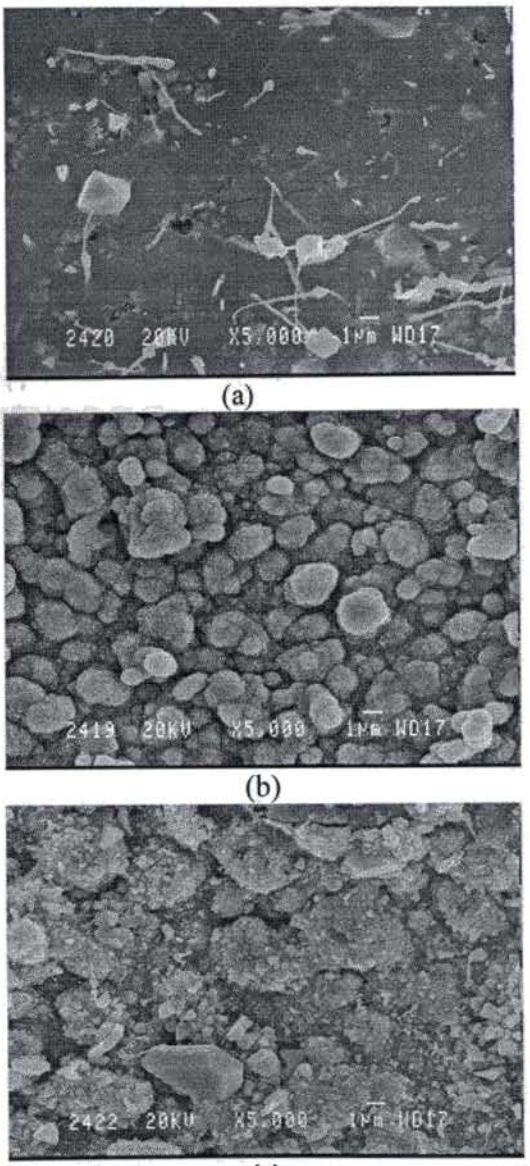

Figure 4.12 SEM micrographs demonstrating the structural features of samples selenized at 350° C for 3 hours using precursor having Cu/In ratio a) 1.2 b) 1.04 c) 0.73.

structure. The visual appearance of indium rich films (Cu/In=0.73) suggests an outer rough surface made of clusters (Fig.4.12).

4.5.2 Optical and Electrical characterisations

The absorption coefficient (α) of the $CuInSe_2$ films was calculated from the absorption spectra. Estimates of the sizes of band gap were obtained by plotting $(\alpha h\nu)^2$ vs. $h\nu$ and extrapolating the linear portion near on set of absorption to the energy axis. The intercept gives the energy.

The variation of the band gap of CIS films with different selenization temperature was also studied. It was observed that the band gap increases with increasing selenization temperature (Fig. 4.13). As the selenization temperature increases from 250^0 C the band gap is found to increase and at selenization temperature 400^0 C the band gap is 1.16 eV. The prepared films have a band gap of 1.05eV at a selenization temperature of 350^0 C, which is close to the theoretical band gap suitable for solar cell [66]. These films were single phase $CuInSe_2$ as indicated by XRD data. The low value of band gap compared to the bulk at lower selenization temperature may be attributed to the presence of secondary phases. At higher selenization temperatures comparatively less secondary phases were observed. The increase in band gap at higher selenization temperature (400^0 C) may be due to the presence of binary phases as evident from the XRD patterns.

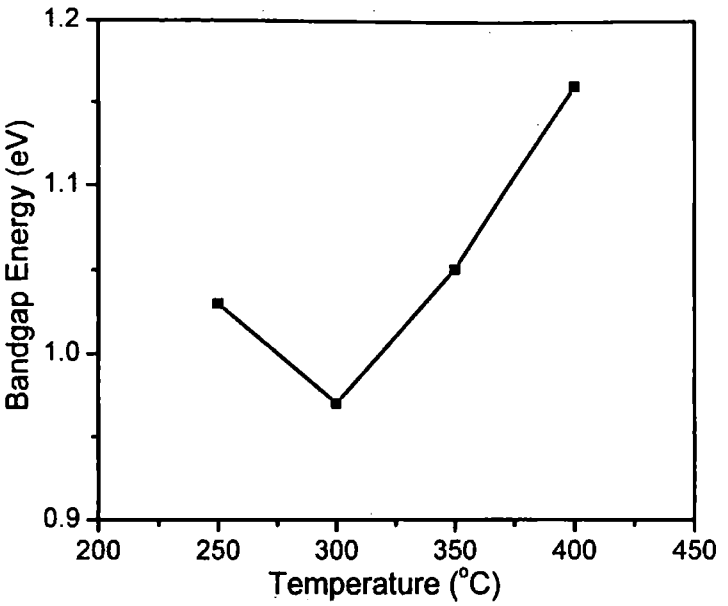

Figure 4.13 Variation of band gap of $CuInSe_2$ (Cu/In =1 in the starting precursor) film with selenization temperature (3 hour selenization)

Resistivity of the samples was determined using two-probe method using silver electrodes in planar geometry. The resistivity was in the order of 10^{-2} Ω cm.

The type of the majority carriers in the present study was determined by hot-point probe method and all the samples were found to be p-type.

4.6 Conclusions

$CuInSe_2$ thin films were grown by a cost effective two stage process which includes the thermal evaporation of metallic bilayers followed by selenization. Single-phase $CuInSe_2$ with (112) preferred orientation was obtained at a selenization temperature of 350^0 C for 3 hours selenization. The presence of some binary phases in films for shorter selenization period and lower

selenization temperature may be due to the incomplete reaction and indium loss. The $CuInSe_2$ thin films prepared under the optimum condition of selenization temperature of 350^0 C and reaction time 3 hours showed optical band gap energy of 1.05 eV and a resistivity of 10^{-2} Ω cm. The CIS films grown by two stage process can be used for the fabrication of solar cells.

References

[1] S. Wagner, J. L Shay, P. Migliorato and H.M Kasper, *Appl. Phy. Lett.* **25** (1974) 434.

[2] T. E. Ciszek, *J. Cryst. Growth*, 70 (1984) 405.

[3] R. Noufi, R. Axton, C. Herrington and S.K. Deb, *Appl. Phys. Lett*, **45** (1984) 668.

[4] R. A. Mickelsen, W. S Chenproc. *16th IEEE, PVSC, IEEEE*, New York, (1982) 781.

[5] K. Ramanathan, M. A. Contreras, C. L. Perkins, S. Asher, F. S. Hasoon, J. Keane, D. Young, M. Romero, W. Metzger, R. Noufi, J.Ward, and A. Duda, *Prog. Photovolt: Res. Appl.* **11**(2003) 225.

[6] J. E. Jaffe. and A. Zunger, *Phys. Review* **29** (1984) 1882.

[7] S. B. Zhang, S. H. Wei, A. Zunger and H. K. Yoshida, *Physical Review B* **57** (1998) 9642.

[8] T. Godecke, T. Haalboom and F. Ernst, *Z.* Metallkd. **91** (2000) 622.

[9] M .L. Fearheily, *Solar Cells* **16** (1986) 91.

[10] D. J. Schroeder, G. D. Berey and A. A. Rockett, *Appl. Phys. Lett.* **69** (1996) 4068.

[11] J. Parkes, R. D. Tomlinson and M. J. Hamphire, *Solid State Electronics* **16** (1973) 773.

[12] Y. Hamakawa and H. Okamoto, *Adv. Solar Ener.* **5** (1988) 201.

[13] L. Kazmerski, F. R. White and G. K Morgan, *Appl. Phys. Lett.* **29** (1976) 268.

[14] D. S. Albin, J. J. Carpella,J .R.Tuttle and R.Noufi, *Mater. Res. Soc. Symp. Proc.* **228** (1992) 267

[15] A. Rockett, F. Abou-Elfotouh, D.Albin, M.Bode, J.Ermer, R.Klenk, T.W.F Russsel, R. D. Tomlinson and T. Walter, *Thin Solid Films* **237** (1994) 1.

[16] N. Kanvar, *Solar Energy Mater. Solar Cells* **52** (1998) 183.

[17] Y. B. He, A. Polity, H. R. Alves, I. O. Terreicher, W. Kriegseis, D. Pfister, B. K. Meyer and M. Hardt, *Thin Solid Films* **403–404** (2002) 62.

[18] S. M. Hasan, M. A. Subhan and Kh. M. Mannan, *Optical Materials* **14** (2000) 329.

[19] O. F. Yuksel, B. M. Basol, H. Safak and H. Karabiyik, *Appl. Phys. A*.**73** (2001) 387.

[20] S. Isomura, S. Shirakata and T. Abe, *Solar Energy Materials* **22** (1991) 223.

[21] H. Neumann, E.Nowak, G.Kuhn and Heise, *Thin Solid Films* **102**, (1983) 201.

[22] M. Alt, H. J. Lawrence and R. Scheer, *J. Appl. Phys* **81** (1997) 956.

[23] J. F. Guillemoles, L. Kronik, D. Cahen, U. Rau, A. Jasenek and H.-W. Schock, *J. Phys. Chem. B* **104** (2000) 4849.

[24] T. Wada, N. Kohara, S. Nishiwaki and T. Negami, *Thin Solid Films,* **387** (2001) 118.

[25] D. Schmid, M. Ruckh, and H.W. Schock, *Solar Energy Mater. Solar Cells* **41/42** (1996) 281.

[26] H. W. Schock and U. Rau, *Physica B* **308–310** (2001) 1081.

[27] J. F. Guillemoles, L. Kronik, D. Cahen, U. Rau, A. Jasenek, and H. W. Schock, J. *Phys. Chem.* B, **104** (2000) 4849.

[28] C. Guillen and J. Herrero *J. Appl. Phys.* **71** (1992) 5479.

[29] V. Sachan and J. D Meakin, *Solar Energy Mater. Solar Cells* **30** (1993) 147.

[30] S. Isomura, S. Shirakata and T. Abe, *Solar Energy Materials* **22** (1991) 223.

[31] S. D. Kim and H. J. Kim, *J. Korean Physical Society* **35** (1999) 403.

[32] S.P. Grindele, A.H. Clark, S. Rezaieserej, E. Falconer, J. McNeily and L. Kazmerski, *J. Appl. Phys.* **51** (1980) 10.

[33] W. Hoig, H. Neumann, H. Sobotta, B. Schumann and G. Kuhn, *Thin Solid Films* **48** (1978) 67.

[34] R. A. Mickelsey and W. S. Chen, *Proc. of 15th IEEE Photovoltaic Specialists Conf.* New York, (1981) p.800.

[35] L. Kazmerski, *Thin Solid Films* **57** (1979) 99.

[36] M. Gorka, P. Bealieu, J. J. Lofeski and B. Roessler, *Solar Energy Materials* **1** (1979) 313.

[37] G. Salviati and D. Scuret, *Thin Solid Films* **104** (1983) L75.

[38] P. Raja, R. Thangaraj and O.P. Agnihotri, *Bull. Mater. Sci.* **8** (1986) 279.

[39] R. N. Bhattacharya and K. Rajeshwar, *Solar Cells* **16** (1986) 237.

[40] J. Herrero and C. Guillen, *J. Appl. Phys.* **69** (1991) 429.

[41] R. Caballero and C. Guillen, *Solar Energy Mater. Solar Cells* **86** (2005) 1.

[42] F. O. Adurodija, M. J. Carter and R. Hill, *Solar Energy Mater. Solar Cells* **40** (1996) 359.

[43] A. Gupta, S. Shirakata and S. Isomura, *Solar Energy Mater. Solar Cells* **32** (1994) 137.

[44] S. Verma, N. Orbey, R.W. Birkmire and T.W. Fraser Russell, *Prog. Photovolt. Res. Appl.* **4** (1996) 341.

[45] S. T. Lalshmikumar and A. C. Rastogi, *J. Appl. Phys.***79** (1996) 3585.

[46] Y. B. He, A. Polity, H. R. Alves, I. Osterreicher, W. Kriegseis, D. Pfisterer, B. K. Meyer and M. Hardt, *Thin Solid Films* **403–404** (2002) 62.

[47] F. J. Pern, J. Goral, R. J.Matson, T. A. Gessert and R. Noufi. *Solar Cells* **24** (1988) 81.

[48] C.D.Lokhande, *J.Electrochem.Soc* **134** (1987) 1727.

[49] R. N. Bahtacharya, *J. Electrochem. Soc.* **130** (1983) 2040.

[50] N. B. Chaure, J. Young, A. P. Samantilleke and I. M. Dharmadasa, *Solar Energy Mater. Solar Cells* **81** (2004) 125.

[51] M. Contreas, B. Eggas, K. Ramanathan, J. Hiltner, A. Swartzlander, F. Hasoon and R. Noufi. *Prog. in Photovoltaics* **7** (1999) 311.

[52] M. Marudachalan, *Processing, Structure and diffusion in* $CuIn_xGa_{1-x}Se_2$ *thin films for solar cells,* Ph.D. thesis, University of Delaware, (1996).

[53] N. G. Dhere and K. W. Lynn, *Proc .of the* 25^{th} *IEEE PV specialists Conf.* Washingtone. D.C **897** (1996) 13.

[54] W. Birkmire and E. Eser, *Annu Rev.Mater.Sci* .**27** (1997) 625.

[55] K. Sato, S. Nakagawa, T. Kamiya, K. Toyoda, T. Ikeya and M. Ishida, 14^{th} *European PV Conference,* Barcelona, Spain (1997).

[56] W.F.Gale, C. J. Smithells and T. C. Totemeier, *Smithells Metal Reference Book*, Butterworth, London **8** (1983) 3-19.

[57] C. Dzonk. H. Metzner, Hessler, H. E. Mahnke, *Thin Solid Films*, **299** (1997) 38.

[58] F. O. Adurodija, J. Song, S.D. Kim, S.H. Kwon, S.K. Kim, K.H. Yoon and B.T. Ahn, *Thin Solid Films* **338** (1999) 13.

[59] P. R. Subramanian and D. E. Laughlin, *Bulletin of alloy phase diagrams* **10** (1989) 554.

[60] O. P. Agnihotri, P. R. Ram, R. Thangaraj, A. K. Sharma and A. Ratur, *Thin Solid Films* **102** (1983) 29.

[61] J. Szot and D. Haneman, *Solar Energy Materials* **11** (1984) 289.

[62] E. R. Don and R. Hill, *Solar Cells* **16** (1986) 131.

[63] J. W. Park, G. Y. Chung, A.T. Ahn and H. B.Im *Thin Solid Films* **245** (1994) 174.

[64] A. Paretta., M. L Addonizio., S. Loreti, L .Quercia. and M. K Jayaraj, *Journal of Crystal Growth* **183** (1998) 196.

[65] H. J. Moller, *Semiconductors for Solar Cells*, Artech House, Inc., London (1993) 292.

[66] V. Alberts, M. Klenk and Bucher. *Jpn. J. Appl. Phys.* **39** (2000) 5776.

Chapter 5

Optimisation of Process for the Growth of $CuIn(Se_{1-x}S_x)_2$ Thin Films

Although $CuInSe_2$ (CIS) has proven to be a promising material for photovoltaic applications with the direct band gap of 1.05 eV, band gap of above 1.2-1.3 eV is considered optimal for maximizing conversion efficiencies. Because the relatively small band gap values of $CuInSe_2$ thin films (close to 1eV) limits the open-circuit voltage to value well below 500mV and thus limits the conversion efficiencies of completed $CuInSe_2$/CdS/ZnO solar cell devices. But it can be adjusted to mach the solar spectrum by substituting part of indium by gallium or part of selenium by sulfur.

5.1. Introduction

Though $CuInSe_2$ cell has reached a development status that makes mass production attractive in the area of thin film solar cell fabrication, research efforts are continuing to further improve preparation technologies and module properties. The area of research for upgrading the fabrication process and device performance include the feasibility of reactive sputtering [1], electrochemical etching of CuS [2], Cd-free buffer layers [3], modifying by incorporating additional elements [4,5] etc. There have been attempts to modify the band gap of $CuInSe_2$ to better suit the solar spectrum. Incorporation of sulfur is recently used with selenide absorbers to increase the band gap. Graded band gaps could be used to improve the V_{oc} of devices by reducing the recombination current in the space charge region while leaving carrier generation and collection relatively unaffected [6, 7]. This can be achieved by alloying of $CuInSe_2$ with $CuInS_2$, i.e. the formation of the quaternary alloy $CuIn(Se_{1-x}S_x)_2$. $CuInS_2$ has a band gap of 1.55 eV [8] and the band gap of CuIn $(Se_{1-x}S_x)_2$ ranges from 1 to 1.55 eV depending on the amount of S in the film [9].

Some studies report significant increases in device performance [10], others only marginal ones [11]. Improvements in device performance have been explained with a reduction of the density of deep trap states in the absorber film which reduces recombination in the space charge region, which improve the open circuit voltage V_{oc} [12]. A V_{oc} of 580 mV has been reported for a $CuIn(S,Se)_2$/CdS/ZnO solar cell devices [13]. Siemens Solar Industries utilizes a graded $Cu(In,Ga)(Se,S)_2$ film structure where the junction region is alloyed with sulfur to increase V_{oc}, while the back contact region is alloyed with gallium [14].

CuIn $(Se_{1-x}S_x)_2$ films were grown by annealing of metallic precursors in a mixture of H_2Se/H_2S gases [15]. Alberts and Dejene have prepared the CuIn

$(Se_{1-x}S_x)_2$ thin films by thermal diffusion of sulfur into $CuInSe_2$ [13]. The formation of CuIn $(Se_{1-x}S_x)_2$ by reacting $CuInSe_2$ thin films in a flowing Ar/H_2S atmosphere has been reported by Engelmann *et al* [16]. The deposition of CuIn $(Se_{1-x}S_x)_2$ by solution growth technique has also been reported in literature [17].

5.2 Diffusion Processes and Reaction Kinetics

Sheppard, *et al* [18] has explained the reaction kinetics of binary phases of $CuIn(Se_{1-x}S_x)_2$ and how it can be accurately controlled to prevent the formation of phase-segregated material. They observed that when the fully formed $CuInSe_2$ films were sulfurised, two discrete ternary phases were formed, $CuInS_2$ and $CuInSe_2$. In another attempt they used partially selenized composite alloys to react with H_2S/Ar. During the sulfurization step, the existing binary phases in the partially selenized films reacted with sulfur to produced ternary sulfoselenides (i.e. Cu(Se, S) and In(Se, S)). The subsequent reaction between the sulfoselenides and the unstable $CuInSe_2$ phase under defined thermal conditions produced uniform, single-phase $CuIn(Se_{1-x}S_x)_2$ compound. The homogeneous incorporation of S into $CuInSe_2$ led to a systematic shift in the lattice parameters and band gap of the absorber films.

An investigation on surface sulfurisation and the effects of sulfur in $CuIn_{1-x}Ga_x(S_{1-x},Se_x)_2$ absorber material and device performance has been carried out by Nakada *et al* [10]. The behaviour of sulfur diffusion is related to the grain structure of the $CuIn_{1-x}Ga_xS_2$ (CIGS) film, since S atoms can easily diffused through grain boundaries. It was proved from the experiment, in which the sulfur concentration seen through the entire film when it is deposited at lower temperature, where as the film deposited at higher substrate temperature was sulfurised only in the surface region. A dramatic increase of solar cell efficiency to 14.3% from a cell efficiency of 8-11%

range before sulfurisation occurred with V_{oc} = 528 mV, J_{sc} = 39.9 mA/cm^2 [10].

The incorporation of S in a $Cu(In,Ga)Se_2$ film has been shown to depend on the composition and structure of the film. The rate of sulfur incorporation found to increasing during co-evaporation of the elements [19] or post-deposition sulfurization of $CuIn_{1-x}Ga_x(S_{1-x},Se_x)_2$ [20], when the copper percentage is more than 25. In addition, films with small grains draw sulfur faster than films with large grains [10, 20]. In Cu-rich $CuInSe_2$ films on silica substrates, S incorporation has been quantitatively described as a combination of bulk and grain boundary diffusion [16]. Post-deposition sulfurization on $CuGaSe_2$ and $CuIn_{1-x}Ga_xSe_2$ films produces a completely sulfurised surface layer that has been correlated with a structure visible in scanning electron microscope (SEM) cross-sectional images. It has also been observed that in sulfurised $CuInSe_2$ films a Na compound tends to segregate at the surface [11].

A model was recently offered to explain the mechanism of S diffusion into $CuInSe_2$ layers by exposing the $CuInSe_2$ surface to S vapours or H_2S gas [21]. According to this model, first a surface reaction which is kinetically controlled occurs between the $CuInSe_2$ surface and the S source, forming a thin $CuInS_2$ layer. This is followed by an inter diffusion process between the $CuInS_2$ and the $CuInSe_2$ layers. Using this model and experimental data, Engelmann and Birkmire derived a bulk diffusion constant of sulfur in slightly Cu-rich $CuInSe_2$ layers as D = $1.5x10^{-12}$ cm^2/sec at 475° C. For a 20-minute sulfurization time at 475° C, the sulfur is expected to extend into the absorber layer by about 0.4 μm [21].

The relation between band gap of $CuIn(S_{1-x}Se_x)_2$ film with sulfur to selenium ratio variation has been studied by Chavan *et al* for $CuIn(Se_{1-x},S_x)_2$ thin films deposited by solution growth technique [17].

Optical band gap varies from 1.44 eV to 1.07 eV as sulfur to selenium ratio changes from x = 0 to 1. The lattice parameters also change with respect to composition x.

In the present study, it has been demonstrated that a classical two step growth process can be utilized to investigate and establish a scientific basis for the graded band gap $CuIn(Se_{1-x},S_x)_2$ thin films. The experimental approach consists of reacting $CuInSe_2$ films in flowing H_2S-N_2 atmosphere to convert films completely to $CuInS_2$, or to produce graded $CuIn(Se_{1-x}S_x)_2$ films by reacting $Cu_{11}In_9$ alloy in a mixture of sulfur and selenium.
The $CuIn(Se_{1-x},S_x)_2$ thin films were obtained by reactive annealing of CuIn precursors in a mixture of sulfur and selenium atmosphere while post sulfurisation of single phase $CuInSe_2$ did not result in $CuIn(Se_{1-x},S_x)_2$ thin films. A band gap of 1.38 eV, obtained for the prepared $CuIn(Se_{1-x},S_x)_2$.

5.3. Experimental Details

The attention was focussed on the effect of sulfur incorporation into the $CuInSe_2$ thin films and thus establish a technique for the growth of graded band gap CuIn $(Se_{1-x}S_x)_2$ thin films. Two thermal profiles were used to study the incorporation of sulfur to increase the band gap of $CuInSe_2$ thin films. One of them was the annealing of the prepared $CuInSe_2$ thin films (CIS) in sulfur atmosphere for different duration. This process called post sulfurisation process however has limited success and the resulting films were not CuIn $(Se_{1-x},S_x)_2$. In the second thermal profile the sulfur was passed through the reaction vessel during the selenization. This thermal profile was named as co- chalcogenisation.
The $CuInSe_2$ thin films for the post sulfurisation process were prepared by selenization of Cu/In alloy precursors as described in chapter 4. $Cu_{11}In_9$ precursors were prepared by sequential vacuum deposition of copper and

indium followed by annealing at 153° C. Heating the prepared CuIn alloy in the presence of selenium vapour under optimised selenization conditions resulted in $CuInSe_2$ films. The CIS film prepared as described above were annealed in sulfur atmosphere for different durations (post sulfurisation). In the co- chalcogenisation process $Cu_{11}In_9$ precursors were annealed in a mixture of sulfur and selenium atmosphere for duration varying from 1 to 3 hours. The optimised $CuInSe_2$ and $CuInS_2$ thin films, discussed in the previous sections were used as reference samples.

The thickness of precursor layers and the deposition rates were controlled during deposition using a quartz crystal digital thickness monitor. The thickness of the prepared films was determined by stylus profiler. The structural studies of the bulk, as deposited and annealed thin films were performed using the X-ray diffractometer and the optical transmission was recorded using the UV-VIS-NIR spectrophotometer. The electrical resistivity of the films was measured using a Keithley source measure unit by two-probe method with electrodes in planar configuration with highly conducting silver paint as the electrodes.

The crystal structure, lattice strain, lattice parameters, absorption coefficient, conductivity, band gap and resistivity were obtained from these studies.

5.4. Results and Discussions

5.4.1 Structural Characterisations

i) XRD Studies on the Prepared Films

In a first profile, the sample were processed under optimised conditions which involved a selenization step at 350 °C for 3 hours to produce a fully reacted $CuInSe_2$ thin film. Details of $CuInSe_2$ thin film preparation is given in chapter 4. The $CuInSe_2$ films prepared so, were annealed in H_2S/N_2 atmosphere.

The figures 5.1, 5.2 and 5.3 depict the XRD pattern of a typical sample prepared under the above described experimental condition at different duration of sulfurisation. The XRD patterns of the single phase $CuInSe_2$ and $CuInS_2$ thin films were used as reference for the structural studies.

The X-Ray reflections from (112) planes of $CuInSe_2$ and $CuInS_2$ phases were present in the XRD pattern. The main peak of the $CuInSe_2$ (112) was shifted from $2\theta = 27^\circ$ to $2\theta = 26.64^\circ$ when these films were annealed in sulfur atmosphere for 1 hour.

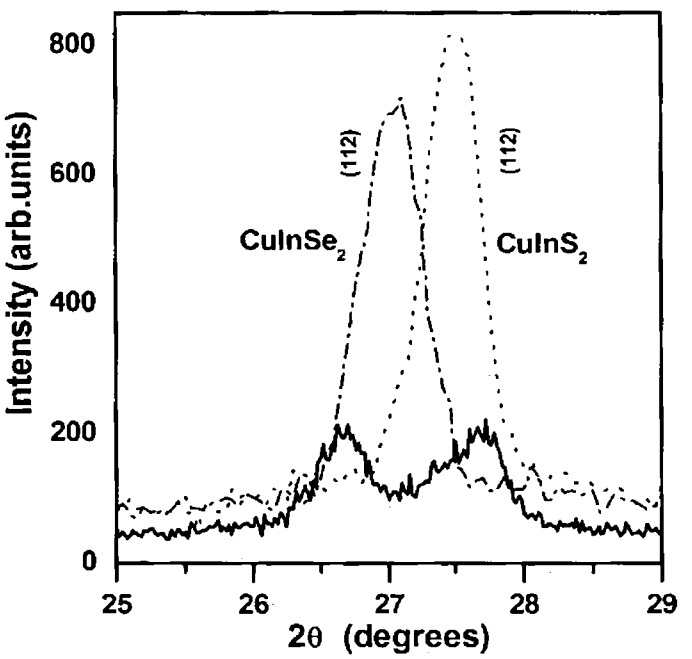

Figure 5.1 XRD pattern (112) peak of the $CuInSe_2$ thin film after post annealing in sulfur atmosphere for a duration of 1 hour (solid line). (112) peaks of $CuInSe_2$ and $CuInS_2$ are also shown (dotted lines)

When the annealing time increased to 2 hours the peak shifted to $2\theta = 26.4^\circ$ from $2\theta = 27^\circ$. The (112) peak was shifted to $2\theta = 26.25^\circ$ for the film prepared by 3 hour sulfurisation.

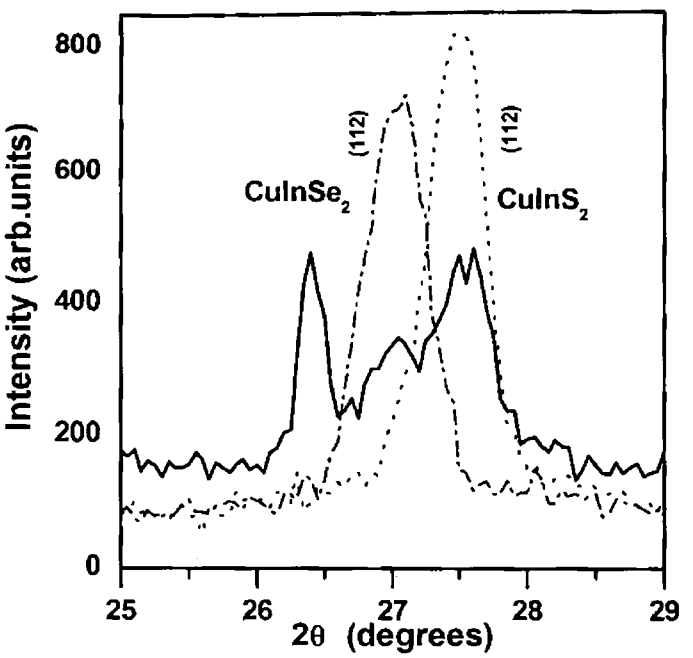

Figure 5.2 XRD pattern (112) peak of the $CuInSe_2$ thin film after post annealing in sulfur atmosphere for a duration of 2hours (solid line). (112) peaks of $CuInSe_2$ and $CuInS_2$ are also shown (dotted lines)

The full width at half maximum (FWHM) values of the (112) peaks of $CuInSe_2$ and $CuInS_2$ phases in the film decrease with the increase of duration of sulfurisation. This indicates the increase in crystalline size with the duration of annealing. The relative intensity of (112) peak corresponding to $CuInS_2$ compared to the (112) peak of $CuInSe_2$ phase increases with the duration of sulfurisation. This indicates that there is an increase in the $CuInS_2$ phase compared to $CuInSe_2$ phase as the duration of annealing increases. The EDX analysis also shows that there is an increase in sulfur content suggesting the increase of $CuInS_2$ phases. However the sulfurisation of $CuInSe_2$ does not lead to the formation of $CuIn(Se_{1-x},S_x)_2$ compound.

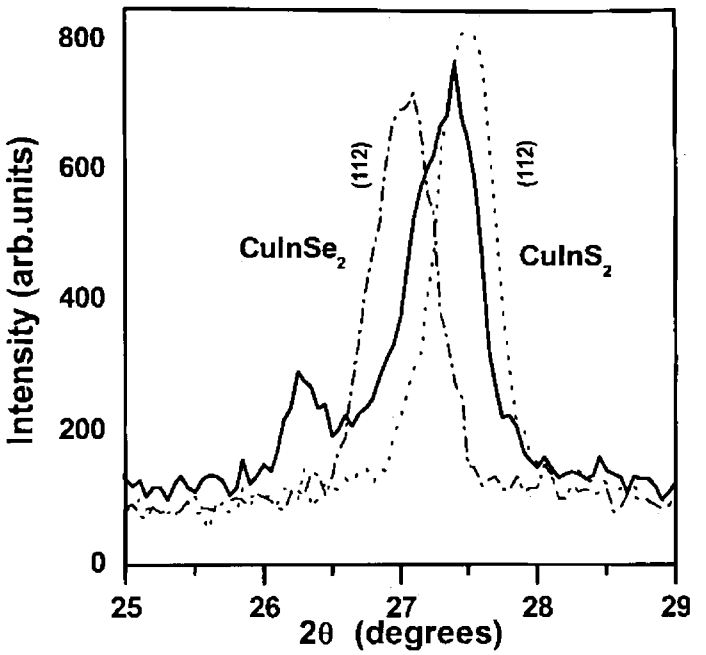

Figure 5.3 XRD pattern (112) peak of the $CuInSe_2$ thin film after post annealing in sulfur atmosphere for duration of 3 hours (solid line). (112) peaks of $CuInSe_2$ and $CuInS_2$ are also shown (dotted lines).

ii) Lattice strain and Volume

Cell volumes were calculated from the lattice parameters and found to be increasing with the duration of the post annealing of the $CuInSe_2$ samples in H_2S atmosphere.

Lattice strains were calculated from the plot of Sin θ versus β Cos θ where β is the full width at half maximum (Fig. 5.4). The strain of the $CuInSe_2$ annealed in sulfur atmosphere was found to increase by ~ 0.1%.

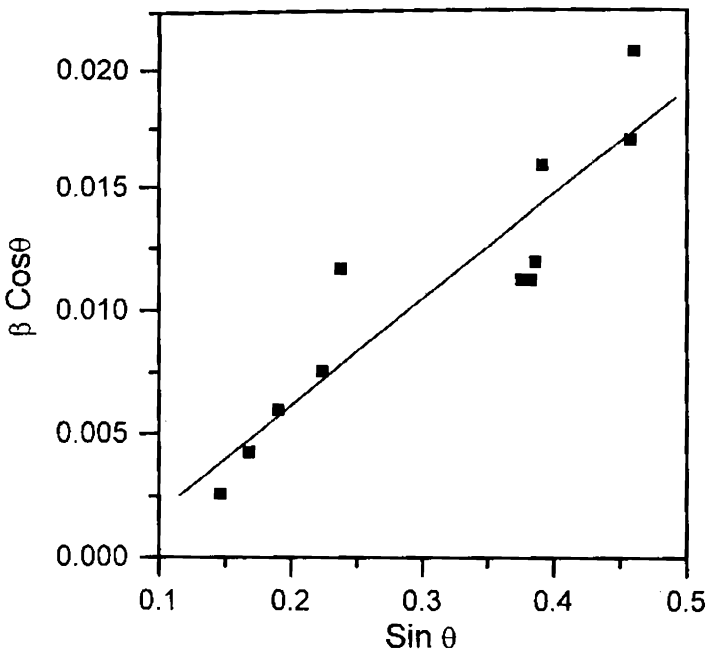

Figure 5.4 Plot of Sin θ vs βCos θ

The XRD pattern of the films prepared by the co-chalcogenisation of $Cu_{11}In_9$ precursors in a mixture of sulfur and selenium atmosphere is shown in figure 5.5. It was found that the position of the dominant peak (112) was at (2θ = 27.2°) significantly higher 2θ value than the expected value for the pure $CuInSe_2$ phase (2θ = 27°). This increase in the 2θ value corresponds to the decrease in lattice parameter. This indicates an incorporation of S in the $CuInSe_2$ absorber layer.

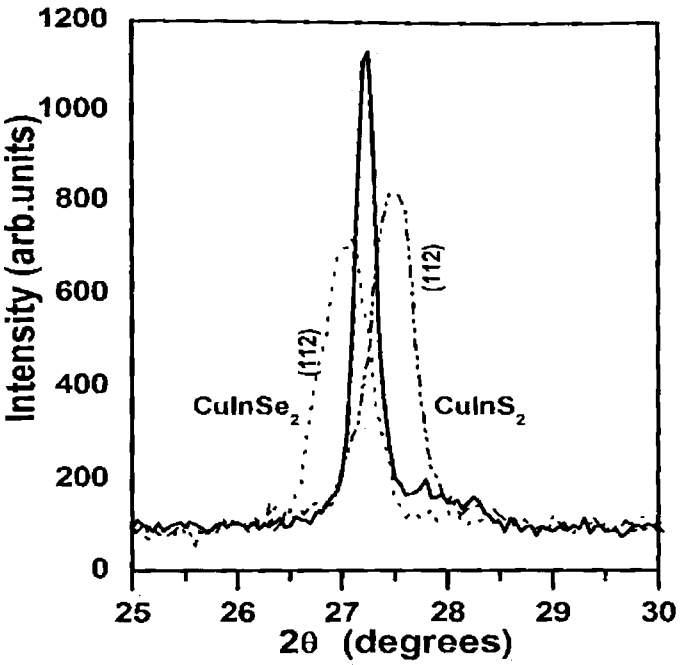

Figure 5.5 The XRD pattern showing the shift in the main peak (112) of $CuIn(Se,S)_2$ thin film prepared by annealing CuIn precursor in Se +S atmosphere. (112) peaks $CuInSe_2$ and $CuInS_2$ are also shown (dotted lines)

The incorporation of sulfur resulted in a shift of the d-values of all peaks towards lower values compared to single phase $CuInSe_2$ (Fig. 5.6). The observed increase in the 2θ of the diffraction peaks can be attributed to the shrinkage of the chalcopyrite lattice. No secondary phases were detected in XRD, this confirms the compound formation. Unlike the post sulfurisation, no phase segregation was observed in the co-chalcogenisation process.

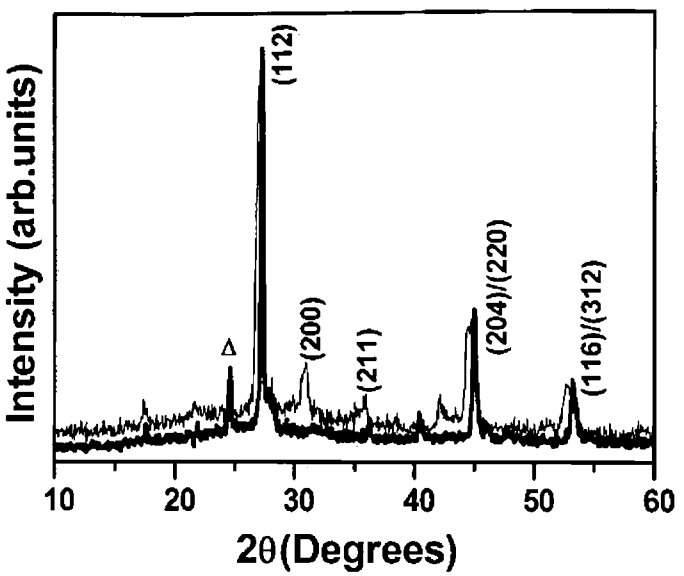

Figure 5.6 XRD pattern of the $CuIn(Se,S)_2$ thin film prepared by annealing $Cu_{11}In_9$ precursor in Se/S atmosphere for 3 hours. Δ –unidentified. The gray line indicates the XRD pattern of single phase $CuInSe_2$

The variation of sulfur diffusion into $CuInSe_2$ for samples having different Cu/In ratio in the precursor was also studied. A large shrinkage was observed for $CuInSe_2$ having Cu/In ratio 1 or greater while a comparatively no shrinkage for In rich samples (Table 5.1).

Table 5.1 The change in the unit cell volume with the Cu/In ratio

Ratio	$CuInSe_2$ $(A^o)^3$	$CuIn(Se/S)$ $(A^o)^3$
Cu/In = 0.77	387.91	382.16
Cu/In = 0.98	382.79	365.7
Cu/In = 1.22	395.02	365.31

For Cu/In ratios of 1 or greater, Cu_2Se is assumed to be present in the film. Engelmann *et al.* [22] described the sulfur incorporation into $CuInSe_2$ films

as two step process. The first step is the chalcogenisation exchange reaction at the solid-gas interface, and the second step is the diffusion of S into the film and Se out of the film. They studied the variation of S diffusion with the presence of Cu_2Se and it was found that Cu_2Se in the film enhances the diffusion of sulfur. So the large shrinkage of the cell volume for Cu/In ratio of 1 or greater may be due to the increased diffusion due to the presence of Cu_2Se.

The structural studies shows that when the single phase $CuInSe_2$ is post annealed in sulfur atmosphere, sulfur might have been incorporated in the interstitial positions, while co-chalcogenisation resulted in $CuIn(Se_{1-x},S_x)_2$.

iii) Morphological Characterisation

Energy dispersive x-ray spectroscopy (EDX) measurements and scanning electron microscopy (SEM) were carried out for post sulfurised samples and co-chalcogenised samples having different Cu/In ratio. The EDX studies showed that the Se content was very low (~ 6 %) in the post sulfurised films while for the films prepared by co-chalcogenisation, the Se content was around 25%. The results points out that by post sulfurisation the sulfur replace the Se in the compound. EDX results also support the observations from XRD.

SEM studies revealed the expected non-uniform crystal size of the heterogeneous alloy. The results presented in figure 5.7 represent the typical structural features of the chalcopyrite alloys, prepared by the post-sulfurization of a fully reacted $CuInSe_2$ thin film.

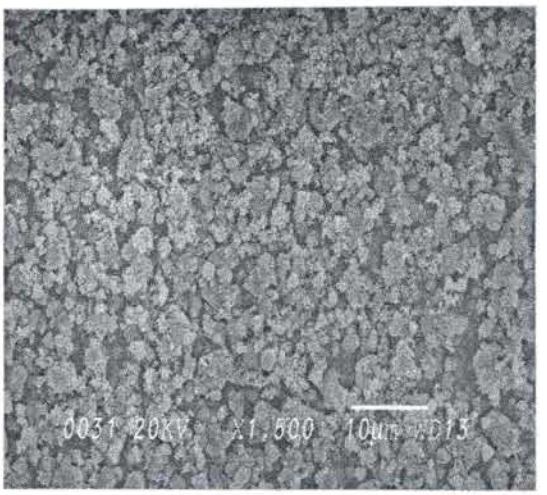

Figure 5.7 SEM picture demonstrating the structural features of post sulfurised $CuInSe_2$

Figure 5.8 SEM micrograph showing typical surface morphology of $CuInSe_2$ thin film

Surface morphology of the films prepared by the co-chalcogenisation of $Cu_{11}In_9$ precursors in a mixture of sulfur and selenium atmosphere (Fig. 5.9) showed a non uniform surface morphology with large irregular shaped grains superimposed on smooth flat background material.

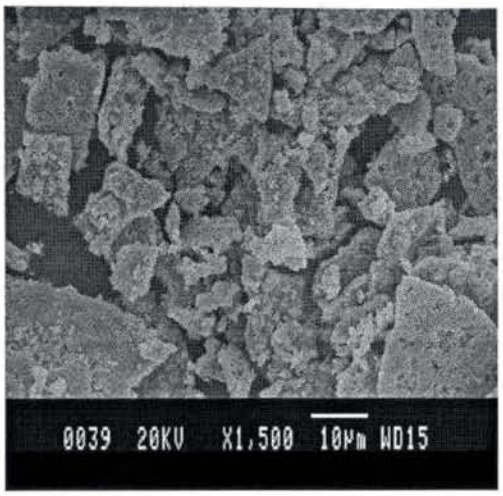

Figure 5.9: Surface morphology of $CuIn(Se_{1-x}S_x)_2$ thin films prepared by co-chalcogenisation.

5.4.2 Optical and Electrical Characterisations

The band gap of the films was determined from the absorption spectra of the samples. The studies showed there was an increase in the band gap for the post sulfurised $CuInSe_2$ films in H_2S atmosphere compared to that of the single phase $CuInSe_2$ (Eg = 1.05 eV). The band gap was 1.2 eV for the post sulfurised $CuInSe_2$ films irrespective of the duration of sulfurisation (Fig. 5.10).

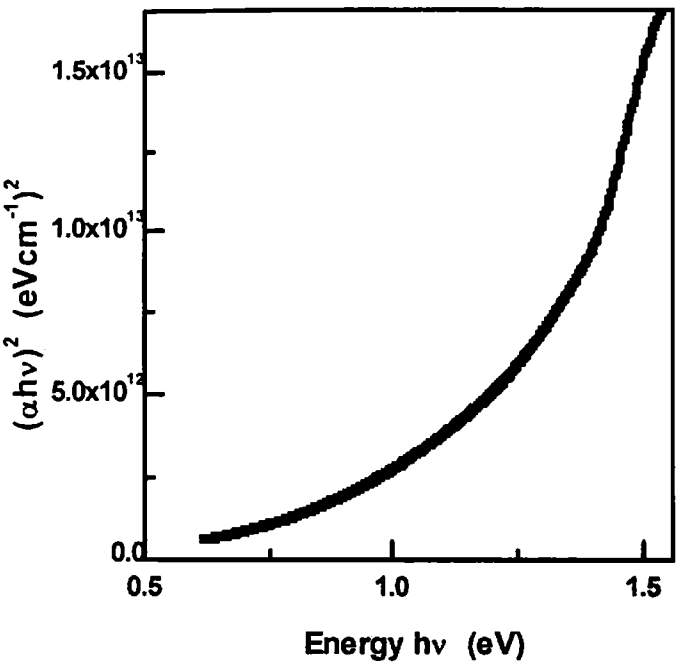

Figure 5.10 Plot of $(\alpha h\nu)^2$ vs the energy of post sulfurised $CuInSe_2$

The $CuInSe_2$ sample after sulfurisation showed the formation of $CuInS_2$ phase as evident from XRD. The increase in the band gap is due to the fact that the measured band gap is the average of the $CuInSe_2$ and $CuInS_2$ phases present in the film. Since $CuInS_2$ has larger band gap, the increase of $CuInS_2$ phase due to the sulfurisation of $CuInSe_2$ resulted in higher band gap values.

The band gap of the $CuIn(Se_{1-x},S_x)_2$ prepared by co-chalcogenisation was 1.36 eV (Fig. 5.11) more close to the obtained band gap obtained for $CuInS_2$ (1.45eV) [23]. This increase in band gap is due to the compound formation.

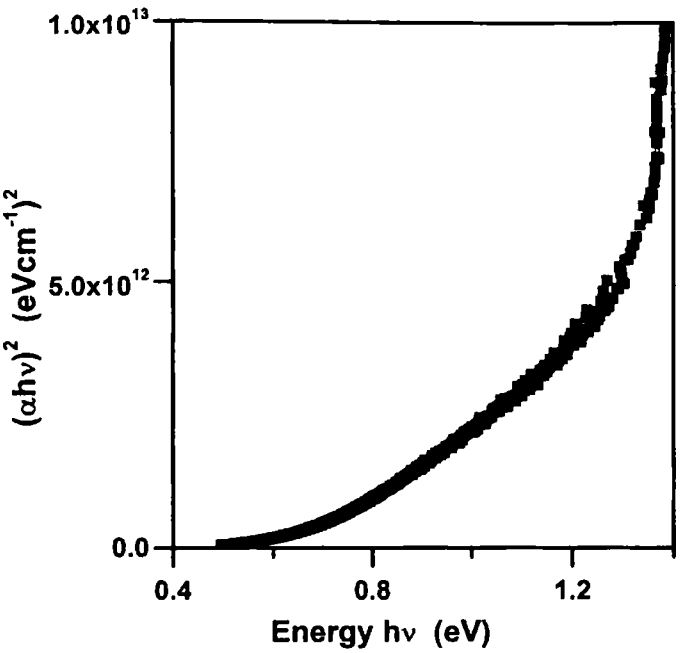

Figure 5.11 The plot of $(\alpha h\nu)^2$ vs the energy $CuIn(Se_{1-x},S_x)_2$ thin films prepared by co-chalcogenisation.

Resistivity of the samples was calculated from the current voltage characteristics. The voltage was varied from 0 to 10 V and the corresponding current through the film was noted. A thin layer of silver was used as the electrode. The resistivity was of the order 10^3 Ω cm.

Thickness of the films was determined by using a stylus thickness profiler and found to be ~ 2 μ m

5.5 Conclusions

The sulfur incorporation into $CuInSe_2$ thin film was investigated by two thermal profiles for the growth of graded band gap thin films. In the case of $CuInSe_2$ films on post sulfurisation, the sulfur may be occupying the interstitial positions or forming a $CuInS_2$ phase along with $CuInSe_2$ phase. The present study shows that the sulfurisation of $CuInSe_2$ is not a feasible

technique for the production of $CuIn(Se_{1-x},S_x)_2$ film. The co-chalcogenisation process of $Cu_{11}In_9$ precursors resulted in a shift of 2θ values and a reduction in cell volume which is indicative of an incorporation of sulfur into the $CuInSe_2$ absorber layer forming $CuIn(Se_{2-x}S_x)_2$. A band gap of 1.38 eV, which is more close to the band gap of $CuInS_2$, obtained for the $CuIn(Se_{1-x},S_x)_2$. It can be concluded that the incorporation of S with the aim of band gap grading of $CuInSe_2$ can be achieved by direct annealing $Cu_{11}In_9$ precursor in S+Se atmosphere.

References

[1] K. Ellmer, J. Hinze and J. Klaer, *Thin Solid Films* **413** (2002) 92.

[2] M. Aggour, U. Stfrkel, C. Murrell, S. A. Campbell, H. Jungblut, R. Hoffmann, R. Mikalo, D. Schmeisser and H. J. Lewerenz, *Thin Solid Films* **403–404** (2002) 57.

[3] C. Kaufmann, P.J. Dobson, S. Neve, W. Bohne, J. Klaer, R. Klenk, C. Pettenkofer, J. Roehrich, R. Scheer and U. Stfrkel, *Proc. 28th IEEE Photovoltaic Specialists Conf.* NJ, (2000) p.688.

[4] D. Braunger, Th. Dqrr, D. Hariskos, C. H. Kfble, Th. Walter, N. Wieser, H.W. Schock, Proc. *25th IEEE Photovoltaic Specialists Conf.*, New York, (1996) p.1001.

[5] A. Werner, I. Luck, J. Bruns, J. Klaer, K. Siemer, D. Braunig, *Thin Solid Films* **361–362** (2000) 88.

[6] D. Tarrant and J. Ermer, *Proc.23rd IEEE PVSC,* Louisville, New York, USA (1993) 372.

[7] A. Dhingra and A. Rothwarf, *IEEE Transactions on Electron Devices* **43** (1996) p.613.

[8] H. J. Moller, *Semiconductors for Solar Cells*, Artech House, Inc., London (1993) 35

[9] T. Walter, M. Ruckh, K. O. Velthaus, and H. W. Schock, *Proc. of the 11th European PV Solar Energy Conference*, Switzerland (1992) p.124.

[10] T. Nakada, H. Ohbo, T. Watanabe, H. Nakazawa, M. Matsui, and A. Kunioka, *Solar Energy Mater. Solar Cells* **49** (1997) 285.

[11] J. Sterner, T. W. Matthes, J. Kessler, J. Lu, J. Keraenen, E. Olsson, and L. Stolt, *Proc. of the 16th European PV Solar Energy Conference* (2000) p.771.

[12] V. Probst, W.Stetter, W.Riedl, H.Vogt, M.Wendl, H.Calwer, S.Zweigart, B.Freienftein and H.Cerva, *Thin Solid Films* **387** (2001) 262.

[13] C. Albert and F. D. Dejene, *J. Phys. D: Appl. Phys.* **35** (2002) 2021.

[14] D.E. Tarrant, J. Bauer, R. Dearmore, M.E. Dietrich, G.T. Fernandez, O.D. Frausto, C.V. Fredric, C.L. Jensen, A.R. Ramos, J.A. Schmitzberger, R.E. Wieting, D. Willett and R.R. Gay, *NREL/SNL PV program review, AIP Conference Proceedings*, **394** (1996) p.143.

[15] J. Bekker V. Alberts, A. W. R. Leitch and J. R. Botha, *Thin Solid Films* **431-432** (2003) 116.

[16] M. Engelmann, B. E. McCandless, and R. W. Birkmire, *Thin Solid Films* **387** (2001) 14.

[17] S. Chawan and R. Sharma, *J. Phys. Chem. Solids* **67** (2006) 767.

[18] C. J. Sheppard, V. Alberts, and W. J. Bekker, *Phys. Stat. Solidi* **201** (2004) 2234.

[19] T. Walter, A. Content, K. O. Velthaus, and H. W. Schock, S *Solar Energy Mater. Solar Cells* **26** (1992) 357.

[20] B. M. Basol, A. Halani, C. Leidholm, G. Norsworthy, V. K. Kapur, A. Swartzlaender, and R.Matson, *Progress in Photovoltaics: Research and Applications* **8** (2000) 227.

[21] R. Birkmire, M. Engelmann, *Proc. 15th NCPV Photovoltaic Review Conference* **23-28** (1998) 462.

[22] M. Engelmann, B. E. McCandless, *J. Appl. Physics* **79** (1996) 7324.

[23] A. Antony, A.S. Asha, Rahana Yoosuf, R. Manoj, M. K. Jayaraj, *Solar Energy Mater. Solar Cells* **81** (2004) 407.

Chapter 6

Fabrication of Chalcopyrite Heterojunctions

The hetero junction is formed by contacting two different semiconductors. The top and bottom layers in a heterojunction device have different roles. The top layer, or window layer, is a material with a high band gap selected for its transparency to light. The window layer allows almost all incident light to reach the bottom layer, which is a material with low band gap that readily absorbs light. This light then generates electrons and holes very near the junction, which helps to effectively separate the electrons and holes before they can recombine.

The advantages of heterojunctions are

- *can be doped both p- and n-type.*
- *high band gap window layer reduces the cell's series resistance.*
- *window material can be made highly conductive.*

6.1. Introduction

Manufacture of solar cells depends on solid-state semiconductor technology, which is very economical in material use. In addition semiconductor technology continues to advance rapidly, and so the prospects for both better performance and reduced costs are improving continually. However, the commercial viability of solar energy suffers the well-known problem of its initial manufacturing cost. So recent research now focuses on large area solar cell fabrication at a minimum capital cost. With this objective we concentrated on the development of relatively scalable cost effective processes for the fabrication of heterojunctions.

The absorber layer $CuInS_2$ is prepared by two stage process which has a high potential for industrial application, because it offers a simple and flexible control over the film stoichiometry. Chemical bath deposition (CBD) technique is used for the preparation of CdS buffer layer. Among various techniques for preparing CdS films, chemical bath deposition is a simple and low cost method that produces uniform, adherent, and reproducible large area thin films for solar related applications. One of the advantages of CBD CdS layers in photovoltaic devices is deposition of a very thin layer (<50nm) on the substrate surface. These characteristics produce an increase in device photocurrent by enhancing the solar absorption spectrum in the UV-range and in the cell open circuit voltage; owing to absorber CdS interface improvement [1]. Two heterojunction were studied with structures Mo/$CuInS_2$/CdS/Ag and Mo/ $CuInS_2$/CdS/ZnO/ ZnO:Al.

6.2 Fabrication of $CuInS_2$ Based Solar Cells

The two stage process is utilised to prepare the $CuInS_2$ films. The first step was the preparation of Cu-In precursors. Cu-In bilayer was deposited on Mo substrates by thermal evaporation and which on annealing at temperature of

153^{0}C for 2 hours resulted in $Cu_{11}In_9$ alloy. The details of the precursor preparation are given chapter 4.

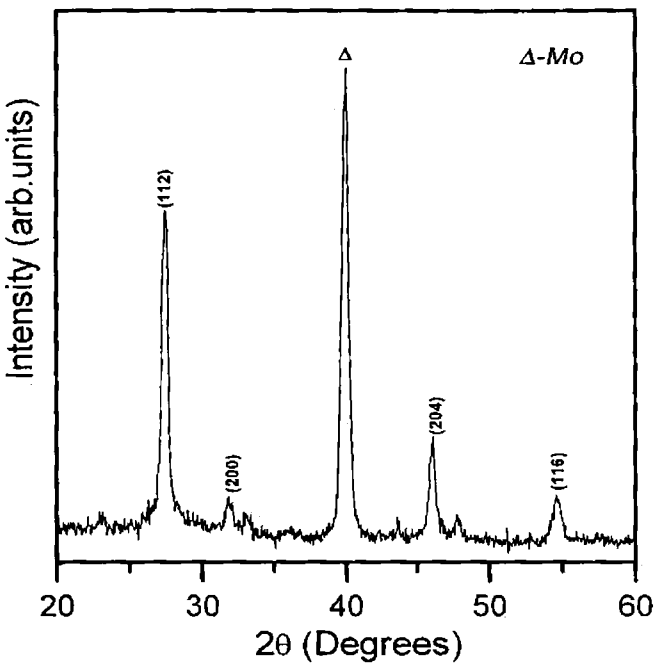

Figure 6.1 XRD pattern of the $CuInS_2$ layer sulfurised at 350°C for a duration of 3 hours. (Δ indicate Mo substrate).

Heating the $Cu_{11}In_9$ alloy in H_2S atmosphere resulted in $CuInS_2$ films. The optimum sulfurisation temperature was 350^{0}C and duration was 3 hours for the growth of single phase $CuInS_2$ which had been optimised in a previous study [2]. The films showed an orientation along (112) plane (Fig. 6.1).

The band gap of the prepared film was 1.45 eV (figure 6.2). The film showed poor adhesion to Mo substrate. So a thin layer of gallium was introduced prior to In coating for better adhesion.

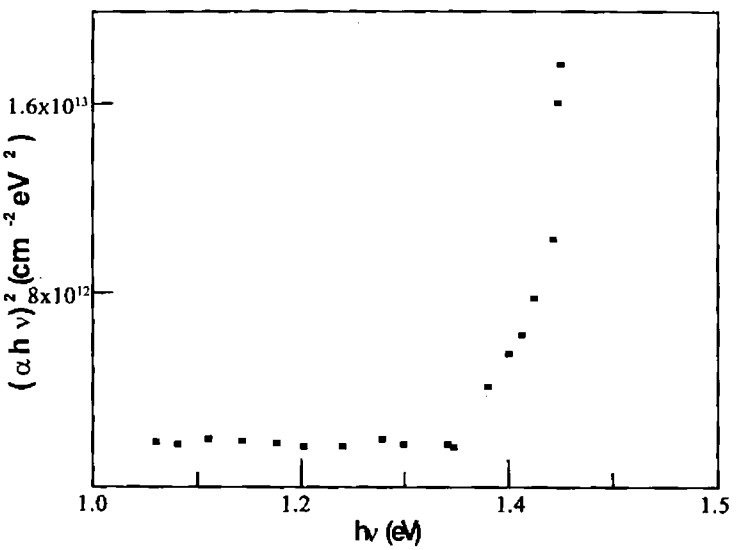

Figure 6.2 The plot of $(\alpha h\nu)^2$ vs the energy for $CuInS_2$ film

The $CuInS_2$/CdS heterojunction was fabricated with the CdS buffer layer grown by chemical bath deposition from a solution of cadmium chloride and thiourea with triethanolamine (TEA) as complexing agent. The volume mixture ratio of the cadmium chloride and thiourea was 1:1 and TEA was added by 4% of the volume of cadmium chloride. The pH of the solution was kept at 10.8 by adding ammonia solution and the bath temperature was maintained constant at 80^0C [3]. The CdS films showed an orientation in (100) plane with band gap of 2.4 eV (figure 6.3).

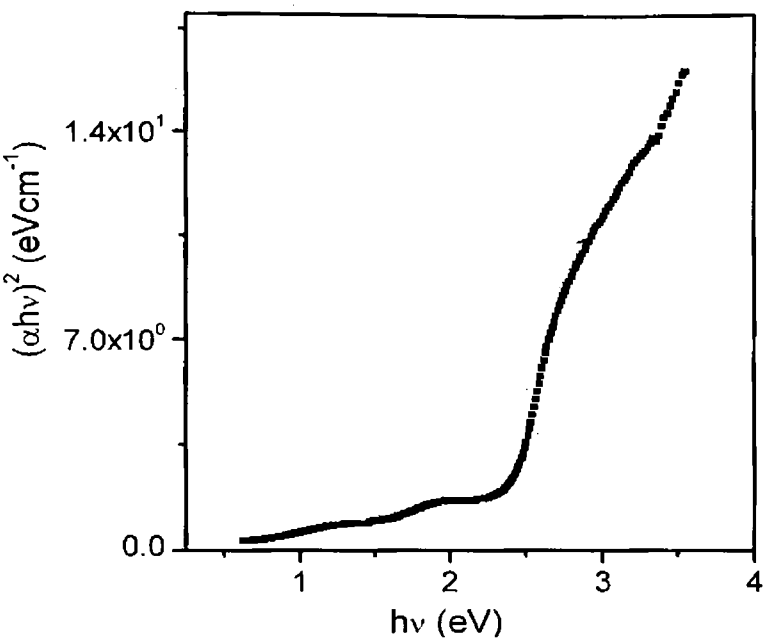

Figure 6.3 The plot of $(\alpha h\nu)^2$ vs the energy for CdS film

The Mo/$CuInS_2$/CdS/Ag heterojunction is completed by depositing silver electrodes by thermal evaporation. Heterojunction were also fabricated with ZnO/ZnO:Al as electrodes. The ZnO/ZnO:Al electrodes were deposited by RF sputtering in Ar atmosphere using ZnO and ZnO:Al(2% Al doped) target [4]. The ZnO:Al film has a conductivity of 4.5×10^4 were prepared. ZnO:Al is frequently used as front contact in thin film solar cells with $CuInS_2$ absorbers because it combines good electrical conductivity with high optical transparency. From the transmission spectra (Figure 6.4) it is seen that the prepared film exhibit a transmission over 85% in the visible region.

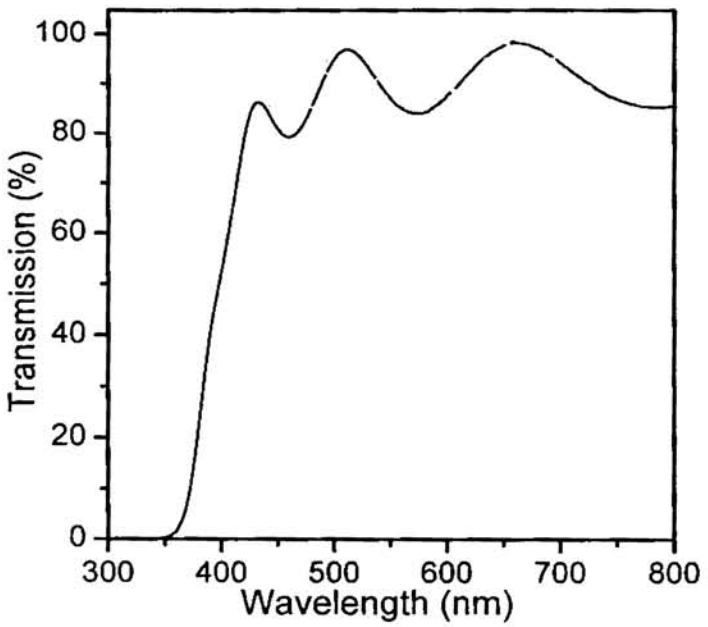

Figure 6.4 Transmission spectra of ZnO:Al thin films

6.3 Solar Cell Characteristics

For the characterisation of the solar cells, J-V characteristics under illumination were studied by a light source having intensity 100 mV/cm^2. Device structure is given in figure 6.5.

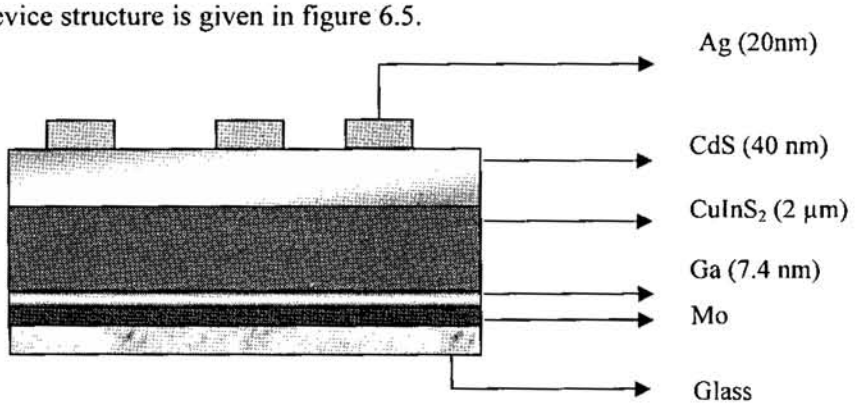

Figure 6.5 Structure of the fabricated solar cell

A typical J vs V plot of the cell with and without illumination is shown in figure 6.6.

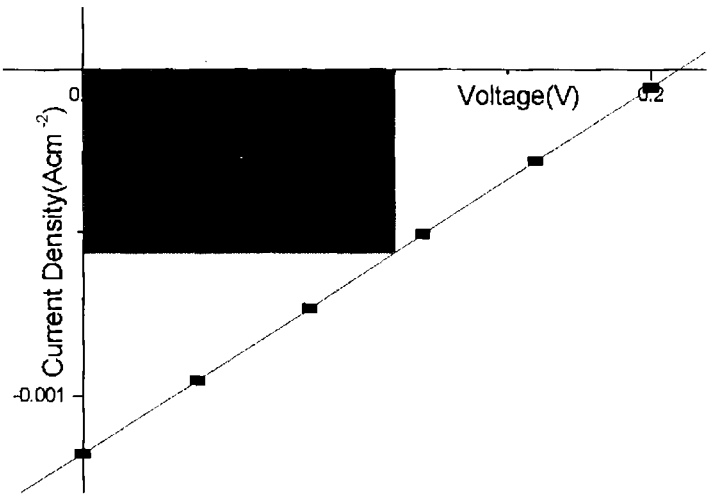

Figure 6.6 Typical J vs V plot of the cell

When silver was used as the electrodes the open circuit was very low but short circuit current was found better compared to that of Mo/$CuInS_2$/CdS/ZnO/ZnO:Al junction. The efficiency increased with the duration of illumination for the junction Mo/ $CuInS_2$/CdS/Ag. This might be due to the diffusion of silver by the heat produced during the illumination. The junctions with ZnO:Al and ZnO/ZnO:Al as electrodes did not show any increase in efficiency with the duration of illumination. Even though the open circuit voltage and fill factor of Mo/ $CuInS_2$/CdS/ZnO/ZnO:Al junction were comparable to the reported values, the efficiency was very low, which was due to the very low short circuit current. This could be due to differences in spectral absorption in window material [5]. The high series resistance can be attributed to the mismatch in CdS/ZnO junction, which was due to the preferred orientation of CdS and ZnO in different planes [6].

6.4

6.3 Summary

Two stage processes consisting of precursor preparation by thermal evaporation followed by chalcogenisation in the required atmosphere is found to be a feasible technique for the PV materials such as n-β In_2S_3, p-$CuInSe_2$, p-$CuInS_2$ and p-$CuIn(Se_{1-x}S_x)_2$. The growth parameters such as chalcogenisation temperature and duration of chalcogenisation etc have been optimised in the present study.

Single phase β-In_2S_3 thin films can be obtained by sulfurising the indium films above 300°C for 45 minutes. Low sulfurisation temperatures required prolonged annealing after the sulfurisation to obtain single phase β-In_2S_3, which resulted in high material loss. The maximum band gap of 2.58 eV was obtained for the nearly stoichiometric β-In_2S_3 film which was sulfurised at 350°C. This wider band gap, n type β-In_2S_3 can be used as an alternative to toxic CdS as window layer in photovoltaics [7].

The systematic study on the structural optical and electrical properties of $CuInSe_2$ films by varying the process parameters such as the duration of selenization and the selenization temperature led to the conclusion that for the growth of single-phase $CuInSe_2$, the optimum selenization temperature is 350°C and duration is 3 hours. The presence of some binary phases in films for shorter selenization period and lower selenization temperature may be due to the incomplete reaction and indium loss. Optical band gap energy of 1.05 eV obtained for the films under the optimum condition.

In order to obtain a closer match to the solar spectrum it is desirable to increase the band gap of the $CuInSe_2$ by a few meV [8]. Further research works were carried out to produce graded band gap $CuIn(Se,S)_2$ absorber films by incorporation of sulfur into $CuInSe_2$. It was observed that when the $CuInSe_2$ prepared by two stage process were post annealed in sulfur

atmosphere, the sulfur may be occupying the interstitial positions or forming a $CuInS_2$ phase along with $CuInSe_2$ phase. The sulfur treatment during the selenization process of $Cu_{11}In_9$ precursors resulted in $CuIn(Se,S)_2$ thin films. A band gap of 1.38 eV was obtained for the $CuIn(Se,S)_2$.

The optimised thin films n-β In_2S_3, p-$CuInSe_2$ and p-$CuIn(Se_{1-x}S_x)_2$ can be used for fabrication of polycrystalline solar cells.

6.3 Future Works

Hybrid solar cell receives great attention now days in PV industry. The advantage of hybrid materials consisting of inorganic semiconductors and organic polymers is that potentially one gets the best of both worlds. Inorganic semiconductors offer excellent, well established electronic properties, and they are very well suited as solar cell materials. Polymers offer the advantage of solution processing at room temperature, which is cheaper and allows using fully flexible substrates, such as plastics [9].

A hybrid solar cell with ITO/In_2S_3/PANI/Ag structure was fabricated using the layers optimised in our laboratory. The advantage in using semi-transparent semiconductor such as In_2S_3 is that they offer the possibility of front wall illumination through the semiconductor avoiding light loss due to absorption in the polymer layer [10]. The polymer for the fabrication of junction used was poly aniline doped with HCl (PANI). PANI was one of the most intensively studied polymers during the last decade [11]. PANI was made into solution by cyclohexanone. A drop of much diluted liquid form of PANI was deposited on ITO/n-In_2S_3 by solution cast. Silver was painted as electrodes.

Though the cell showed only poor junction behaviour, we hope a better efficiency cell by improving the characteristics of polymer layer. Photovoltaic characteristics are mainly controlled by the electrical properties

of the polymer film which depend strongly on the synthesis conditions [12]. So more sophisticated predation methods like spin coating can be applied for polymer deposition.

References

[1] J. Herrero, M. T. Gutierrz, C. Guilten, J. M. Dona, M. A. Martinef, A. M. Chaparro and R. Bayon, *Thin Solid Films* **361-362** (2000)26.

[2] Aldrin Antony. A. S. Asha, Rahana Yoosuf, R.Manoj and M. K. Jayaraj, *Solar Energy Mater. Solar Cells* **81** (2004) 407.

[3] Aldrin Antony, R. Manoj and M.K.Jayaraj, in: Proc. National conf. Thin Film Techniques and Applications (2002) 68.

[4] M. K. Jayaraj, Aldrin Antony and R. Manoj, *Bull. of Mater. Sci.* **25** (2002) 227.

[5] R. Scheer, T. Walter, H. W. Shock, M. L. Fearheiley and H. J. Lewerenz, *Appl. Phys. Lett.* **63** (1993) 1859.

[6] S. H. Jeong, J. K. Kim and B. T. Lee *J. phys. D: Appl. phy.* **36** (2003) 2017.

[7] N. Naghavi, S. Spiering, M. Powalla, B. Cavana and D. Lincot, *Prog. Photovolt: Res. Appl.* **11** (2003) 437.

[8] C. J. Sheppard, V. Alberts, and W. J. Bekker, *Phys. Stat. Sol. (A)* **201** (2004) 2234.

[9] P. J. Sebastian, S. A. Gamboa, M. E. Calixo, H. N. Cong, P. Chartier and R. Perez, *Semicond.Sci. Technology* **13** (1998) 1459.

[10] A. J. Frank, S. Glenis and A. J. Nelson, *J. Phys .Chem.* **93** (1989) 3818.

[11] A. G. MacDiarmid, *Synth. Met.* **84** (1997) 27.

[12] H. N. Cong, C. Sene and P. Chartier, *Solar Energy Mater. Solar Cells* **29** (1993)127.